T.R.
EGE UNIVERSITY
Graduate School of Applied and Natural Science

PREPARATION AND CHARACTERIZATION OF METAL OXIDE NANOPARTICLES MODIFIED CARBON NANOTUBE-CONDUCTING POLYMERS BASED COMPOSITE ELECTRODE FOR SIMULTANEOUS DETERMINATION OF MELATONIN AND CAFFEINE

Tansu DOĞAN

Supervisor : Prof. Dr. Zekerya DURSUN

Department of Chemistry

İzmir
2020

Tansu Doğan tarafından **Yüksek Lisans** tezi olarak sunulan **"Preparation and characterization of metal oxide nanoparticles modified carbon nanotube-conducting polymers based composite electrode for simultaneous determination of melatonin and caffeine"** başlıklı bu çalışma EÜ Lisansüstü Eğitim ve Öğretim Yönetmeliği ile EÜ Fen Bilimleri Enstitüsü Eğitim ve Öğretim Yönergesi'nin ilgili hükümleri uyarınca tarafımızdan değerlendirilerek savunmaya değer bulunmuş ve 14.02.2020 tarihinde yapılan tez savunma sınavında aday oybirliği/oyçokluğu ile başarılı bulunmuştur.

Jüri Üyeleri:		**İmza**
Jüri Başkanı	**: Prof. Dr. Zekerya DURSUN**	.....
Raportör Üye	**: Prof. Dr. H. İsmet GÖKÇEL**	.....
Üye	**: Prof. Dr. Yusuf DİLGİN**	.....

EGE ÜNİVERSİTESİ FEN BİLİMLERİ ENSTİTÜSÜ

ETİK KURALLARA UYGUNLUK BEYANI

EÜ Lisansüstü Eğitim ve Öğretim Yönetmeliğinin ilgili hükümleri uyarınca Yüksek Lisans Tezi / Doktora Tezi olarak sunduğum **"Preparation and characterization of metal oxide nanoparticles modified carbon nanotube-conducting polymers based composite electrode for simultaneous determination of melatonin and caffeine"** başlıklı bu tezin kendi çalışmam olduğunu, sunduğum tüm sonuç, doküman, bilgi ve belgeleri bizzat ve bu tez çalışması kapsamında elde ettiğimi, bu tez çalışmasıyla elde edilmeyen bütün bilgi ve yorumlara atıf yaptığımı ve bunları kaynaklar listesinde usulüne uygun olarak verdiğimi, tez çalışması ve yazımı sırasında patent ve telif haklarını ihlal edici bir davranışımın olmadığını, bu tezin herhangi bir bölümünü bu üniversite veya diğer bir üniversitede başka bir tez çalışması içinde sunmadığımı, bu tezin planlanmasından yazımına kadar bütün safhalarda bilimsel etik kurallarına uygun olarak davrandığımı ve aksinin ortaya çıkması durumunda her türlü yasal sonucu kabul edeceğimi beyan ederim.

14 / 02 / 2020

İmzası

Tansu DOĞAN

ÖZET

MELATONİN VE KAFEİNİN EŞZAMANLI TAYİNLERİ İÇİN METAL OKSİT NANOPARÇACIK İLE MODİFİYE KARBON NANO TÜP-İLETKEN POLİMER TEMELLİ KOMPOZİT ELEKTROTLARIN HAZIRLANMASI VE KARAKTERİZASYONU

DOĞAN, Tansu

Yüksek Lisans Tezi, Kimya Anabilim Dalı
Tez Danışmanı: Prof. Dr. Zekerya DURSUN
Şubat, 2020, 128 sayfa

Bu tez çalışması kapsamında, camımsı karbon elektrot yüzeyine sırasıyla elektropolimerizasyon ile polikresol kırmızısı döngüsel voltammetri ile film oluşturularak, oluşan film yüzeyi üzerine çok duvarlı karbon nanotüp ve çok duvarlı karbon nano tüp üzerine çinko oksit metal nano parçacıkları kronoamperometri ile elektrokimyasal olarak depolanmıştır. Oluşturulan kompozit modifiye elektrotların morfolojik, kimyasal ve elektriksel yüzey özellikleri aydınlatıldıktan sonra, melatonin ve kaffeinin tekli ve bir arada olduğu koşullardaki elektrokimyasal davranışı farklı pH'larda incelenmiştir.

Yalın ve kompozit elektrotlarda melatonin ve kaffeinin pik akım yüksekliği ve pik potansiyelleri karşılaştırıldığında en uygun çalışma pH'ının 7.0 fosfat tamponu olduğu saptanmıştır. Aynı zamanda pH=7.0 fosfat tamponu ortamında tüm elektrotların melatonin ve kaffein yükseltgenmesine davranışları incelendiğinde, polikrezol kırmızısı-çok duvarlı karbon nanotüp-çinko oksit depolanmış kompozit elektrodun (ZnO/MWCNT/PCR/GCE) en yüksek katalitik etkinliğe sahip olduğu saptanmıştır. Polikrezol kırmızısının elektrot yüzeyinde oluşturulmasına ilişkin, krezol kırmızısı derişimi ve döngüsel voltammetrik döngü sayısı optimize edilmiştir. Ardından MWCNT/PCR/GCE üzerine kronoamperometri ile depolanan çinko oksit metal nano parçacıklarının sırasıyla

derişim, potansiyel ve biriktirme süresine ilişkin optimizasyon çalışmaları gerçekleştirilmiştir. Optimum deney koşulları saptandıktan sonra, differansiyel puls voltammetrik teknikle melatonin ve kaffeinin duyar tayinine yönelik deneysel çalışmalar yalın camımsı (GC), PCR/GC, MWCNT/PCR/GC, MWCNT/GC, ZnO/MWCNT/GC ve ZnO/MWCNT/PCR/GC elektrotlarıyla yapılmış ve elde edilen veriler karşılaştırıldığında, en yüksek etkinliğe sahip olan elektrodun kompozit yapıdaki ZnO/MWCNT/PCR/GC elektrodu olduğu saptanmıştır. ZnO/MWCNT/PCR/GC kompozit elektrotta pik akım yüksekliğinin melatonin ve kaffein derişimi ile değişimi $4.0x10^{-8}$ M – $4.0x10^{-7}$ M aralığında doğrusal bulunurken, belirtme alt sınırı ise sırasıyla $1.38x10^{-8}$ M ve $1.33x10^{-8}$ M olarak saptanmıştır (S/N=3).

Hazırlanan kompozit elektrotların, morfolojisi taramalı elektron mikroskobu, yüzeyin kimyasal bileşenleri X-ışını fotoelektron spektroskopisi ve elektriksel özellikleri ise elektrokimyasal impedans tekniği ile aydınlatılmıştır.

Anahtar sözcükler: Melatonin, kaffein, çok duvarlı karbon nanotüp, iletken polimer, polikrezol kırmızısı, metal nano parçacık, voltammetri.

ABSTRACT

PREPARATION AND CHARACTERIZATION OF METAL OXIDE NANOPARTICLES MODIFIED CARBON NANOTUBE-CONDUCTING POLYMERS BASED COMPOSITE ELECTRODE FOR SIMULTANEOUS DETERMINATION OF MELATONIN AND CAFFEINE

DOĞAN, Tansu

MSc in Chemistry Department
Supervisor: Prof. Dr. Zekerya DURSUN
February, 2020, 128 pages

In this thesis study, highly effective zincoxide metal nano particles electrodeposited by chronoamperometry on multi-walled carbon nanotube and polycresol red film based composite modified surfaces were prepared onto glassy carbon electrode surfaces and after the examination of morphological, chemical and electrical properties of these modified electrodes, the electrochemical behavior of melatonin and caffeine was investigated at different pHs.

When peak currents and peak potentials of melatonin and caffeine were compared at bare and prepared composite electrodes, it was determined that the optimum working pH was obtained as 7.0 by using phosphate buffer. Moreover, when the behavior of all electrodes against melatonin and caffeine oxidation was examined in pH 7.0 phosphate buffer solutions, zincoxide-multi-walled carbon nanotube-polycresol red composite electrode (ZnO/MWCNT/PCR/GCE) was observed to have the highest activity. Regarding to the formation of polycresol on the electrode surface, cresol red concentration and number of cyclic voltammetric cycles were optimized. Then, zincoxide optimization parameters such as concentration, deposition of potential and deposition time were studied

respectively. After the optimization of experimental conditions, experimental studies for the sensitive detection of melatonin and caffeine were highlighted utilizing at bare GC, PCR/GC, MWCNT/PCR/GC, MWCNT/GC, ZnO/MWCNT/GC ve ZnO/MWCNT/PCR/GC electrodes by performing differential pulse voltammetry technique and when the obtained data was compared to each other, finally ZnO/MWCNT/PCR/GC composite electrode has the highest activity. For this electrode, linear range was found to be $4.0x10^{-8}$ M– $4.0x10^{-7}$ M for melatonin and caffeine, while limit of detection was calculated as $1.38x10^{-8}$ M and $1.33x10^{-8}$ M (S/N=3), respectively.

Keywords: Melatonin, caffeine, multi-walled carbon nanotube, conductive polymer, polycresol red, metal nano particles, voltammetry.

ÖNSÖZ

Elektrokimyasal analiz teknikleri, özellikle voltammetri, elektrokimya alanında son yıllardaki gelişmelere paralel olarak ve analizlerde sağladığı bazı üstünlükler nedeniyle giderek artan bir uygulama alanına sahiptir. Mekanizmaların açıklanmasını daha da aydınlatmak için özellikle indirgenme olaylarına oranla elektrokimyasal yükseltgenme olaylarının da bu yöntemlerle incelenip araştırılması yeni ufukların açılmasına önemli ölçüde katkı sağlamıştır. Bununla birlikte "modifiye elektrotlar" yani özellikleri değiştirilerek geliştirilmiş elektrotlar tasarlanmıştır. Bu sayede yeterli bir tekrar edilebilirlik sağlanabildiği gibi kantitatif analizlerde duyarlılık ve seçimlilik arttırılmış dolayısıyla klinik analizlerde ve çevre çalışmalarında modifiye elektrotların kullanılması oldukça popüler hale gelmiştir.

Birden fazla maddenin bir araya getirilerek oluşturulduğu kompozit malzemelerin, bileşenlerine göre daha iyi elektriksel, kimyasal, katalitik vb. özelliklere sahip olabilmesi ve nano parçacıklar ile modifiye edilebilmesi son yıllarda elektrokimyasal tekniklerle yoğun bir şekilde çalışılmaktadır. İletken özellikteki polimerlere metal/metal oksit parçacıklar katlandırıldığında ya da karbon nanotüp gibi karbon esaslı malzemeler ile birlikte hazırlandıklarında iletkenlikleri önemli ölçüde artırılabilir.

Bu tez kapsamında, yüksek elektrokatalitik etkinliğe sahip, kararlı, düşük maliyetli metal/metal oksit nano parçacık modifiye-iletken polimer kompozit elektrot geliştirilerek, farmakolojik ve biyolojik önemi olan melatonin ve kafeinin eşzamanlı seçimli ve duyar voltammetrik tayinleri yapılmıştır. Melatonin ve kafeinin tekli veya bir arada oldukları koşullarda elektrokimyasal davranışlarının incelenebilmesi, voltammetrik sinyallerinin bir biriyle çakışmaması, her iki molekülün pik akım değerlerinin metal/metal oksit modifiye kompozit elektrotlarla yalın camımsı karbon elektroda göre daha yüksek olması gibi sonuçlar bir arada tayinler için başarı ölçütü olacak ve akademik düzeyde yapılacak çalışmalar açısından fayda sağlayacaktır.

İZMİR

14 / 02 / 2020

Tansu DOĞAN

FOREWORD

In recent years, electrochemical analysis techniques, especially voltammetry, have been increasing in parallel with the developments in electrochemistry field and due to some advantages in analysis. To further clarify the explanation of mechanisms, in addition to the reduction events, the analysis of oxidation events with these methods contributed significantly to the opening of new horizons. However, “modified electrodes” that is, developed electrodes by changing their properties are designed. In this way, sufficient reproducibility can be ensured and sensitivity and selectivity have been increased in quantitative analysis, and therefore the use of modified electrodes in clinical analysis and environmental studies has become very popular.

In recent years, composite materials have better electrical, chemical and catalytic properties compared to their constituent components and their modification with nanoparticles has been continuing intensively with electrochemical techniques. The conductivity can be significantly increased when the metal / metal oxide particles are folded into the conductive polymers or they are prepared together with carbon-based materials such as carbon nanotube.

In this thesis, stable, low cost metal / metal oxide nanoparticle modified-conductive polymer composite electrode with high electrocatalytic activity was developed. With the help of this electrode, sensory voltammetric assays were performed simultaneously for pharmacological and biological importance of melatonin and caffeine. To be able to investigate the electrochemical behavior of melatonin and caffeine in single or combination conditions, voltammetric signals do not coincide with each other, peak current values of both molecules are higher than metal glass oxide carbon electrode with metal / metal oxide modified composite electrodes, the combination of all the results listed above will be a criterion of success and will be beneficial in academic studies.

İZMİR

14 / 02 / 2020

Tansu DOĞAN

CONTENTS

Page

CONTENTS (continued)

Page

CONTENTS (continued)

Page

CONTENTS (continued)

Page

CONTENTS (continued)

Page

FIGURE LIST

Figure **Page**

FIGURE LIST (continued)

Figure **Page**

FIGURE LIST (continued)

Figure **Page**

FIGURE LIST (continued)

Figure **Page**

FIGURE LIST (continued)

Figure **Page**

FIGURE LIST (continued)

Figure **Page**

FIGURE LIST (continued)

Figure **Page**

FIGURE LIST (continued)

Figure **Page**

FIGURE LIST (continued)

Figure **Page**

FIGURE LIST (continued)

Figure **Page**

FIGURE LIST (continued)

Figure **Page**

FIGURE LIST (continued)

Figure **Page**

FIGURE LIST (continued)

Figure **Page**

FIGURE LIST (continued)

Figure **Page**

TABLE LIST

TABLE LIST (continued)

Table **Page**

TABLE LIST (continued)

Table **Page**

ABBREVIATIONS

Symbol	Explanation
A	Electrode area
C	Analyte concentration
CPs	Conducting Polymers
PCR	Poly Cresol Red
CFME	Carbon fibre micro electrophoresis
CL	Chemiluminescence
CNT	Carbon Nanotubes
C_{ox}	Concentration of oxidized form
C_{red}	Concentration of reduced form
CV	Cyclic Voltammetry
D	Diffussion coefficient
DPV	Differential Pulse Voltammetry
E^0	The standart potential
E_p	Peak potential
E_{pa}	Anodic peak potential
E_{pc}	Cathodic peak potential
Eq	Equation
EIS	Electrochemical impedance spectroscopy
GCE	Glassy carbon electrode
i_l	Limiting current
i_{pa}	Anodic peak current
i_{pc}	Cathodic peak current
LOD	Limit of Detection
LR	Lineer range
MNP	Metal nano particle
MWCNT	Multiwalled Carbon Nanotubes
SWCNT	Single Walled Carbon Nanotubes
Ox	Oxidized form
Red	Reduced form
SEM	Scanning Electron Microscopy
v	Scan rate

1. INTRODUCTION

Preparation and application of nano-sized materials in different fields of science and technology have been greatly studied due to their unique optical, electrical, catalytic and magnetic properties of these materials. The materials have also high specific area, subtle electronic characteristics, strong adsorptive ability and promote the electron-transfer reactions of electroactive molecules. The properties of nano materials are usually dissimilar from their bulk counterparts due to their extremely small size, special shape and large surface-to-bulk ratio. The increasing surface area to volume ratio provides to an enhancement in the superiority of the surface atoms of the nanoparticles over those in its inside structure (Abid et al., 2013).

As with many alternative disciplines, the applications of nanotechnology (for example in steelmaking and painting) were used centuries prior to the official definition of the field. It occurred in the early eighties and early nineties. Although the 1950s were seen as the earliest time for conceptualization and concerns concerning nanotechnology. Semiconductor technology (electronic technology), biotechnology (growths in biological structures, eg cell-level growths) and nanotechnology are pioneers in technological advances that can be defined as direct applications of basic sciences. Richard Zsigmondy received the Nobel Prize in 1925 for the first time for expressing the concept of “nanometer” (Hulla et al., 2015).

Scientists were able to make observations at an atomic level that was comparable to that of IBM Zurich scientists in the 1980s, when they created a scanning tunneling microscope and an atomic force microscope that followed their findings. Comprehensive substance system simulations using supercomputers were made feasible by the increasing number of advanced computers during this time. These investigations were supplied by understanding nano-extent substance constructions and components. Nano-extent studies gained momentum in the 1980s

ascribed to the additional activities of modeling and simulation, atomic extent imaging and classification, and empirical synthesis (Hulla et al., 2015).

Meanwhile, in order to grasp the quantum components of nanosubstances, it is significant to consider the elements of the subject as atoms, molecules or crystals in the collective phase. Nano-mixtured metals with extent ranging from 1-100 nm (span, width, thickness) are called metallic nanoparticles. The first research of metallic nanoparticles in solution was made by Faraday in 1857 (Kumar et al., 2018).

Almost all significant characteristic of nanoparticles is the surface area / volume proportion that permits them to interact with unalike particles. The prominent surface area / volume proportion accelerations diffusion and requires lower temperatures to be accessible. Unalike studies have shown that empirical factors, the adsorption progress of the stabilizing envoy and the kinetics of the relationship of metal ions with reducing envoys (Khan et al., 2019).

Nanotechnology, together with nanochemistry, has shed light on the growth of electrochemistry and the identification of many biological and habitatal specimens by designing electrodes alter with nano-compounded substances.

Nanotechnological growths have permitted the manufacture of adaptable conductive polymer nanosubstances with upgrade interpretation. In the last decade, conductive polymers (CPs) have attracted get bigger awareness ascribed to their powerfull potential as an feasible to their inorganic equivalents, and have open on to significance basic and empirical research attempts. In the late 1970s, most scientists thought that CPs (or "synthetic metals") were stubborn and unable to be solved. Since the invention of polyamethylene in 1977 by A. Heeger, A. Mac Diarmid and, H. Shirakawa a number of significant CPs have been continuously explored, counting polypyrrole (PPy), polyaniline (PANI), polythiophene (PT), poly (3,4-ethylenedioxythiophene). (PEDOT), trans-polyacetylene and poly (p-phenylene vinylene) (PPV) (Thanh-Hai et al., 2017).

Generally, CPs have feasible single (σ) and double (π) bonds, and these (π)-conjugated systems have optical, electrochemical and electrical / electronic structures specific to CPs. Conductive polymers have chemical diversity, low density, elasticity, corrosion resistance, easy-to-control shape and morphology, and adjustable conductivity to reprinciple inorganic equivalents (Huang et al., 1986). It is recognized that the parameters have an impact on the physical structures of CP are conjugation span, degree of crystallinity and interchain and interchain interactions (Thanh-Hai et al., 2017).

The privatization of substance structures at extremely small levels to obtain specific components guides to broad nanotechnology profits by broadening substance science broadly. For example, polymer nanocompounds (PNC) are noted for a variety of potential component improvements that can be achieved by incorporating unalike types of nanofiles into polymer matrices. Over the past few decades, PNCs have been given increasing concern as, unlike alternative metal options, they are lightweight, incostly and easy to progress, and have individual ability to replace components. Subject to the end-use application, the precise PNC components are guided and the formulation and proportion of the PNC can be admixtured to obtain the required components (Zhu et al., 2004).

The logical integration of CPs with alternative substances could consequence in substances with absorbing structures and new demand chances in a change of fields, from electronics to energy tools (Thanh-Hai et al., 2017).

In 1985, a big leap was made by finding new form for the carbon molecules called 60 bukyball circular 60, which are circular and have sixty carbon atoms. This open on to the formation of a reporter molecular form in 1991 called “carbon nanotube’’ (Iijima et al., 1991).

CPs, concerning 100 times powerful than steel and only one-sixth of the weight, are now emerging areas of nanotechnology; they have outstanding thermal and conductivity structures. Similarly, research on semiconductor nanocrystals has

open on to the progression of quantum dots whose components are located on either side bulk semiconductors and separatio molecules (De Volder et al., 2013).

Researchers in this area have detail unalike stratiogies for obtaining CP-based compoundeds and hybrids with new assembly and grow better structures (Wang et al., 2005).

The illustrative example, CP nanocompoundeds involve carbon nano-species such as graphene, carbon nanofibers and carbon nanotubes have been evolved (Gupta et al., 2016).

In order to understand the size of a single carbon atom with the use of carbon and carbon-based materials in nanotechnology, examples of nano-sized materials were shown in Figure 1.1 compared to many smaller sizes, such as carbon nanotubes, quantum dots, and red blood cells. Nanotechnology has grow an ever-increasing nanoelectrochemistry for academic studies, and this has grow more significant through scientific studies.

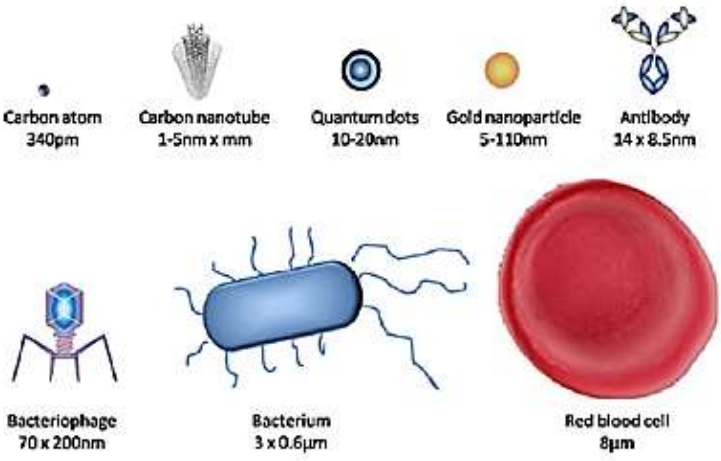

Figure 1.1 Some nanoparticles in comparison with biological molecules (Lahiff et al., 2010)

1.1. The Purpose of the Thesis

There are two main goals of this thesis; the first aim was to design various composite electrodes, which prepared by composition of conducting polymer and multiwalled carbon nanotubes on glassy carbon electrodes (GCE) and then modified by various metal/metal oxides for electrocatalytic oxidation of melatonin and caffeine. A series of optimization studies were performed by changing the concentration of cresol red monomer, cycle number, amount of carbon nanotube, concentration metal ions, type of supporting electrolyte and concentration of electrolyte using cyclic voltammetry, chronoamperometry to obtain the best catalytic active electrode surfaces.

The second goal of this thesis was characterized the chemical, morfological and electrical properties of the composite electrodes by CV, XPS, SEM,EDX and EIS.

1.2. Carbon Nanotubes

Carbon is an significant element for a change of sciences, from the sciences of physics, chemistry and substances to life sciences, but the conventional carbon formulation on a micron extent it may not be the optimal insert substance (Mortier and Engelhardt, 2000). Carbon based structures such as nanotubes, fullerenes, carbon onions are characteristic derivates of nano-structured carbons to which are significant in nano-sciences. (Sun et al., 1996).

After the discovery of the extraordinary structures of carbon nanotubes, it was extensively studied, and this notice open on to the conversion of substance into a "phenomenon" in many areas, particularly in nanoscience. In most performed and theoretical studies, carbon nanotubes have grown a "model system" for nanotechnology (Ando et al., 2004). Subsequently, nanosubstances such as carbon nanotubes (CNTs) with individual electrical, mechanical and surface structures drew notice and aroused the notice of many scientists (Kam et al., 2005).

Elemental carbon has long been recognized to have only three forms-amorphous, graphite and diamond. Unalike carbon species in sp^2 hybridization can form a change of surprising structures. One of these surprising structures is Kroto and fullerene (Kroto et al., 1985). Similar to Fullerenes It has a graphite structure and be composeds of a layer of connected hexagonal rings, but they contain pentagonal (or sometimes heptagonal) rings that prevent the layer from being planar. New forms of carbon were identified shortly after the discovery of fullerenes.

In 1991, Iijima (Iijima, 1991) first observed the tubular carbon structures of a variety of tens of graphite shells MWCNT. Two years after, Iijima and Ichihashi (Iijima and Ichihashi, 1993) and Bethune Synthesized Single-Walled Carbon Nanotubes (SWNT). Regardless of the method used in the synthesis of (MWCNT), carbon nanostructures, graphite sheets, amorphous carbon, metal catalyst and a small amount of fullerens.

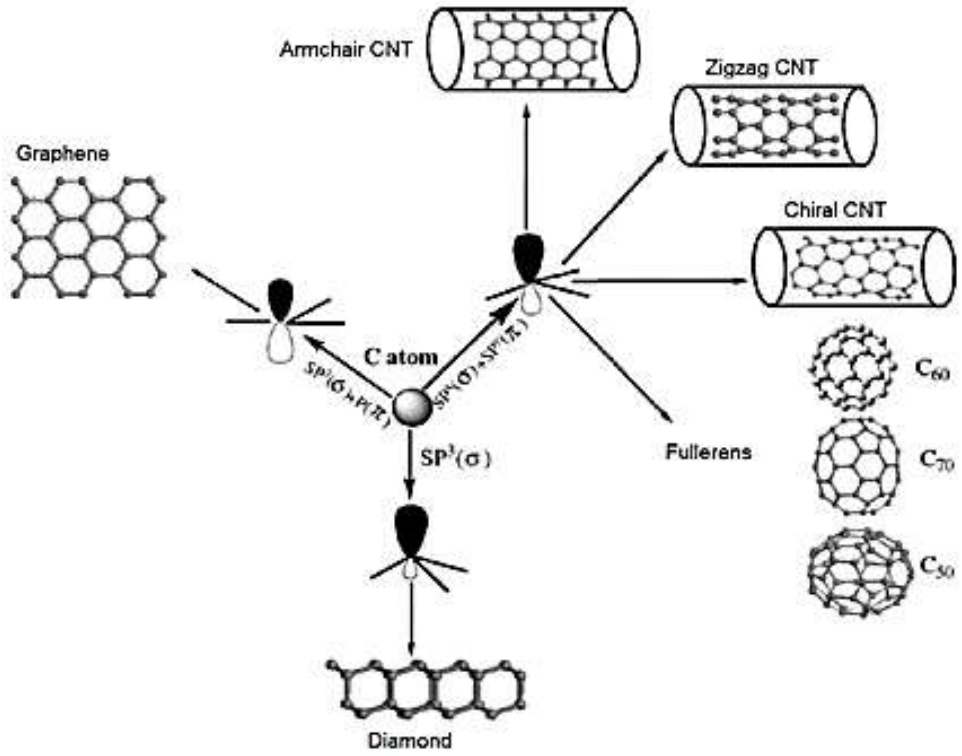

Figure 1.2 Chemistry of carbon substances (Li et al., 2007)

CNTs and similar structures also have at least one dimension below 100 nm. Concave-1B nanosubstances with a 1B or very high-rise span / width proportion are particularly relevant to CNTs (Kuchibhatla et al., 2007). As can be seen from Figure 1.3, the nanosubstances 1B can be in many unalike forms.

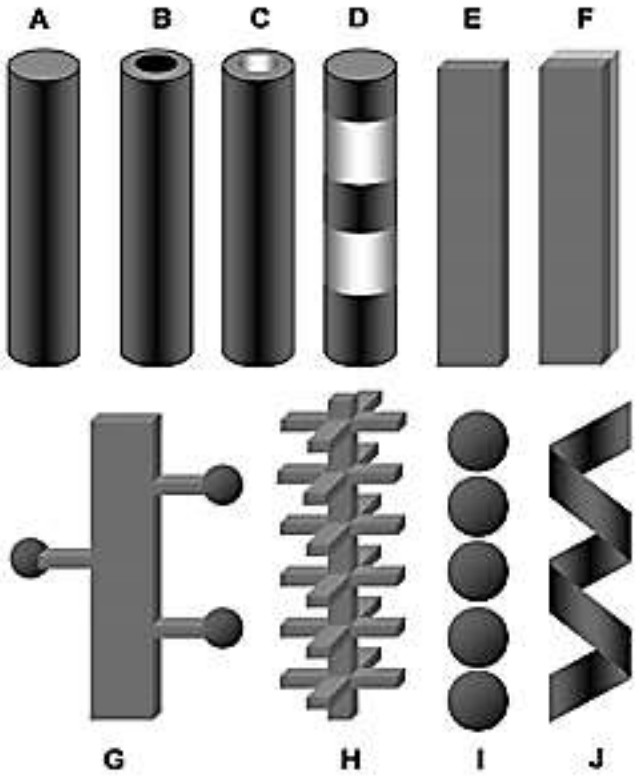

Figure 1.3 1B nano-substances. (A) nano-wires and nano-rods, (B) nuve-shell structures, (C) nano-tubes, (D) hetero-structures, (E) nano-belts, (F) nano-cerps, (G) dendrites, (H) hierarchical nano-structures, (I) nano-particles (J) nano-helices (Kuchbhatla et al., 2007)

CNTs are probably the most significant of all 1B nanosubstances. Simply put, CNT is a tubular structure with nanometer diameter and μm span (Dresselhaus et al., 2004, Charlier et al., 2007). In alternative words, from a structural point of view, CNTs may be considered as a hollow cylinder made of one or more graphene layers (a single graphite layer). The diameter of said cylinder may be from 0.4 nm to 100

nm or high-riseer (Maultzsch, 2004, Kuchibhatla et al., 2007). However, Dresselhaus et al. It proposes to classify tubular structures larger than 15 nm in diameter as "carbon nanofibers" (Dresselhaus et al., 2004). CNTs, which can be very unalike depending on the manufacture method and conditions, can mixture from hundreds of μm to cm (Dai, 2002).

The number of graphene walls that adjust it generally classifies CNTs. The final nanotube structure is graphite tubular single-walled carbon nanotubes (Figure 1.4). SWCNTs have diameters showing the mixture of 1-2 nm and Gaussian distribution (Maultzsch et. al., 2004) (Ajayan et al., 1999, Maultzsch, 2004). SWCNTs can be of three unalike types, depending on the direction of the graphene cylinder forming it relative to the tube axis: "seat", "zigzag" and "chiral" nanotubes (Chen et al., 2000). SWCNTs are usually found in hexagonal packed crystalline bundles (ropes) (Dresselhaus, 2004, Maultzsch, 2004). These bundles are connected by van der Waals forces (Sinnot et al., 2001).

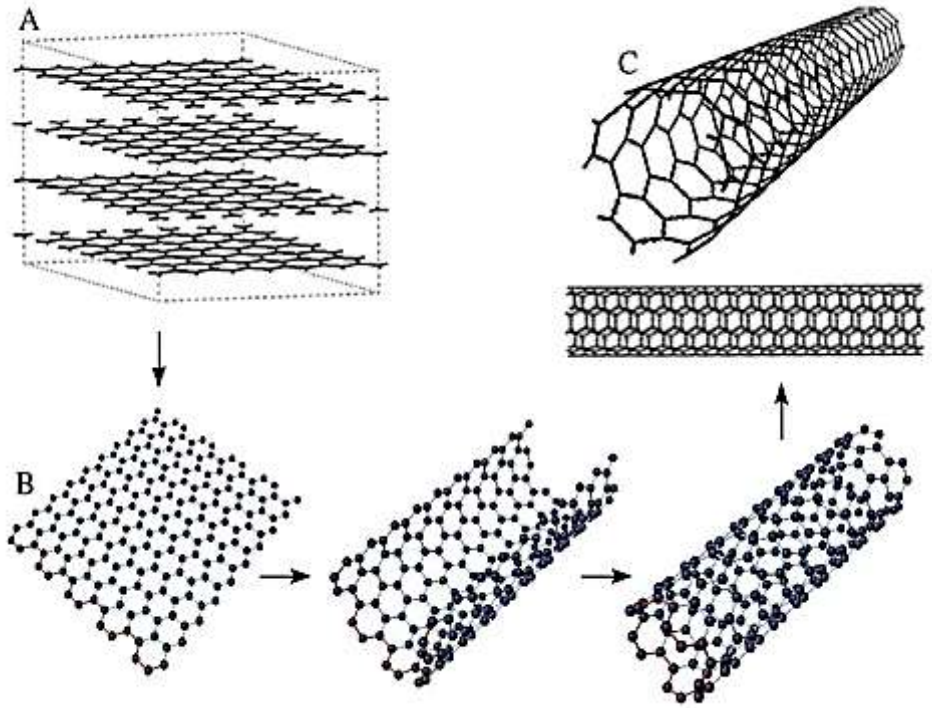

Figure 1.4 Graphite (A), graphene sheet (B) and carbon nanotube (C) (Kuchibhatla et al., 2007)

MWCNTs are nanotubes with more than two graphene walls (Figure 1.4). The internal diameters of the MWCNTs can be lessen to 0.4 nm, but to concerning 5 nm (Maultzsch, 2004). As noted earlier, the outer radius is 15 nm (Dresselhaus et al., 2004). The interval on either side the walls in the MWCNTs was estimated to be 0.339 nm. In XRD and TEM analyzes, the interval of graphene walls to each alternative was measured in the mixture of 0.34-0.39 nm (Sun et al., 1996, Chen et al., 2000, Sinnott et al., 2001). In addition, the calculations show that inter-wall interactions are low in neighboring MWCNTs and that the walls are capable of independent rotation and translation movements (Sun et al., 1996, Kuchibhatla et al., 2007).

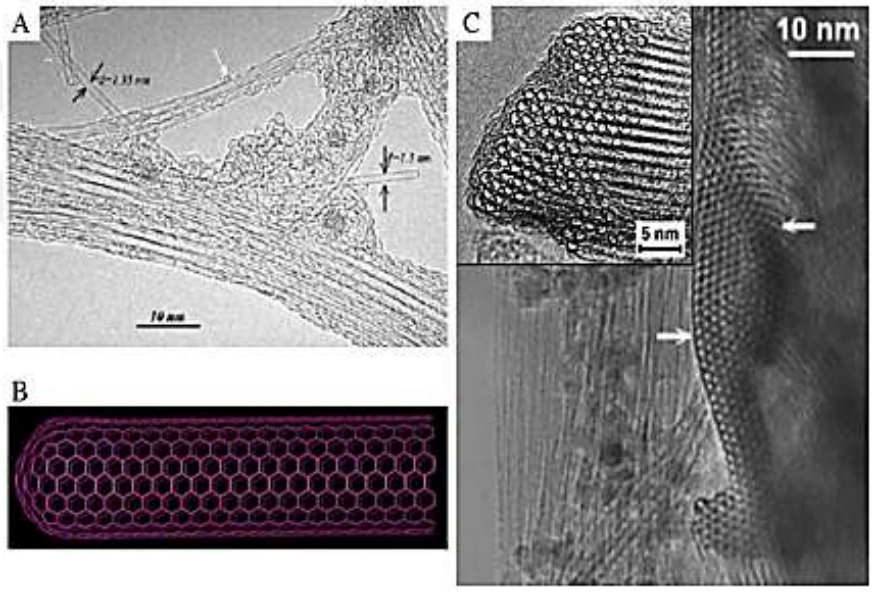

Figure 1.5 SWCNT (A) TEM image of SWCNTs with unalike by-manufactured, (B) Schematic structure of SWCNT, (C) SWCNT bundles (Colomer et al., 2002, Eklund et al., 2002)

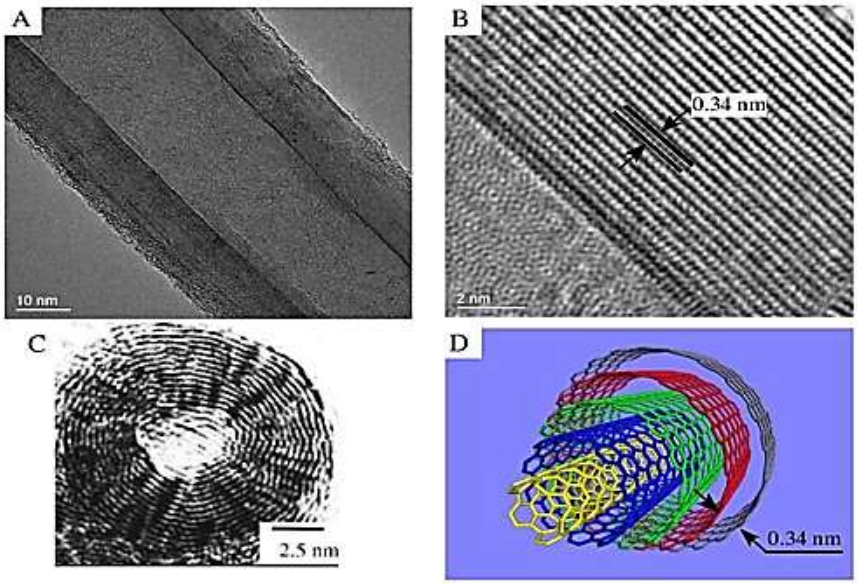

Figure 1.6 MWCNT (A) lateral TEM image, (B) high-rise resolution lateral TEM image, (C) TEM anterior cross-sectional view, (D) schematic structure of MWCNT (Kiselev and Zakharow, 2001)

1.2.1. Crystal structure of CNT

While describing CNTs, Hamada et al. and graphene is based on the crystal lattice structure (Figure 1.7) (Hamada et al., 1992). In this method, which can fully define the nanotubes geometrically (Charlier et al., 2007), each CNT is assigned a chiral vector - Ch (Terrones, 2003, Dresselhaus et al., 2004):

$$C_h = na_1 + ma_1 \equiv (n,m) \qquad (1)$$

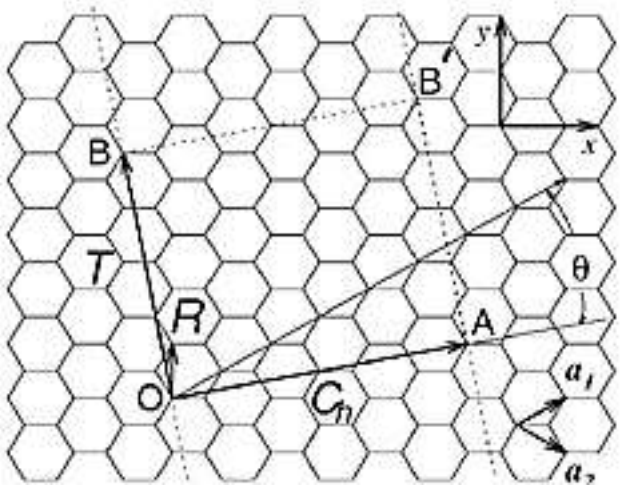

Figure 1.7 Graphene lattice (Dresselhaus et al., 2004)

In Equation 1, a_1 and a_2 are unit vectors the chiral vector resolves the direction of folding in the geometric transformation of a graphene layer into the nanotube (Kuchibhatla et al., 2007). More specifically, the chiral vector, the ends and tail of O and A, are crystallographically identical when the chiral vector is folded into an overlapping circle (Charlier et al., 2007). The AB and OB lines are also combined so that the unit cell of the nanotube is obtained. The corresponding nanotube formation for a Ch given in Figure 1.7 is presented. As can be seen, Ch is the sum of unit vectors. The diameter of CNT (dt) is communicated by correlation (2) (Terrones, 2003):

$$d_t = \frac{C_h}{\pi} = \frac{a_{C-C}}{\pi}\sqrt{3\,(m^2 + mn + n^2)} \qquad (2)$$

In the above equation a_{C-C} is the span of the carbon-carbon bond and a_{C-C} = 0.1421 nm can be taken onto the graphite.

$$C_h = \pi d_t$$

As can be understood from the above description, Ch corresponds to the CNT habitat (Charlier et al., 2007). The angle on either side the A1 line ("zigzag" direction) and Ch is called "chiral angle -" (Mauron, 2003, Dresselhaus et al., 2004, Maultzsch, 2004). The value of the chiral angle can be communicated in terms of (n, m) (Terrones, 2003, Dresselhaus et al., 2004):

$$\theta = tan^{-1}\left(-\frac{m\sqrt{3}}{m+2n}\right) \qquad (3)$$

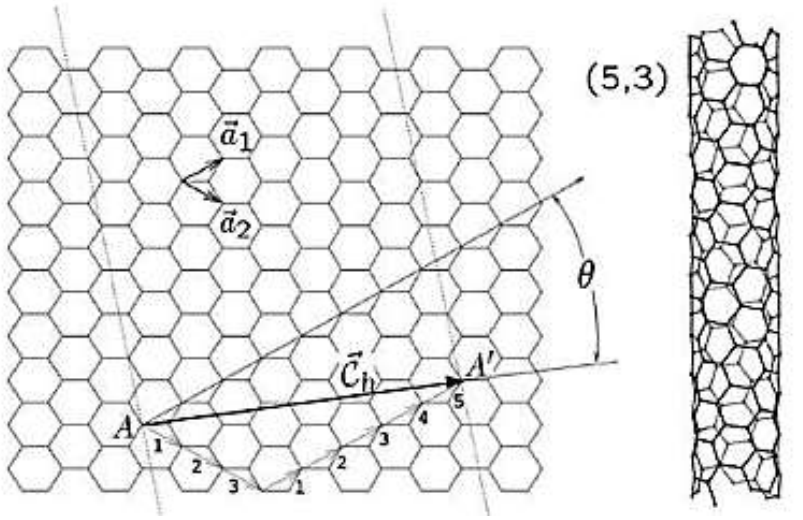

Figure 1.8 Ch = $5a_1 + 3a_2 \equiv (5,3)$ nanotubes (Charlier et al., 2007)

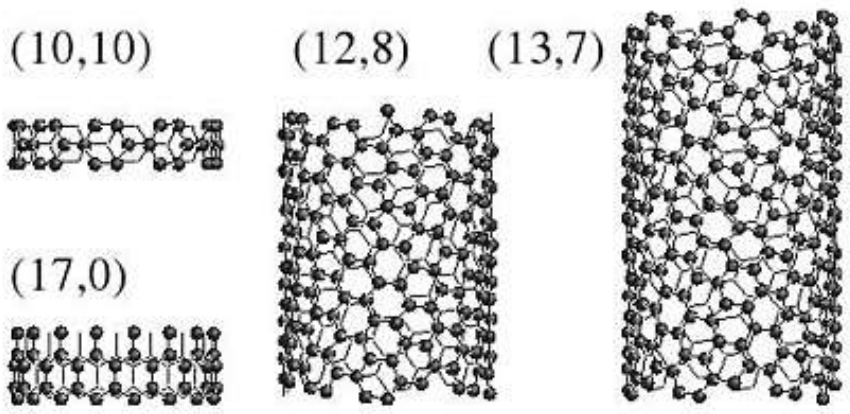

Figure 1.9 Unit cells for unalike CNTs (Reich, 2002)

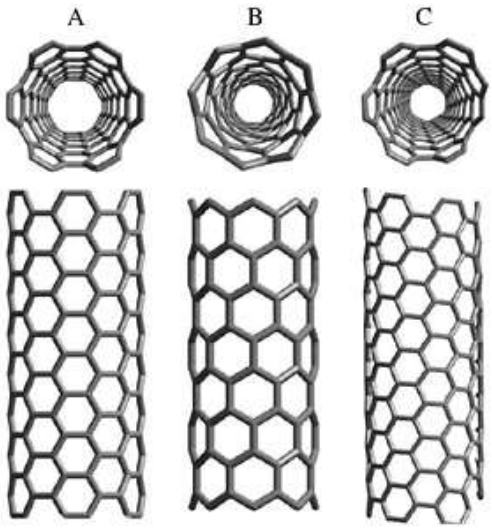

Figure 1.10 CNT species. (A) armchair, (B) zigzags and (C) chiral nanotubes (Terrones, 2003)

Table 1.1 Type of CNTs (Ajayan, 1997)

Type of CNTs	*Chiral angle*	(n,m)	*Structure*
Armchair	$\theta = 30°$	$n = m$	*trans-*
Zigzag	$\theta = 0°$	$m = 0$	*cis-*
Chiral	$0 < \theta < 30°$	$n \neq m$ ve $m \neq 0$	*trans- ve cis-*

1.2.2. Carbon Nanotubes Synthesis

1.2.2.1. Arc discharge procedures

In this procedure, two graphite electrodes are placed at a interval of concerning one millimeter. İllustrative electrode temperature is around 2737-3737 ^{0}C. An arc is manufactured through electrodes having a large DC current of 50-300 A (10-30 V) at a pressure of 50-760 Torr in an He atmosphere. After evacuation for concerning one hour, an accumulated carbon rod forms the cathode end. The bar

section be composed of three zones- a gray core, a black ring and an outer gray shell. The black ring is the incomplete carbon nanotubes shaped in a beam called “buckybundle”. The gray districts are amorphous carbon. This procedure is a dirty progress and is hard to progress because of the soot that can be carried effortlessly in the air. Effective refreshing is required to ensure a homogeneous assertion of CNTs. SWNTs can be manufactured by incorporating graphite electrodes with transition elements such as Fe, Co, or Cu (Guo et al., 1995).

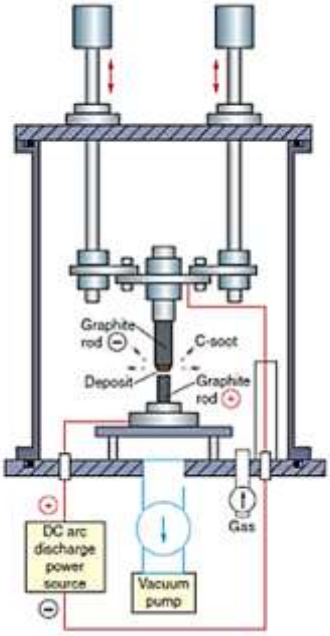

Figure 1.11 CNT formation equipment diagram by the arc-discharge method (Ando et al., 2004)

Figure 1.12 High-rise-resolution TEM of H_2-arc MWNTs (Ando et al., 2004)

1.2.2.2. Laser-furnace method

These findings were made in 1996 to make CNTs, particularly SWNTs (Thess et al., 1996). Figure 1.13 be seen the installation of a laser furnace comprising a quartz tube with window, a furnace, a water-cooled trap, a target carbon compounded doped with catalytic metals, and flow systems for buffer gas to retain constant pressures and flow ratios (Guo et al., 1992). A laser beam (illustratively a YAG or CO_2 laser) is initiated through the window and focuses on the target in the middle of the oven. The target is evaporated in high-rise temperature Ar buffer gas and forms SWNTs. Ar flow ratio and pressure are illustratively 1 cm s^{-1} and 500 torr, respectively. The manufactured SWNTs were transported into the trap where they were composed by buffer gas. The evaporation plane is hold as newly as feasible by altering the focal point or moving the target. The procedure has a variety of benefits such as high-rise grade SWNT manufacture, diameter control, research of growth dynamics and the manufacture of new substances. High-rise-grade SWNTs with least imperfections and pollutants such

as amorphous carbon and catalytic metals have been manufactured using the laser kiln technique with purification progresses (Bandow et al., 1997).

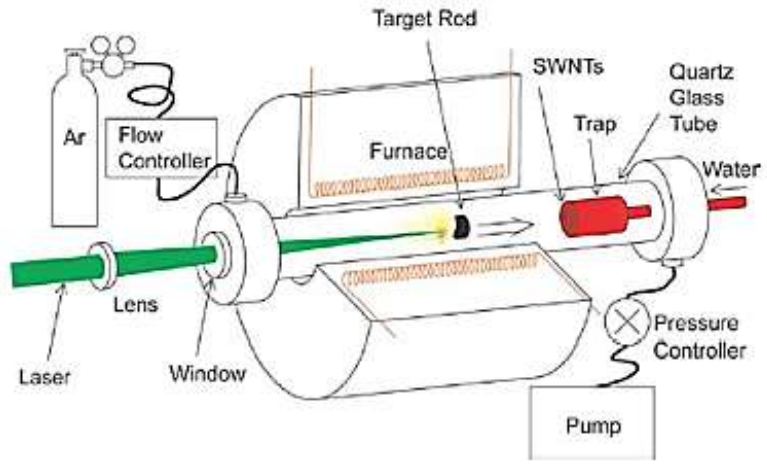

Figure 1.13 Schematic diagram of the laser-furnace equipment (Ando et al., 2004)

1.2.2.3. Chemical Vapor Deposition

Chemical Vapor Deposition (CVD) is one more satisfactorily received method for manufacturing CNTs in which a hydrocarbon vapor is thermally perished by means of a metal catalyst. This technique is also recognized as thermal or catalytic CVD to unalike it from many alternative types of CVD used for unalike motivation. Anologized to arc discharge and laser techniques, CVD is a easy and economical procedure for synthesizing CNTs at low temperature and surrounding pressure at the expense of crystallinity. In any case, the use of unalike hydrocarbons (solid, liquid or gas) is adaptable to allow the use of unalike substrates and allow CNT growth in unalike shapes such as powder, thin or thick films. or a mixed, flat or curled or required nanotube construction in predefined areas on an enhanced substrate. It supplies good control over growth parameters too.

CVD is the simplest form of CNT growth. The progress concern fleeting a hydrocarbon vapor (illustratively 15-60 minutes) through a pipe furnace in which a

catalyst substance for decomposition of the hydrocarbon is at a adequate high-rise temperature (600-1200 ° C). The CNTs grow on the catalyst and are composed upon refreshing the system to room temperature. In this situation liquid hydrocarbon (alcohol, benzene, etc.), the liquid is made warm in a bottle and an inert gas is washed through it to transport the vapor to the reaction furnace. Evaporation of a solid hydrocarbon (camphor, naphthalene, etc.) could be readily obtained prior to the principle, high-rise temperature reaction furnace shown at one more low temperature in one more furnace (Figure 1.14(a)).

The three principle parameters required for CNT growth in CVD are hydrocarbon, catalyst and growth temperature. According to previous practicle knowledge, the low temperature yields CNT (600-900 °C) MWCNT, while the high-riseer temperature (900-1200 °C) promotes SWCNT growth, demostrating that the SWCNTs have probably a high-riseer formation energy. Because of their small diameter consequence in high-rise curvature and high-rise strain energy (Baker et al., 1983). This may explain why MWCNTs are not difficult to grow from most hydrocarbons and can only be get bigger from selected hydrocarbons (eg CO, CH_4, etc. having a sensible firmness in the temperature mixture of 900-1200°C). Commonly effective precursors of MWCNTs (eg, acetylene, benzene, etc.) are unsafe at high-riseer temperatures and guide to the accumulation of large quantity of carbonaceous admixture alternative than CNTs (Ago et al., 2000).

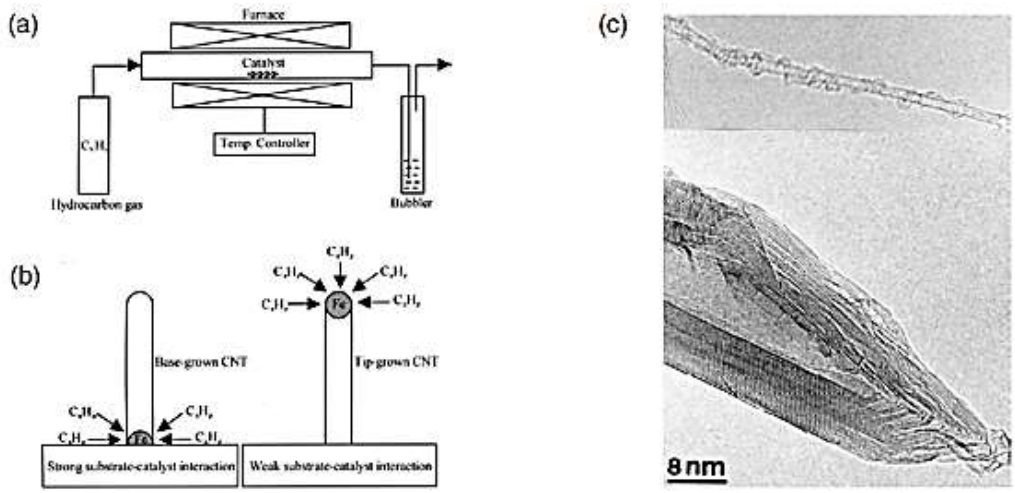

Figure 1.14 (a) CVD setup diagram (b) Probable models for CNT growth. (c) SWCNT and a MWCNT get bigger from camphor via CVD (Ando et al., 2004)

1.2.3. Applications of Carbon Nanotubes

The carbon-carbon bond in graphene is the powerfulest bond ever observed in nature (Terrones, 2003, Dresselhaus et al., 2004). As can effortlessly be understood, the mechanical structures of the nanotubes are much high-riseer than that of steel recognized for their durability in daily use. The high-rise surface areas and low resistances of CNTs have aroused appreciable notice in the field of electrochemistry (Robertson, 2004). CNTs can replace accustomed carbon black, which is used as metal support in fuel cells. (Serp et al., 2003). In addition, CNTs are the ideal electrode substance for supercapacitors with the high-risest conductivity per unit weight and high-rise surface areas. Anologized to amorphous carbon electrodes, CNTs exhibit benefits such as high-rise conductivity, structural strength, and the ability to prepare films without binders (Kaempgen et al., 2007). Furthermore, the nanotubes are satisfactorily suited for self-shrinkage and agglomeration ascribed to their high-rise surface area and span / diameter proportion, flexibility. Therefore, researchers want to distribute CNTs to their isolated states and prepare their suspensions and use them as 1B (fibrous structures), 2B (membranes) or 3B (bulk solids) (Hilding et al., 2003).

Today, CNTs are also used as electrode alter substances because CNTs offer very specific benefits such as grow better electronic structures, vast edge plane / basal plane proportion, and electron transfer reactions (Wang et al., 2008). For example, they alter the (GCE) with MWCNT (Dursun et al., 2018) and then growed the electrocatalytic commotion of the copper phthalocyanine / multi-walled carbon nanotube compounded electrode through Pt nanoparticle alteration for oxygen fraction. In the alternative study (Dursun et al., 2018), electrochemical resolution of serotonin was emphasized using a pre-treated Multi-Walled Carbon Nanotube-polyaniline compounded electrode. One more example of a alter electrode (Dursun

et al., 2010) described the prepaproportionn of alter poly pyrrole film electrodes of metal nanoparticles and explored their electrocatalytic commotion.

1.3. Conducting Polymers

Polymers compete with natural and inorganic substances in applications requiring good mechanical structures and low weight. Conventionally, polymers are considered insulators. However, in 1977, A. G. MacDiarmid, H. Shirakawa and A. J. Heeger were changed the conventional concept. The conductivity of polyacetylene- after doping with electron-withdrawing AsF5 - growed nine-fold and 103 S / cm row (Shirakawa et al., 1977). The individual property of conductive polymers is conjugated molecular structure of polymer principle chain where all electrons are delocalized polymer chain (Chiang et al., 1978). Shortly after this discovery, from the late 1970s to the early 1980s, a number of stable conductive polymers were detail, counting polyprol (PPy), polyaniline (PAn), and polythiophene (PTh) conductive polymers. For the significance of conjugated polymers, Heeger, Mac Diarmid and Shirakawa were assigned the Nobel Prize in Chemistry in 2000 for their appreciable contribution to the discovery and growth of conductive polymers.

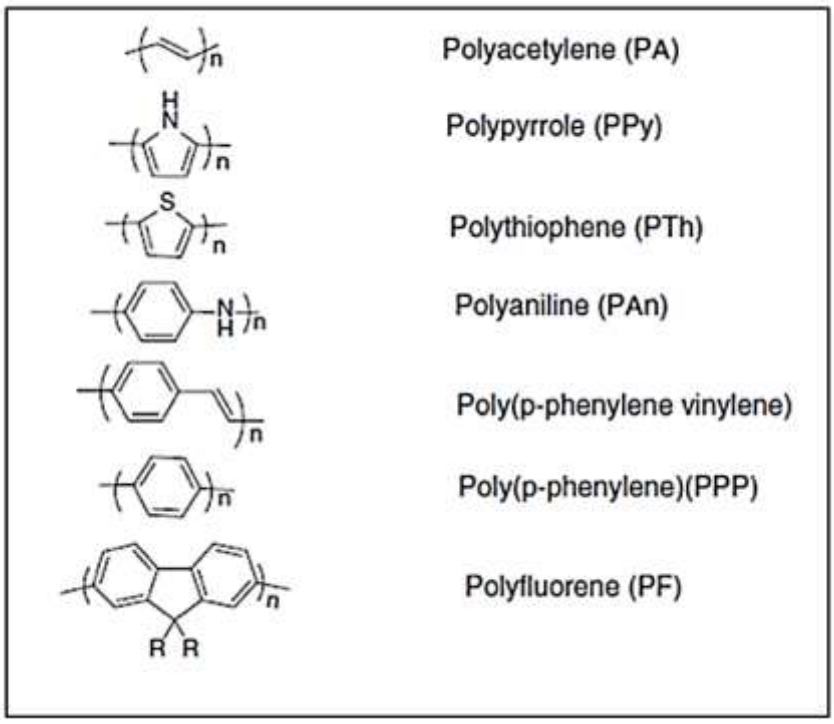

Figure 1.15 Principle chain structures of a variety of illustrative conjugated polymers (Shirakawa et al., 1977)

Table 1.2 Structures and applications of some illustrative conjugated polymers (Shirakawa et al., 1977)

Conjugated polymers	Stable structure	Preparation method	Solubility	Application fields
Polypyrrole (PPy)	p-Doped conducting state	PPy films can be obtained by electrochemical oxidation polymerization from aqueous or organic solution. PPy powder can be prepared by chemical oxidation polymerization	Insoluble	Modified electrode, enzyme electrodes (biosensors), electrochromics, conducting polymer films
Polyaniline (PAn)	p-Doped conducting state (proton-acid doping)	Electrochemical or chemical oxidation polymerization from strong acidic aqueous solution	Insoluble for the PAn doped with common anions, but it can become soluble by counteranions doping induced solubility	Modified electrodes, enzyme electrodes (biosensors), electrochromics, electrode materials for batteries and solid capacitors, anti-corrosion, microwave absorption, electrode buffer layer for optoelectronic devices
Polythiophene (PTh)	Intrinsic semiconducting state	Electrochemical oxidation polymerization from organic solution, or chemical oxidation polymerization in organic solvent	Insoluble	Electrochromics, conducting polymer films
PEDOT:PSS	p-Type doped conducting state	Electrochemical oxidation polymerization from organic solution, chemical oxidation or chemical synthesis in organic solvent	Aqueous solution	Transparent conducting polymer films, anode buffer layer materials in organic/polymer light-emitting diodes and organic/polymer solar cells, anti-static-electricity coating layer materials, electrode materials in solid state capacitors, etc.
Poly(3-hexylthiophene) (P3HT)	Intrinsic semiconducting state	Chemical synthesis in organic solvents	Soluble in THF, chlorobenzene, dichlorobenzene, etc.	Donor material in polymer solar cells, semiconductors in field effect transistors
MEH-PPV and MDMO-PPV	Intrinsic semiconducting state	Chemical synthesis in organic solvents	Soluble in organic solvents	Orange electroluminescent material for polymer light-emitting diodes

The principle benefits of conductive polymers are not only the electronic and optical structures of metals and inorganic semiconductors, but also the elastic mechanics and progressability of polymers. It also has exceptional electrochemical redox commotion with conductive polymers. Obviously, conductive polymers, counting doped conductive polymers and intrinsic semiconductor conjugated polymers, will play an significant role in the future growth of organic optoelectronic and electrochemical tools.

Replacing the electrode surface by coating it with a polymer sights to get larger the selectivity, accuracy and reproducibility of a voltammetric measurement. When the electrode is coated with an ionic polymer, substances exhibiting redox structures are concentrated on the film as a result of electrostatic interaction with the ionic districts in the polymer film (Rocheleau and Purdy, 1991). In this respect, there is a similarity on either side this procedure and stripping voltammetry. The condensation can also be carried out by placing a complexing envoy in the film for metal ions and complexing with the metal. When the electrode is coated with ion

exchange films, the concentration of the substance to be examined on the electrode surface is made according to the ion exchange principle. This layer also has ions similar to the electrode surface.

It also supplies selectivity by inhibiting diffusion. This selectivity may based on the charge as satisfactorily as the hydrophilic and hydrophobic basic nature of the molecules. It is also selective according to the size of the pores in the film layer. Polymer coated electrodes contain chemically and electrochemically active centers. The polymer coating on the electrode surface can also be carried out in the form of electropolymerization based on the monomer structure. The selectivity may be better with respect to the particle size than with the film layers thus shaped. The permeability of such films rest on the electrical charge fleeting through the electrode during anodic progressing (Wang, 1991).

In this study, nano polymeric cresol red film was synthesized by electropolymerization method. The data obtained showed that the poly-cresol red films were deposited on the surface of the GCE by electropolymerization. The electrochemical behavior of poly cresol red in GCE is in good agreement with the previous findings, referring to the electrochemical answers of a variety of organic polymerized admixture in the solid electrode.

1.4. Chemical structures of Melatonin

Melatonin, N-acetyl-5-methoxypriptamine, is actually a hormone synthesized in the pineal gland and its accumulation rest on cyrcadian rhythms. Melatonin is an significant neurohormonal chemical charged with for modulate sleep. Most melatonin is manufactured overnight (Reiter, 1986). Melatonin is also a significant signaling molecule in the gastrointestinal tract and is also described (Bubenic, 1999).

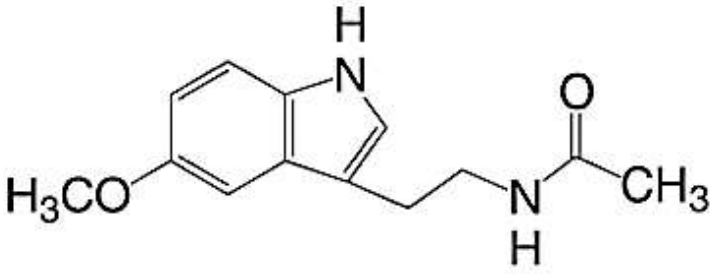

Figure 1.16 Chemical structure of melatonin

This hormone has appreciable impact on unalike physiological and behavioral progresses as neurological, psychiatric (Reiter, 1991) reproductive (Cardinali, 1981) and neuroprotective envoy in Alzheimer's and Parkinson's disease models (Mayo et al., 2005).

Melatonin is synthesized from plants and animals on either side tryptophan and melatonin. Serotonin is an significant halfway because the biosynthetic progress uses two potential pathways, each involve two successive enzymatic steps to make melatonin (Tan et al., 2015), (Back et al., 2016).

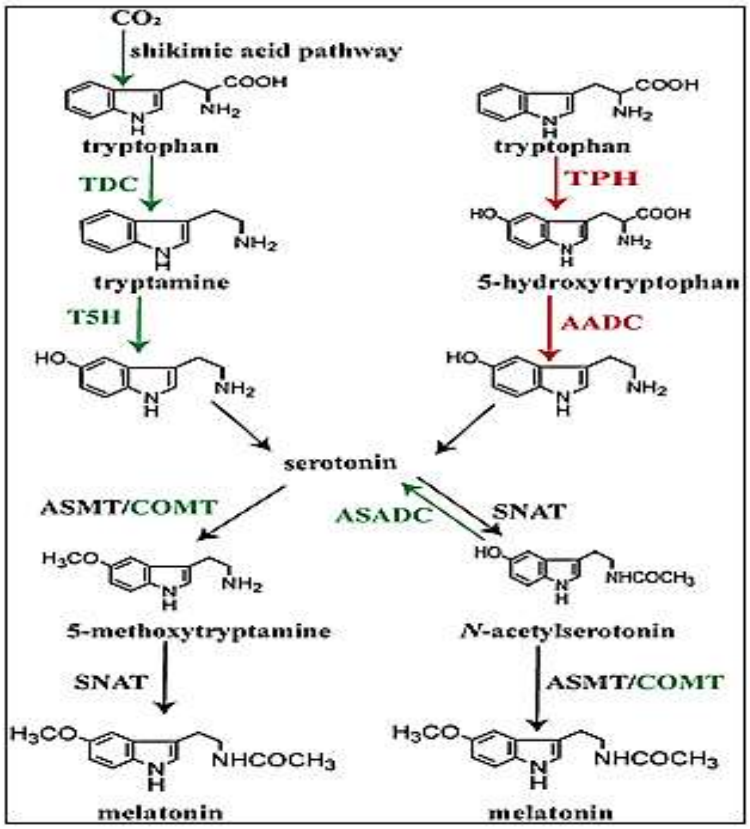

Figure 1.17 Melatonin synthesis pathways in unalike plant (left) and animal (right) taxa. (Melatonin synthesis pathways in unalike plant (left) and animal (right) taxa. (Depending on the organism, not all events need to be in chloroplasts or mitochondria of each species. The published data for the species, plants and animals examined supply powerful proof that these organelles are critically related to melatonin manufacture.)

Because of its significant role in a large number of pathological, physiological and biological progresses, melatonin has been extensively studied and has grow satisfactorily received in late years. To date, many methods have been used in the quantitative determination of melatonin, high performance liquid chromatography (HPLC) (Mills et al., 1986) voltammetry (Radi and Bekhiet, 1998) amperometric observation of in a flow injection analysis system (FIAED) (Corujo-Antuna et al., 2003) and radioimmunoassay (RIA) (Miles et al., 1985)

However, many of these detail procedures are costly, complex progresses and often require time-consuming specimen progressing prior to analysis. On the

alternative hand, electrochemical techniques are more acceptable and cheaper than accustomed analytical procedures. A voltammetric procedure has high selectivity and repeatability at fast answer and low cost (Agrawal et al., 2013).

In the electrochemical analysis of melatonin, a change of electrode types with unalike surface alterations, counting carbon paste electrodes, were used as a working electrode (Radi and Bekhiet, 1998). (PEDOT) hybrid film alter glassy carbon electrode (Tsai et al., 2011) glassy carbon electrode (Uslu et al., 2001).

The latest studies are as follows, nanopalladium modified granular polymer nanocompounded based sensor (Kumar et al., 2016), electrocatalytic properties with a nanostructured film electrode (Qu et al., 2005) , Fe_3O_4 nanoparticle decorated reduced graphene oxide modified electrode (Bagheri et al., 2015).

1.5. Chemical structures of caffeine

Caffeine, (3, 7-dihydro-1, 3, 7-trimethyl-1H-purine-2, 6-dione), is exist together with other trace purines, in coffee, tea and soft drinks. Caffeine has many significant physiological success, such as gastric acid secretion, diuresis, and stimulation of the central nervous system (Spataru et al., 2002), (Pizzariello et al., 1999).

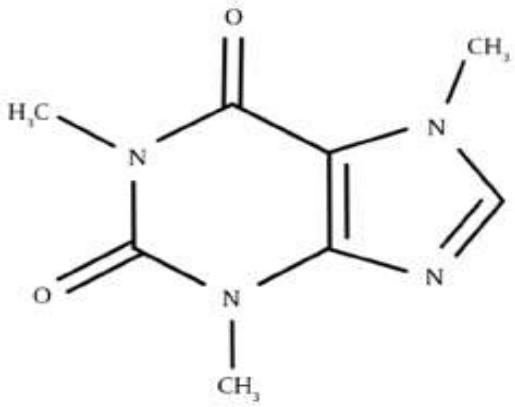

Figure 1.18 Chemical Structure of the Caffeine Molecule

Further, when over-consumed, it can cause negative mutation success (Pons and Muller, 1990) such as reserve of DNA repair and cyclic AMP

phosphodiesterase commotion (Blecher et al., 1997). It can also cause to cancer, heart disease and difficulty in pregnant women and aging (Kalmar and Cafarelli, 1999), (Srisuphan and Bracken, 1986). Various methods have been developed for determination of caffeine in in coffee, tea and cola beverages by high performance liquid chromatography (Sharma et al., 2005), (Fernandez et al., 2000) capillary chromatography (Wang et al., 2000) capillary electrophoresis, (Regan and Shakalisava, 2005), spectroscopy (Lopez-Martinez et al., 2003) and liquid chromatography tandem mass spectroscopy (Jones et al., 2011).

Anologized to these accustomed analytical methods, electroanalytical methods are fast, suitable, cost effective and habitatally friendly (Rawat et al., 2010). Polymer based electrodes (PMEs) have received sizeable awareness in late years ascribed to their good firmness, reproducibility, growed active sites, homogeneity in electrochemical assertion and powerful adhesion to the electrode surface (Horiuchi and Fujita, 2003), (Sun et al., 2008). Resolution of caffeine in unalike analytical methods such as MWCNT given alter GCE. For example, Nafion / MWCNT compounded film electrode, graphene based electrodes. (Sun et al., 2011).

1.6. Voltammetry and Voltammetric Procedures

Voltammetry is an analytical procedure with a potential screening based on measuring current flowing from an electrode submerged in a solution involve electroactive admixture. This electrode is called the working electrode and can be made with a change of substances. Generally, it has very few surfaces to fast and correctly accept the potential of the electric circuit. The electrode may be solid (gold, platinum or glassy carbon) or may be shaped by a drop of mercury frontal from the end of the capillary portion. If the electrode is shaped with a drop of mercury rhythmically falling from the capillary vessel, the analytical procedure is called Polarography.

Voltammetry is a adaptable research procedure that allows to look in to unalike features of electrochemical reactions, ie, reactions involving the exchange of electrons on either side reenvoys and manufactured. For these reactions, it is feasible to look in to the laws modulate the reliance on of current and potential on an electrode immersed in the reaction medium. In general, these laws are very complex, just like redox reactions and their habitat.

The use of voltammetric procedures is fundamental to understanding the laws of unalike electrochemical phenomena and is of appreciable significance in unalike technological fields such as: examination of corrosion-resistant substances (corrosion is the result of a series of electrochemical reactions), investigation of new electrodic progresses for the chemical industries (in fact millions of tons of aluminum, chlorine, soda are manufactured by electrochemical reactions), manufacture of new types of batteries that can supply large quantity of energy.

One of the well-known applications of voltammetry is quantitative analysis of metals (or whatever, these reducible or oxidizable chemicals) at levels of μg/L or less. This introduction discusses the qualitative features of voltammetric analysis of detect of heavy metals and organic matter in solution (Kissinger and Heineman, 1983).

1.6.1. Cyclic Voltammetry

Cyclic voltammetry (CV) has turn out to be a extremely ordinary procedure for the opening electrochemical learning of newborn systems and has bear out to be extremely practical in acquiring understanding regarding complex electrode reactions. The CV assay is the first in an electroanalytical study because it gives details regarding the position of the redox potentials of electroactive types and the effect of the media on the redox affair.

Cyclic voltammetry comprise of a linear scould of a potential of a fixed potential electrode, which is placed in an unstable elucidation using a triangular

potential waveform. In potential screening, the current effect from the petition potential is measured and the effect current-potential graph is called a cyclic voltammogram.

Important details regarding chemical reactions or soaking up affaires could be acquired by this procedure combined with the thermodynamics of redox affaires and the kinetics of heterogeneous electron convey reactions. The formation and enlargement of the diffusion covering near the electrode surface could be comprehend by mindfully examining the form of the curve during potential scouldning. The first potential for this is pick out for a redox reaction Ox^{+} $ne^{-}\rightarrow$ Red, where no reduction happens and the potential petition to the working electrode increases negatively. The current happens after a certain reduction potential, which leads to a reduction in the surface congregation (Co) of Ox. At high enough potentials and in the speedy electrode kinetics stage Co goes to zero, giving the maximum current value. A further increase in potential due to the enlargement of the diffusion covering causes a decrease in the current.

In an inert elucidation of an electroactive types in a pick out hold up (inert) electrolyte, electrochemical measurements are performed in conventional CV experiments. The promoter electrolyte typically has a congregation of 0.10 M due to oxygen depletion and possible subordinate reactions with dissolved oxygen, while the congregation of electroactive types is typically in the middle of 10 mM and 1 mM. The elucidation is purged with nitrogen or argon for 5-15 minutes.

The CV procedure comprise of applying a linearly increasing (or decreasing) potential as a function of time with respect to:

$$E = E_i + vt$$

Where E_i is the first potential and v is the scanning rate indicated as $mV.s^{-1}$ or $V.s^{-1}$).

In general, the opening potential value E_i is pick out such that the chemical types investigated are inceptively oxidized or not oxidized or lessen.

$$I_p = 2.99 \times 10^5 n(\alpha n_a)^{1/2} A D^{1/2} v^{1/2} C$$

The potential is then brush to either positive or negative scanning E_{max} or E_{min} voltage, respectively. E_f Potential limits, E_{max} and E_{min}, are pick out to include scould direction, potential range oxidation or reduction affaires scanned to the indigenous or a unalike potential value. The current and petition potential curve are recorded in a separate loop or multiple cycles (Figure 1.20)

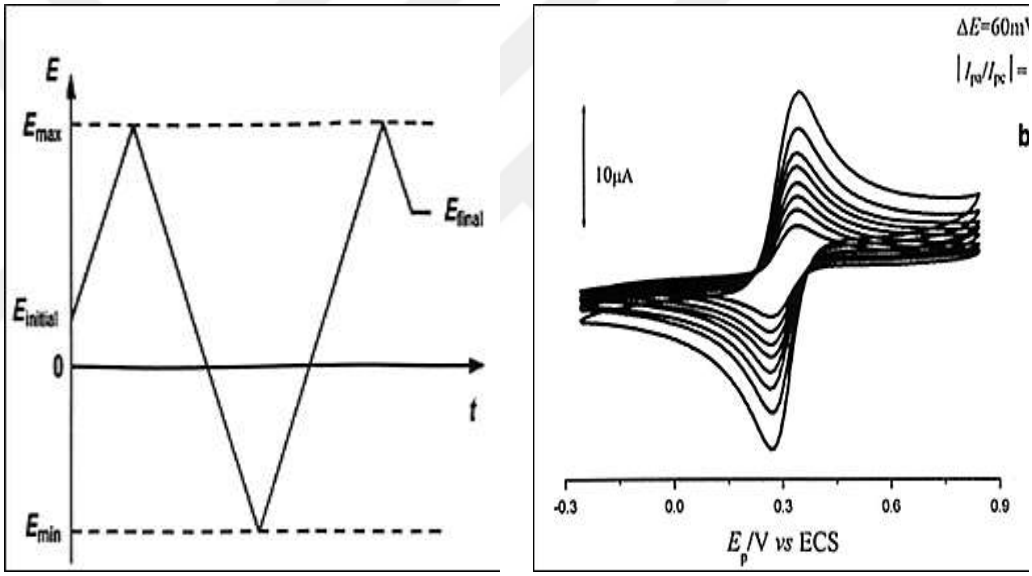

Figure 1.19 (a) Potential waveform of (CV) (b) I-V characteristic of (CV)

At the irreparable boundary, as with most pharmaceutical compounds, no adverse reaction is observed. Electrochemical systems are characterized in that the following peak potential is irreversibly shifted by the scanning speed:

$$E_p = E^{0'} - \frac{RT}{\alpha nF}\left[0.78 - \ln\frac{k^0}{D^{1/2}} + \ln\left(\frac{\alpha nFv}{RT}\right)^{1/2}\right]$$

Here α is the convey coefficient, n is the electron numbers connected in the impose convey pace, and k^o is the quality ratio sustained of the electron convey reaction. For a system with irreparable peak current:

Here n_a is electrons number in the rate-determining pace of the electrode affair. In this irreparable situation , CV is identical.

Generally analytical work, the basic rewards of CV is:

- Specificity attributable to a large acquireable time scale and a superior intention of peak-formed curves.

- Swiftly recuperated current-potential curves

- Enough sensitivity

1.6.2. Pulse Voltammetry

The foundation of all pulse procedures be composed of the ratio of impose deterioration and the variance of faradaic currents after a potential pace (or "pulse"). As the impose current exponentially decreases, the faradaic current (for diffusion-controlled current) 1/(time) function deteriorates as a function; that is, the ratio of deterioration of the expect current is much speedy than the faradaic current.

Consider of a lowering case if the beginning potential is satisfactorily positive than the redox potential, the demand of small amplitude pulses doesn’t creator any faradaic reactions, so no available answer is present. When the pulse amplitude is big enough to the pulse potential is nearly equal to the redox potential, a faradic reaction happens in reply to the potential pulse (assuming moderately speedy electron convey kinetics), and the magnitude of this current based on both the velocities and the diffusion electron convey ratio. When pulsed potentials are adequate negative to the redox potential at which the electron convey reaction

happens quickly, the faradaic current at most rest on the diffusion ratio which means that, a threshold current is acquired.

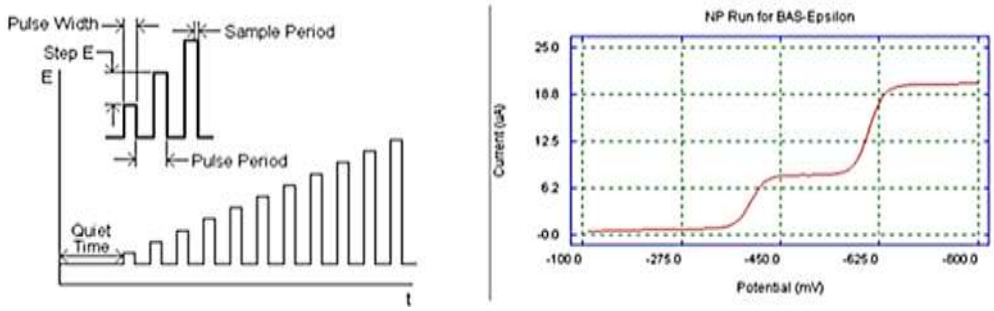

Figure 1.20 (a)Normal pulse voltammetry, (b) Schematic I-E profile.

Both procedures Normal pulse voltammetry (NPV) and unalike pulse voltammetry (DPV) procedures are alike procedures. There are two important variances that distinguish these procedures. The base potential increases in the middle of pulses and these increases are equal. The current is measured immediately before and end of the pulse and the variance in the middle of the two currents is recorded.

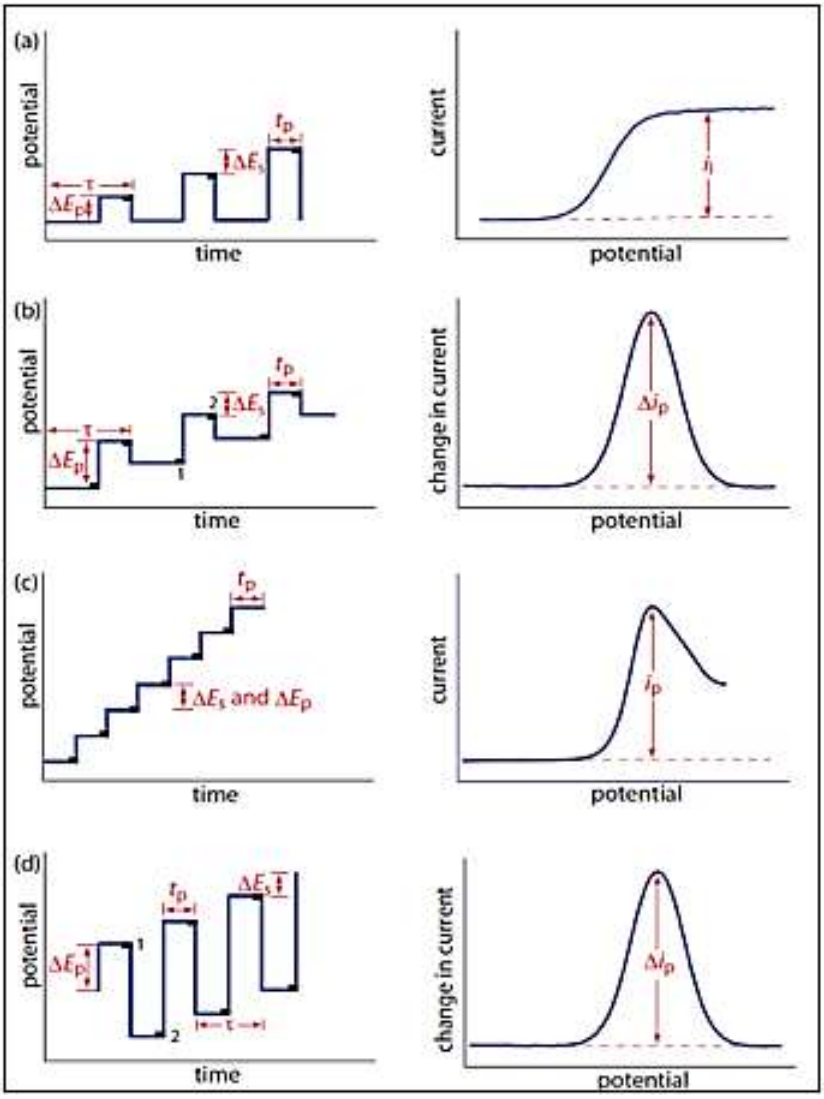

Figure 1.21 voltammetric procedures, (a) NPV, (b) DPV, (c) Staircase pulse voltammetry (d) Square-Wave pulse voltammetry and I-E profiles

The potential time waveform placed on a potential ramp is shown in Figure 1.22. It is easier to use for the computing system that controls the ladder waveform. Since DPV is a unalike procedure, it is alike to the first derivative of a conventional voltammogram. The highest potential E_p could be roughly represented by $E_{1/2}$. With the increasing irreversibility Ep, the distance to $E_{1/2}$ increases with increasing peak width and decreasing altitude. Because the time scale of normal pulse voltammetry is the same, the degree of reversibility of an electrode reaction is clearly alike to that observed (Brett et al., 1993).

1.7. Surface Characterization Procedures

Surface characterization procedures have an important role in the analysis of modified surfaces (eg. modified electrodes), in elucidating the constructional properties of advanced substance, in determining and improving the relationship in the middle of the properties and performance of the substance.

It is ordinary for many to need to investigate an unnoted specimen with a variety of analytical procedures to acquire a practical result. In this study, (SEM), (XPS) and (TEM) learning were investigated to understand the electrochemical experiments.

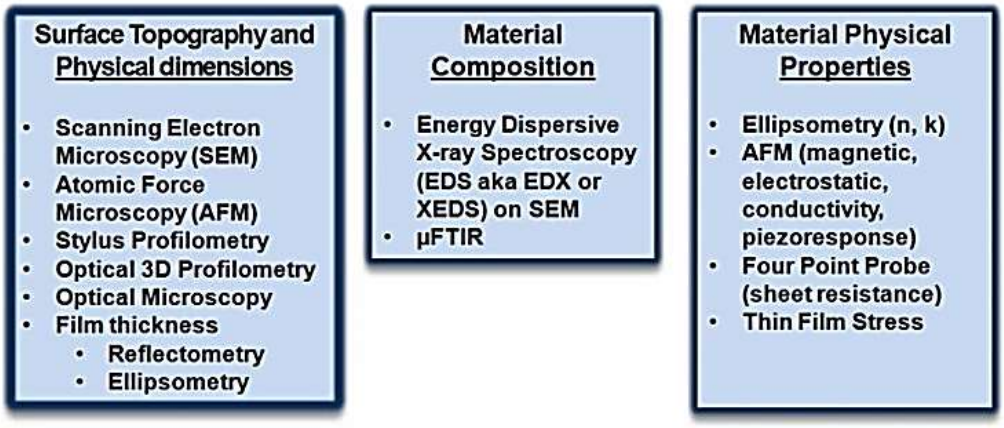

Figure 1.22 The metrology of the characterization micro-nano-structures and substance broad range of technologies and unalike procedures

1.7.1. Scanning electron microscope (SEM)

A strong enlargement instrument that uses centred electron purlins to acquire details is the Scanning Electron Microscope (SEM). The three-dimensional high-elucidation morphological and topographic images construct by SEM give details and enable them to retrieve priceless data in a variety of science and industry applications (Brabazon and Raffer, 2010).

The brief operating concept of the SEM device is depend on the concept that the principal electrons emitted from the specimen give energy to the atomic electrons of the specimen, which could then be released as subordinate electrons (SE) and could be generated by gathering these subordinate electrons from every one point. For example, SEM is required to work under vacuum to prevent the interaction of electrons with gas molecules and to achieve high solubility. Here, principal electrons construct and propagated from the electron gun by warming or high energy in the range of 1−40 keV are accelerated (Goldstein et al., 1992).

The electrons emitted by magnetic field lenses and metal housings in a vacuum column are cramped to a monochrome purlin (diameter of 100 nm or less). The limited principal electrons are scanned along the specimen surface by scanning the coils in a quick design. The scattering and interaction volume of the electrons depends on the number of atoms, the atomic congregation of the examined specimen and the incoming electron energy (accelerating voltage).

In Figure 1.23 the electron purlin interaction with the specimen and the signal emitted from the specimen could be seen. Larger escape depths generally turn into a larger sidewise dimension and therefore potential reelucidations that the signal could produce, but the actual size and form of the interaction volume depends on the accelerating voltage, the number of atoms, and the slope (Zhou et al., 2006).

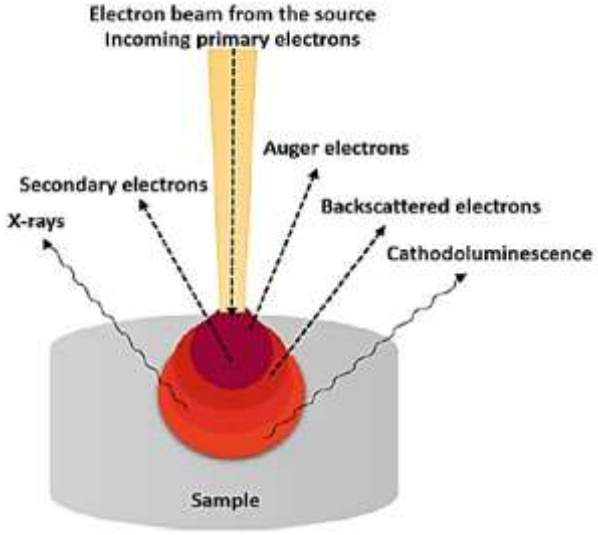

Figure 1.23 Electron beam interaction with sample

The following parameters could measure and analyse by using SEM: (Alyamani and Lemine, 2012)

- Extent of films and thin coverings.

- Morphology and aspect of surface.

- Size and size handing.

- Form and dispersion of tiny piece, fibres, nanosubstance or any other ingredient in componds and mix.

- Altitude and sidewise dimensions of nanometre-sized substance.

- Chamber size and size handing in foam substance.

- Chemical constitution and basic analysis of nano- and micro-substance.

- Breaking and constructional flaws analysis.

1.7.2. X-Ray photoelectron spectroscopy (XPS)

X-ray photoelectron spectroscopy (XPS), also noted as basic spectroscopy (ESCA) for chemical analysis, is a extremely important procedure used to identify chemical types on the surface of the material. Although the advantages of these procedures are due to their internal surface sensitivity, they could also be used to determine the constitution of deeper coverings.

Figure 1.25 shows a specimen manipulation with unalike linear and revolving degrees of freedom, electron optics, an energy distributor analyzer and a detector. In addition, XP spectra are shown by element-specific handing of core-level photoemission for four unalike metals.

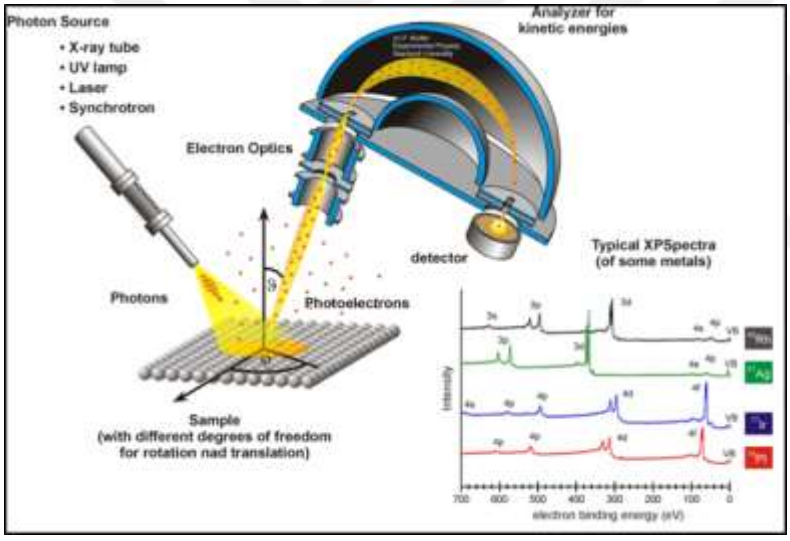

Figure 1.24 Typical XPS set-up with photon source

The energy required to remove the electron from any specimen could be defined as the ionization energy or the binding energy of the electron. It could be indicated as the energy *(hv)* of the radiation used to break the electron. Thus, by computing the kinetic energy of the photoelectron ($KE_{electron}$), we could calculate the bonding energy of the electron in the specimen:

$$\mathrm{BE} = h\nu - \mathrm{KE}_{\mathrm{electron}}$$

The removal of electrons could be achieved by bombarding a specimen material with XPS mono-energetic soft x-rays. From the kinetic energies of these projected photoelectrons, the components found in the example could be directly identified. The chemical state of an atom is sensitive to its electron-binding energies. Although XPS is designed for solids, specimens may be gas, liquid or solid. XPS could be used for the analysis of metals, ceramics, semiconductors and organic, biological and polymeric substance (Miyoshi, 1996).

The interaction in the middle of the atoms of the material AND the incident purlin causes an electron emission at the core level. XPS determines the kinetic energy of electrons. This electron kinetic energy details contains details regarding the nature of the atom and its environment (Ratner et al., 1996).

One of the advantages of using XPS is the characterization of biosubstance. The possibility of analyzing specimens without a specific specimen preparation is an important advantage here. Disadvantages include the need for vacuum, the possibility of specimen damage and the availability of equipment.

1.7.3. Electrochemical impedance spectroscopy (EIS)

Electrochemical impedance spectroscopy is widely operated for improve the understanding of multi-step reactions such as charge transfer, diffusion impedance, solution resistance, double-layer capacitance. EIS have been also used to identfy of corrosion, electron kinetics of membranes, conduction polymers, semiconductors, batteries and fuel cells, interfaces, etc. For impedance measurements, a periodic small amplitude sinusoidal AC signal is applied, and the current response is determined. These measurements are performed different ac frequencies (Suni, 2008), (Uygun and Uygun, 2014).

1.7.3.1. Electrical circuit components

The EIS data could be examined by attaching to an identical electrical circuit model. In this model, circuit components are generally ordinary electrical components such as resistance, capacitor and inductor. To ensure efficiency, the circuit components in the model must have a basis in the physical electrochemistry of the system. For example, most models contain a parameter that models the elucidation resistance of the chamber.

Component	Current Vs.Voltage	Impedance
resistor	E= IR	Z = R
inductor	E = L di/dt	Z = jωL
capacitor	I = C dE/dt	Z = 1/jωC

Figure 1.25 Electrical Circuit Components

1.7.3.2. Physical electrochemistry and identical circuit components

An important element in the impedance of the electrochemical chamber is elucidation resistance. The elucidation resistance in the middle of the meter and the mention of electrodes make amends for a modern 3-electrode potentiostat. However, any elucidation resistance in the middle of the mention of electrode and the working electrode should be think about when modeling your chamber**.**

The components used in identical circuits are stated in the following Figure 1.27 Priority and impedance equations are stated for every one element.

Equivalent Element	Admittance	Impedance
R	$1/R$	R
C	$j\omega C$	$1/j\omega C$
L	$1/j\omega L$	$j\omega L$
W (infinite Warburg)	$Y_0\sqrt{(j\omega)}$	$1/Y_0\sqrt{(j\omega)}$
O (finite Warburg)	$Y_0\sqrt{(j\omega)}Coth(B\sqrt{(j\omega)})$	$Tanh(B\sqrt{(j\omega)})/Y_0\sqrt{(j\omega)}$
Q (CPE)	$Y_0(j\omega)^{\alpha}$	$1/Y_0(j\omega)^{\alpha}$

Figure 1.26 Circuit Components Used in the Models

EIS is generally preferred for determining the accuracy of electrode affairing by computing electrode impedance in the presence of a faradic reaction. Transformations at the electrode-elucidation interface happen during electrochemical measurement and these transformations could be visualized using modules of electronic identical circuits. In an electrochemical experiment, the combination of components such as impedance, elucidation resistance (Rs), double covering impose on electrode surface (Cdl), impose convey resistance (Rct), and Warburg Element (Zw) as depicted is noted as the Randles circuit; (MacDonald, 1987).

Applying the Ohm's law impedance could be acquireed and this impedance comprise of two parts, a real Z′ and an imaginary Z″:

$$Z(\omega) = R_s + R_p/(1+\omega^2 R_p^2 C_d^2) - j\omega R_p^2 C_d/(1+\omega^2 R_p^2 C_d^2) = Z' + jZ''$$

where $j = \sqrt{-1}$.

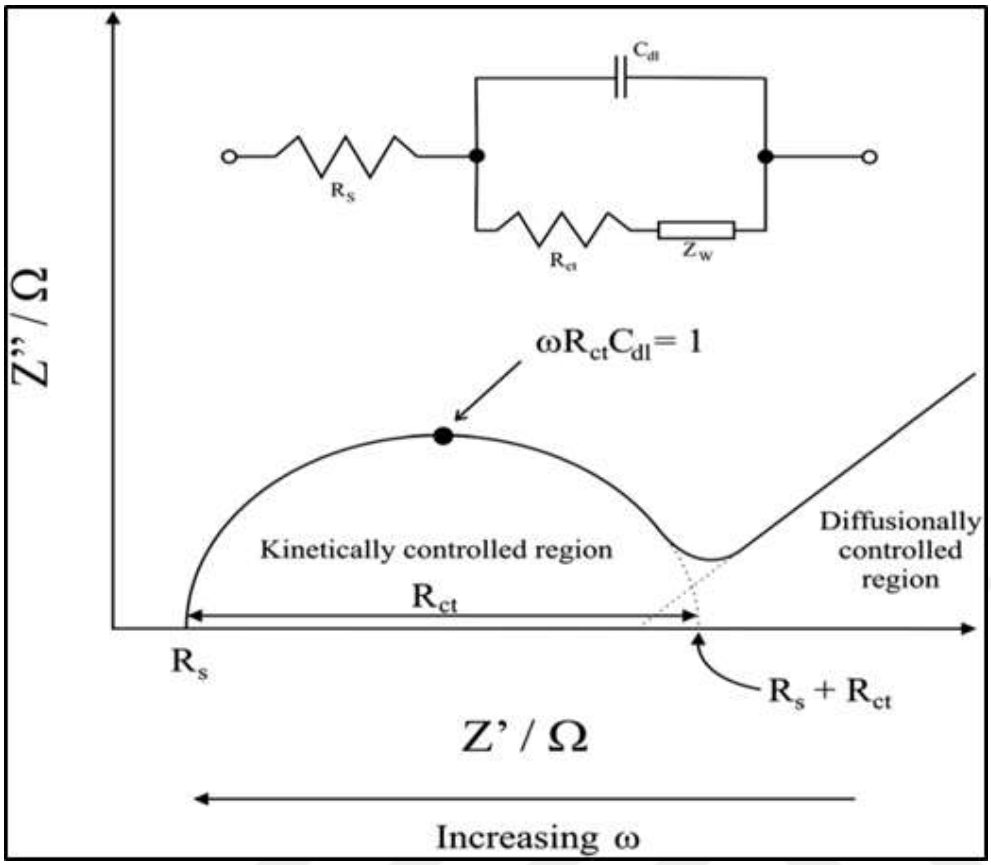

Figure 1.27 A Randles circuit for an identical electrochemical chamber

2. EXPERIMENTAL

2.1. Instrumentation

Voltammetric measurements were carried out using Autolab 101 Potentiostat Electrochemical Analyser equipped with three electrodes system consisted of a working electrode (GCE, MWCNT/GCE, PCR/GCE, MWCNT/PCR/GCE, ZnO/MWCNT/GCE, ZnO/MWCNT/PCR/GCE), auxilary a platinum electrode and an Ag/AgCl (sat.KCl) used as reference electrode. Cyclic and differential pulse (dp) mode and chronoamperometry were used through the electroanalytical studies. The pH measurements were carried out with Mettler Toledo handheld Seven Compact ion analyzer pH-meter. Electrochemical impedance measurements were realized by Autolab 302N. The SEM/EDX measurements were performed using the Thermo Scientific Apreo S for the characterization of modified electrode surfaces. X-ray photoelectron spectroscopy (XPS) spectra of the modified electrodes were collected via Thermo Scientific Spectrometer with K-Alpha Surface Analysis. Bandelin Sonorex model ultrasonic bath was used for preparation of solutions and cleaning the electrodes**.**

2.2. Reagents and Solutions

All reagents were of analytical reagent grade. Melatonin ($C_{13}H_{16}N_2O_2$), caffeine ($C_8H_{10}N_4O_2$), cresol red ($C_{21}H_{18}O_5S$), zinc sulfate heptahydrate ($ZnSO_4.7H_2O$) ethanol (C_2H_5OH), sulfuric acid (H_2SO_4), multiwalled carbonanotube (MWCNT), sodium dihydrogen phosphate (NaH_2PO_4), disodium monohydrogen phosphate (Na_2HPO_4), acetic acid (CH_3COOH), sodium acetate (CH_3COONa), potassium hexacyanoferrate(II) ($K_4Fe(CN)_6$), sodium hydroxide (NaOH), alimuna (Al_2O_3), N,N-dimethylformamide (DMF) were supplied from Merck, Sigma and Aldrich.

Buffer solutions were prepared from differnet compounds. These were acetic acid/sodium acetate, sodium dihydrogen phosphate/sodium hydrogen phosphate

species. The pH of the buffer solutions were changed between 3.76 - 8.00, respectively. Ionic strength was aimed and kept approximately constant for each buffer solutions as 0.1 M. All buffer solution was prepared from analytical grade reagents and in ultrapure water [Millipore Milli Q system (18.2 MΩ)].

Stock standart solutions of melatonin ($1.0x10^{-2}$ M) were freshly prepared in ethanol and caffeine were also prepared in ultrapure distillated water. The metal ion solution ($1.0x10^{-3}$ M $ZnSO_4.7H_2O$ in H_2SO_4 (0.1 M) were prepared by dissolution of metal salt in acidic solution. All experiments were studied at atmospheric temperature and high purity nitrogen kept flowing over the solution during the experimental studies.

2.3. Methods

2.3.1. Pre-conditioning of GCE

The bare GCE surface was polished carefully using with various grade of Al_2O_3 slurry (0.05-3 micron) mixture with the help of synthetic cloth. Subsequently, rinsed thoroughly with pure water and ultrasonicated for 3 minutes in ethanol and ultra pure water (1:1 v/v) mixture. GCE was also electrochemically cleaned by keeping 10 minutes at constant potential at 1.0 V in 0.1M HCl.

2.3.2. Preparation of Polycresol Red Film Modified Electrode

Electrochemical polymerization of cresol red was carried out in 0.1 M pH: 7.00 PBS solution containing ($5.0x10^{-4}$ M) cresol red by cycling the potential from -1.1 to 2.0 V vs. Ag/AgCl (sat.KCl) at a scan rate of 100 mV/s for 5 cycles. The obtained electrode was ready for use after the final wash with ultra pure water and denoted as PCR/GCE.

2.3.3. Pre-treatment of Multiwalled Carbon Nanotubes

0.04 grams of weighed CNT is treated with 8 mL of concentrated nitric acid and then boiled together until the acid is evaporated. After that washed several times with ultra pure water and keep to dry at 60 °C in oven. The 15 mg acid-treated MWCNT are dispersed in ultrasonic bath for 30 min in 2 mL DMF untill homogeneous suspension would be achieved.

2.3.4. Preparation of MWCNT Modified GCE

A 10 μL this suspension was put on the surface of bare polished GCE or PCR/GCE. It was seen that the suspension covered total surface area of the GCE. The DMF of the suspension on the GCE surface was then evaporated by keeping the electrode in furnace at 60°C for 45 minutes.

2.3.5. Preparation of Zn metal nanoparticles modified MWCNT/PCR/GCE

Zn/ZnO MNPs were formed on MWCNT/PCR/GCE surface by chronoamperometric technique. The electrodeposition of Zn/ZnO on the MWCNT/PCR/GCE from 0.1 M H_2SO_4 solution containing 1.0 mM $ZnSO_4$ by applying a constant potential electrolysis at –0.9 V for 60 s. After electrodeposition of Zn/ZnO particles on the electrode surface, denoted as ZnO/MWCNT/PCR/GCE, the composite electrode was washed with ultrapure water.

3. RESULTS AND DISCUSSION

In this thesis, in order to design and develop a modified electrode based on the simultaneous determination of melatonin and caffeine, in the first step polymerization of the GCE surface with cresol red was achieved. A preconditioned multi-walled carbon nano-tube was dropped onto the formed polymer film surface. To the e final surface layer, zinc oxide nanoparticles was deposited by chronoamperometric method. Thus, the optimization conditions for the modified electrode will be examined in this section.

3.1. Preparation of Polycresol red Modified Electrode

The PCR/GCE was prepared by electropolymerization of cresol red on GCE with CV by scaning the potentail-current between -1.1 mV/s and 2.0 mV/s in pH: 7.00 PBS solution containing ($5.0x10^{-4}$ M) cresol red at a scan rate of 100 mV/s for 5 cycles. Figure 3.1 shows the oxidation reactions of PCR.

The polymerization of CR on GCE surface by CV was carried out at pH 7.00 phosphate buffer. As following in Figure 3.2 two irreversible oxidation peaks were observed at –0.3 V and 1.0 V while a well defined reduction peak was observed about – 1.0 V during the first potential-current scan. The increasing of peak current depending on cycles number shows that the increasing the content of polymer on the electrode surface.

The mechanism of cresol red electropolymerization can be clarified as: the ortho-methyl phenol ring of cresol red is first oxidized to form 2-methylcyclodienone. A Michael addition reaction between the main molecule and the oxidized cresol red form produces a dimer (Jayakumar et al., 2017).

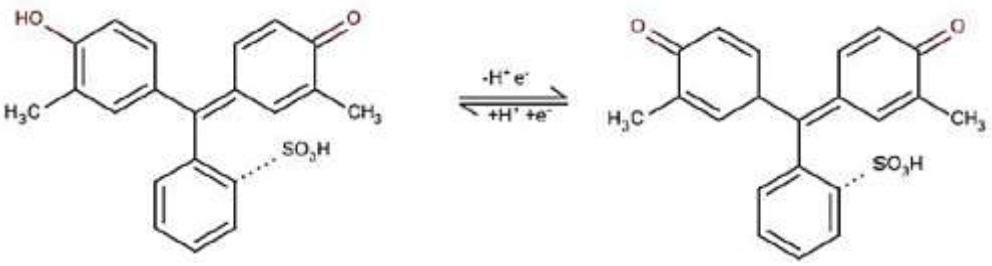

Figure 3.1 Oxidation reaction of Poly CR over the surface of GCE (Jayakumar et al., 2017)

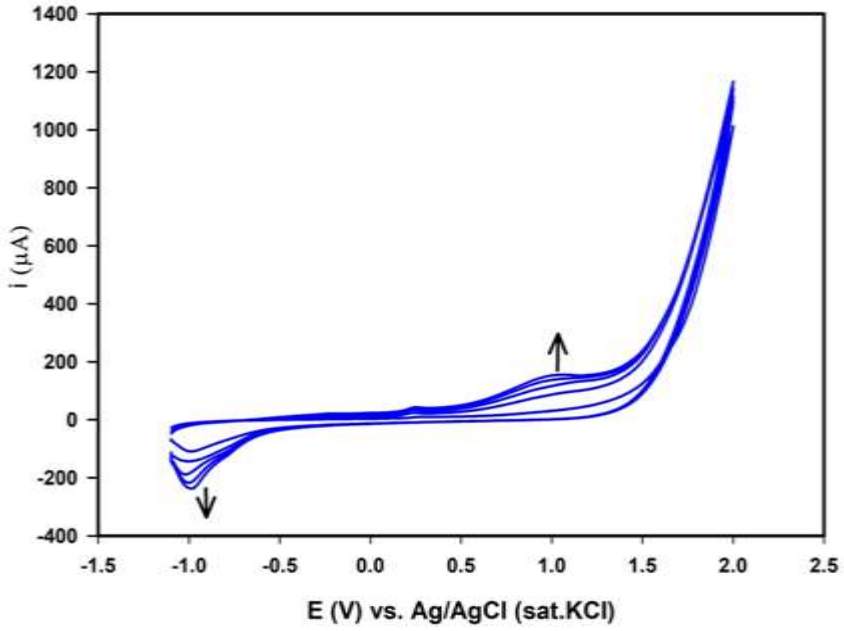

Figure 3.2 CVs of PCR electropolymerization in 0.1 M pH: 7.00 PBS solution containing ($5.0x10^{-4}$ M) cresol red at a scan rate 100 mV/s for 5 cycles

3.2. Preparation of MWCNT Modified PCR/GCE

After polycresol red film was formed by electro-polymerization on the electrode surface, 10 microliters of pre-conditioned multi-walled carbon nanotubes were dropped onto the PCR/GC electrode surface. The electrode was held for about half an hour in an oven set at 60°C to evaporate the DMF solution in which the multi-walled carbon nanotube was suspended.

3.3. Preparation of Various Metal Nanoparticles Modified MWCNT/PCR/GCE

Metal/metal oxide particles have been widely used as an modifier for electrochemical reactions due to their unique properties, which exactly dissimilar from their bulk forms such as improve the electron transfer rate and catalyse the reactions. In this thesis, metal/metal oxides were prepared as a component of composite electrode material that serves to obtain the more catalytic electrode surfaces to individiual and simultaneous determination of melatonin and caffeine.

Figure 3.3 A, B and C displays repetitive cyclic voltammograms of copper, gold, and Co particles electrochemical deposition from their metal ion solutions on MWCNT/PCR/GCE surfaces in acidic mediums. On the other hand Figure 3.3 D and E shows chronoamperometric deposition of Zn/ZnO and Ni/NiO from their metal ion solutions.

Cu metal particles deposited on composite electrodes by CV scanning between 0.2 to -1.1 V in 0.1 M H_2SO_4 + $1.0x10^{-3}$ M $CuSO_4$ solution and the CV showed that, Cu metal particles obtained by Cu(II) ions reduction at -0.80 V and reoxidation at -0.6 V (Figure 3.3 A). To prepare a fixed metal nano particles deposited modified electrode surface, E-i scanning was repeated for 10 cycles.

Figure 3.3 B demostrate well-defined peak observed at -0.35 V for reduction of Au(III) ions in the first current-potential scan. As current-potential scans were continued, the reduction peak potentail was shifted to positive potentials while the peak located at -0.25 V and the second reduction peak appeared at 0.0 V. In addition, an anodic peak was obseved at - 0.1V by oxidation of deposited Au metal.

Co particles were electrochemically deposited on MWCNT / PCR / GCE by current potential scan ranges between (-1.0 V - 1.0 V). The peak at -0.5 V corresponds to the Co(II) ions reduction to Co metal particles on the surface while the re-oxidation peak was recorded at -0.45 V in Figure 3.3D.

Zn/ZnO or Ni/NiO particles were formed on MWCNT/PCR/GCE surface by chronoamperometric technique (Fig.3.3 D and E). The electrodeposition of Zn/ZnO on the MWCNT/PCR/GCE from 0.1 M H_2SO_4 solution containing 1.0 mM $ZnSO_4$ was applied a constant potential electrolysis at –0.9 V for 60 s. The electrodeposition of Ni/NiO on the MWCNT/PCR/GCE from 0.1 M H_2SO_4 solution containing 1.0 mM $NiSO_4$ was applied a constant potential electrolysis at –1.3 V for 120 s.

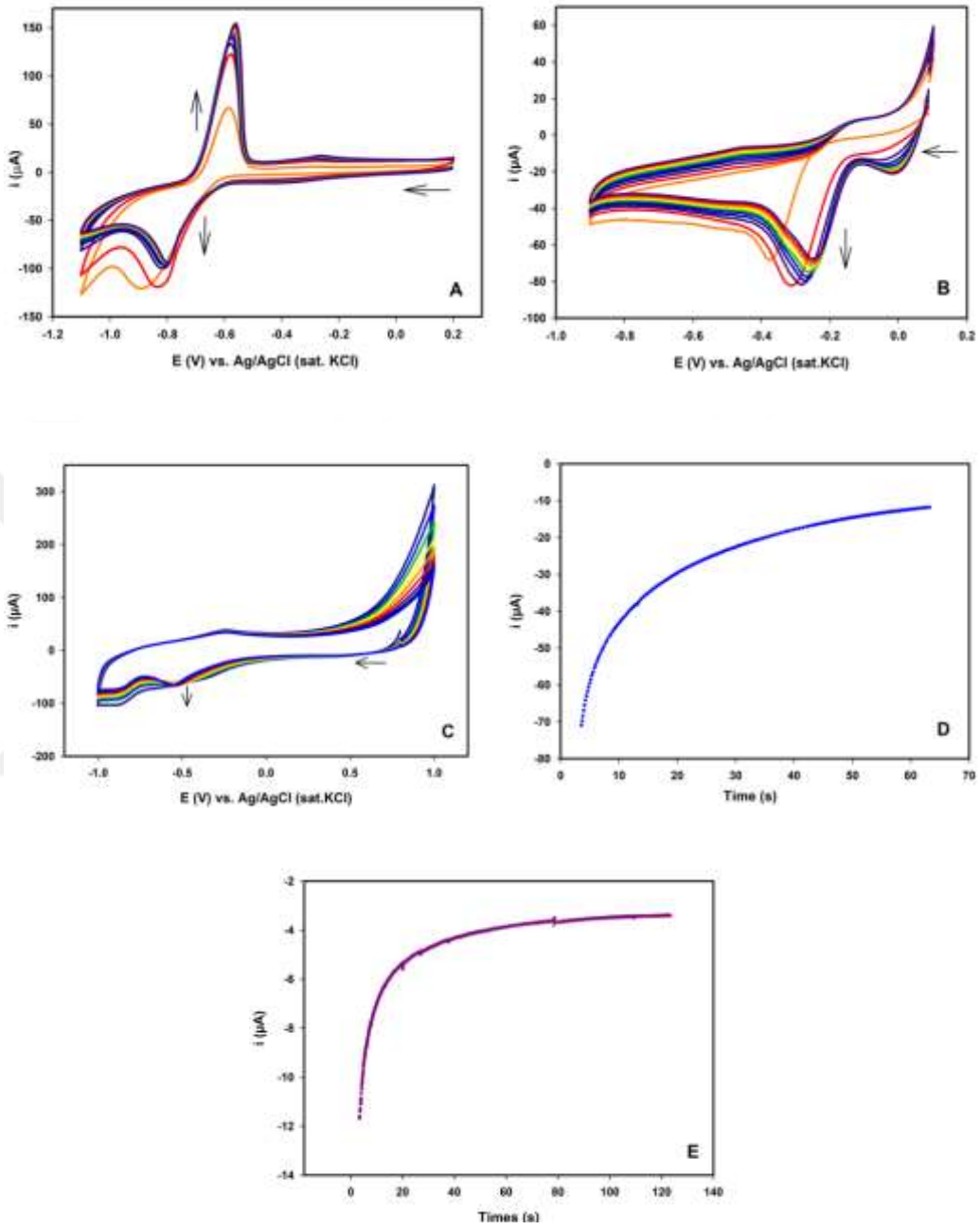

Figure 3.3 Sequential cyclic voltammograms and chronoamperometromograms of electrochemical deposition of different metal nanoparticles on the MWCNT/PCR/GC electrode surface by cyclic voltammetry and chronoamperometric method. A) Cu, B) Au, C) Co, D) Zn, E) Ni. The concentration of Cu^{2+} , Co^{2+}, Ni^{2+}, Zn^{2+} ions in 0.1 M H_2SO_4 solutions. $1.0x10^{-3}$ M $HAuCl_4$+ 0.1 M HCl solution at 50 mV/s scan rate.

3.4. Characterization of Composite Electrodes

3.4.1. SEM Images of Composite Electrodes

The surface morphology of PCR/GCE, MWCN/GCE, MWCNT/PCR/GCE and ZnO/MWCNT/PCR/GCE was characterized by SEM. Figure 3.4A shows an polymer content of PCR that could be clearly observed on the GC electrode surface. The average size of the PCR particles on this electrode surface was about 184 nm. Figure 3.4 B indicates the SEM image of the electrode surface containing multi-walled carbon nanotube. This image consists of a random distribution of MWCN that resemble thin-long tubes. Figure 3.4 C demostrate the MWCNT-PCR composite structure on the GCE surface. On the other hand, Figures D and E show that at different magnification of Zn/ZnO nanoparticles were deposited on the composite structure and the surface image obviously change compare with MWCNT/PCR/GCE. The SEM image of ZnO/MWCNT/PCR/GCE shows many observable particles on the MWCNT/PCR/GCE surface (Figure 3.4D end E). Energy dispersive X-Ray spectroscopy (EDX) study confirmed the presence of Zn/ZnO particles on MWCNT/PCR/GCE decorate with the electrochemical deposition.

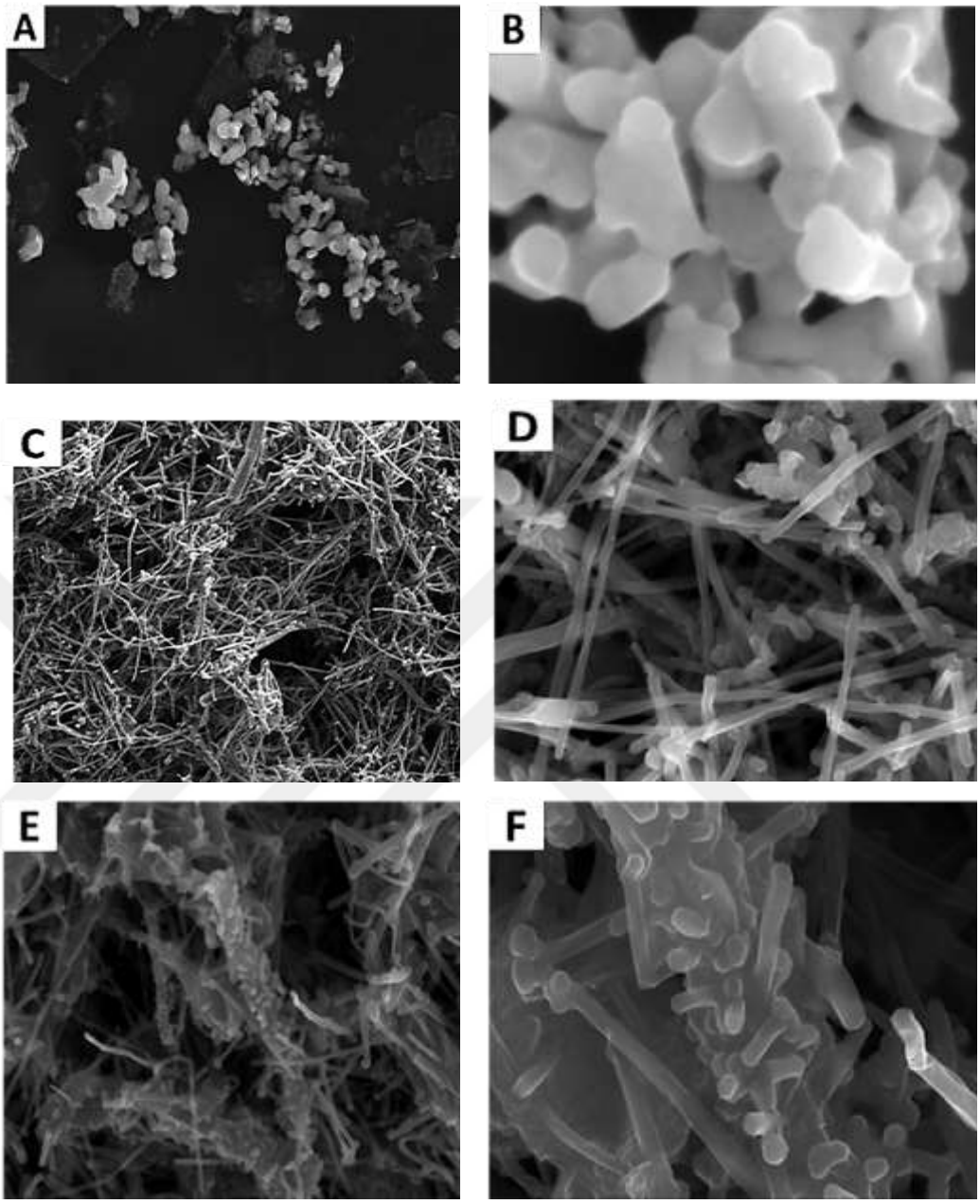

Figure 3.4 SEM images of the (A) PCR/GCE (50 000x), (B) PCR/GCE (250 000x), (C) MWCNT/GCE (50 000x), (D) MWCNT/PCR/GCE (50 000x), (E) ZnO/MWCNT/PCR/GCE (25 000x) and (F) ZnO/MWCNT/PCR/GCE (100 000x)

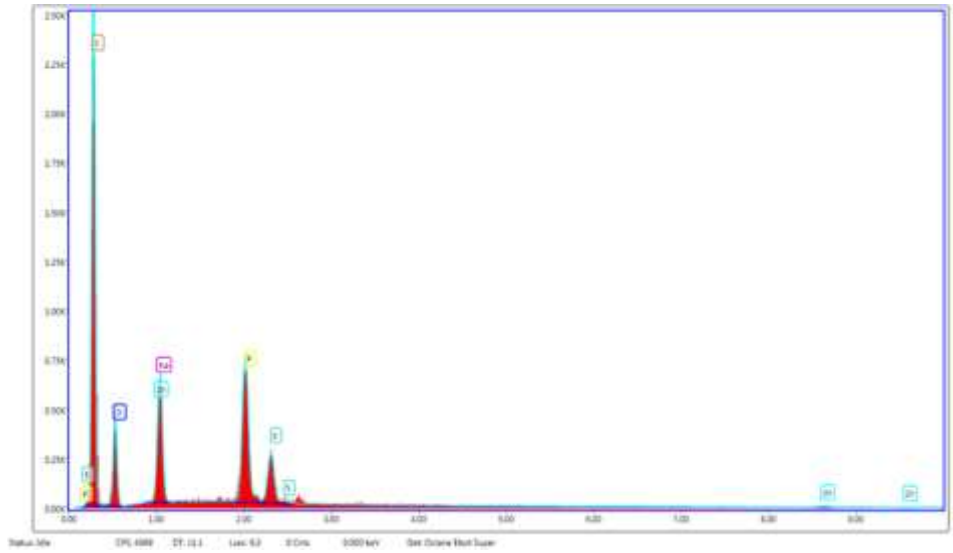

Element	Wt%	Atomic %
C	71.93	81.15
O	14.15	11.98
Na	5.79	3.41
P	5.78	2.53
S	2.05	0.87
Zn	0.35	0.06
Total:	100.00	100.00

Figure 3.5 EDX results of the ZnO/MWCNT/PCR/GCE

3.4.2. Chemical characterization of modified electrodes by XPS

The XPS is that one of the highly surface-sensitive spectroscopic techniques used to illuminate the chemical composition of electrode surfaces. In this study, XPS measurements for three different modified electrodes were studied and the data were discussed below detaily. Figure 3.6 A, B and C indicates the XPS survey spectra and high resolution spectrum of the MWCNT/GCE to improve the presence of C-C and O=C-O structures. The binding energies obtained as 284.6 eV for C-C bond and 532.6 eV for O = C - O prove the content of pre-treatated MWCNT on GCE. The presence of PCR on the composite electrode, the curve fitting data of S2p orbital is shown in Figure 3.7C. The deconvolution of the S2p peak gives two doublet peaks at about 168 eV and 169 eV allocated to the $–SO_3H$ and $–OSO_3H$ groups in polymeric film, respectively. In Figure 3.8 binding energies of $Zn2p_{3/2}$ and $Zn2p_{1/2}$ were observed at 1021.9 eV and 1044.82 eV, are assigned the presence of Zn species on MWCNT/PCR/GCE. On the other hand, the peaks at the binding energies of 530.6 eV for O1s can indicates the oxide structure of zinc.

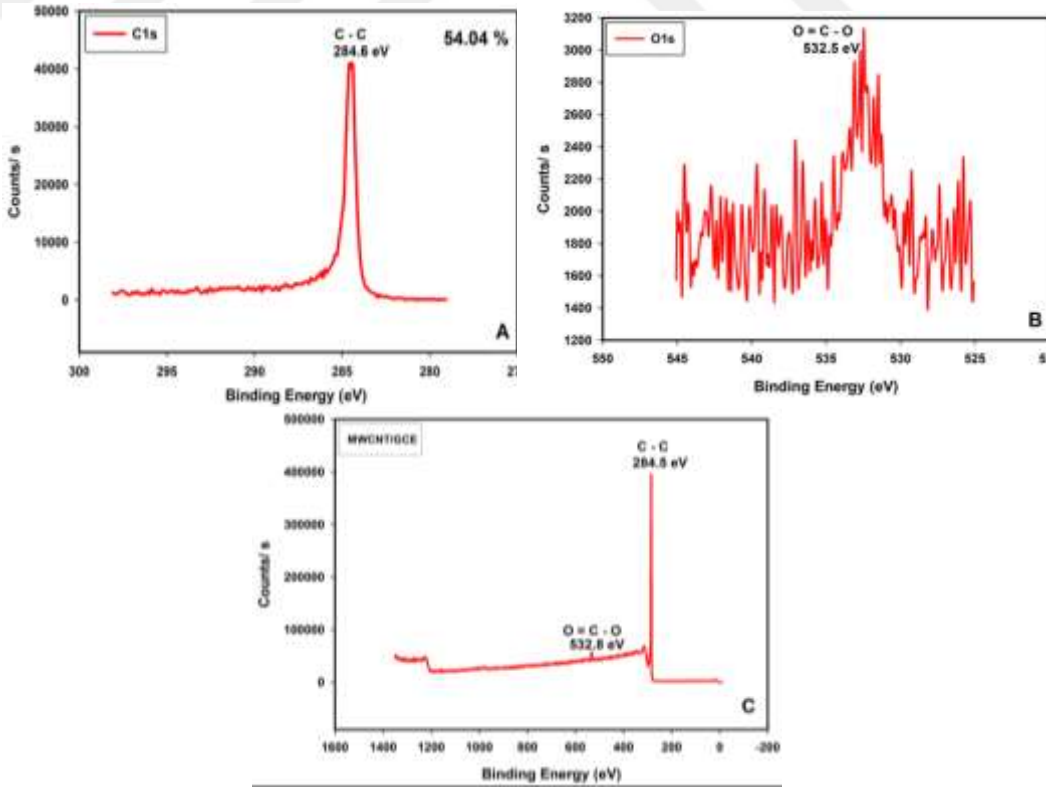

Figure 3.6 The XPS spectra of A) C1s, B) O1s, C) MWCNT/GCE.

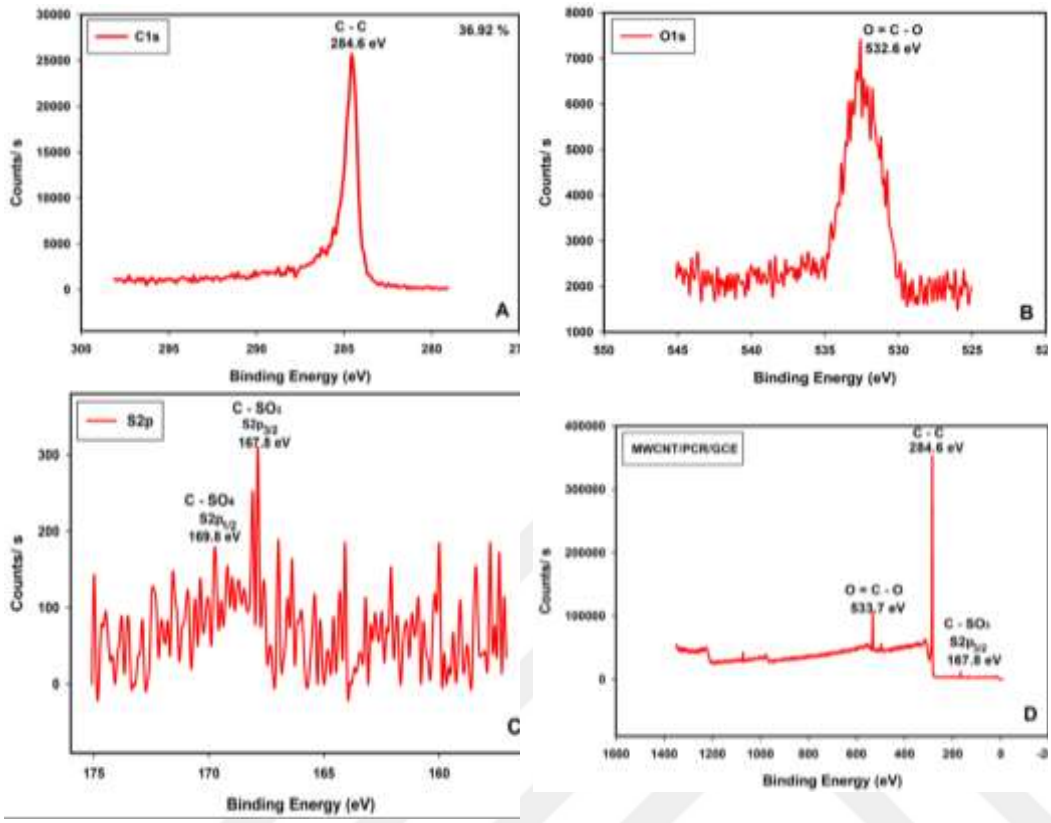

Figure 3.7 The XPS spectra of A) C1s, B) O1s, C) Sp^2, D) MWCNT/PCR/GCE

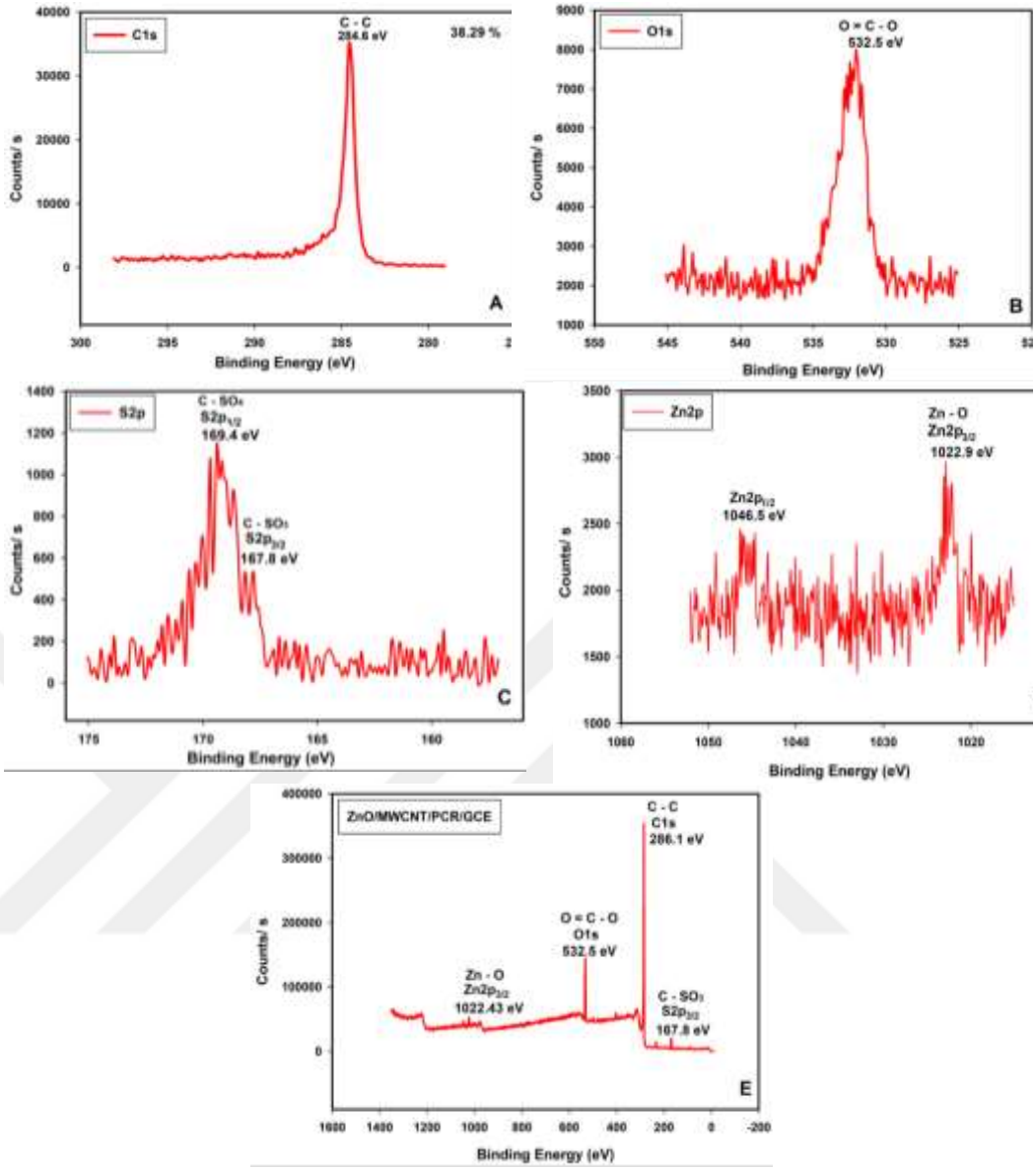

Figure 3.8 The XPS spectra of A) C1s, B) O1s, C) Sp^2, D) Zn2p, E) ZnO/MWCNT/PCR/GCE.

3.4.3. Electrochemical characterization of modified electrodes by EIS

Electrochemical impedance spectroscopy (EIS) is a versatile technique for investigating the electrical properties of a variety of different electrochemical materials and modified electrodes. The typical EIS curve was contained of a semicircular part at high frequencies and linear part at lower frequencies. The semicircular part comprises the electron transfer limited electrochemical reactions.

The diameter of semicircle is equal to the electron transfer resistance (R_{ct}). The linear part which appears represents the diffusion limited process.

The results of electrochemical impedance spectroscopy (EIS) for bare GCE, PCR/GCE, MWCNT/GCE, MWCNT/PCR/GCE, ZnO/MWCNT/PCR/GC electrodes were shown in Figure 3.9-10. Measurements were taken at 0.05 to 5.000 Hz at varying frequencies in 0.1 M KNO_3 support electrolyte containing 5 mM $[Fe(CN)_6]^{3-/4-}$.

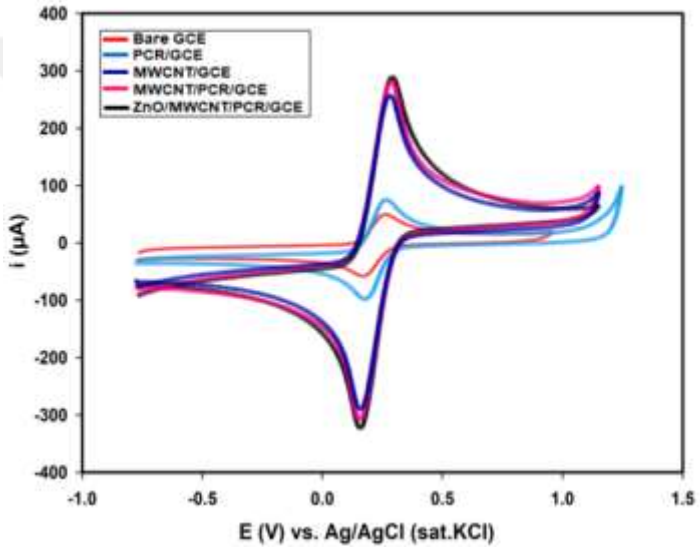

Figure 3.9 Cyclic Voltammetric behaviors of all electrodes in 0.1 M KNO_3 solution + 5 mM $Fe(CN)_6^{-3/-4}$.

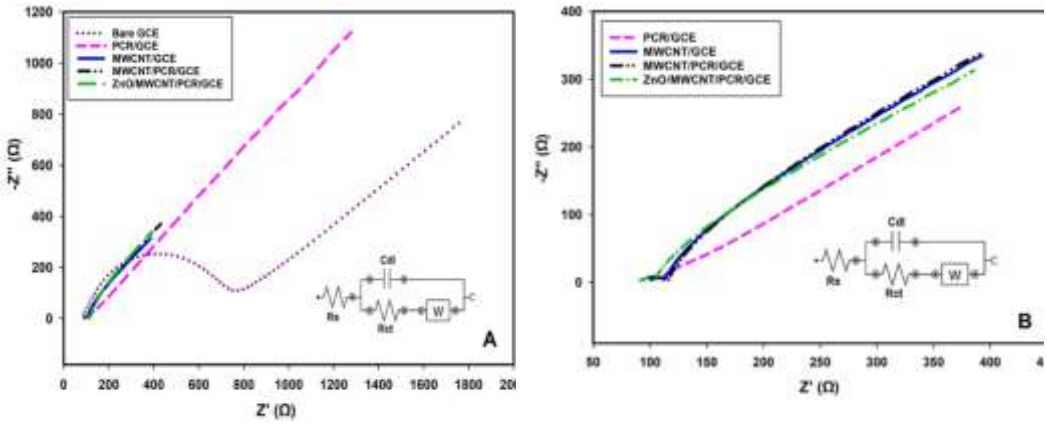

Figure 3.10 Nyquist curcit of GCE, PCR/GCE, MWCNT/GCE, MWCNT/PCR/GCE and ZnO/MWCNT/PCR/GCE. The frequency range was from 0.05 to 5.000 Hz at the formal potential about 238 mV.

Table 3.1 The stated values for Rs, Rct, Cdl and W for bare and modified electrodes.

	Bare GCE	PCR/ GCE	MWCNT/ GCE	MWCNT/PCR/GCE	ZnO/MWCNT/ PCR/GCE
Rs (Ω)	136	107	112	107	99.3
Rct(mΩ)	**562000**	**7640**	**0.0019**	**0.00188**	**0.0011**
Cdl (mF)	0.000586	0.0137	1.58	1.14	1.12
W(mMho)	0.946	1.14	3.60	3.40	3.99

The EIS values calculated for each electrode according to the R (C (RW)) circuit were given in the Table 3.1. The Rct value with the highest electron transfer resistance was measured on a 562 Ω at bare electrode. The largest semicircle between the electrodes belongs to the GC electrode in Figure 3.10A. The modification of the electrode surfaces was further signified in Figure 3.10B, where the semicircle decreases gradually for each electrode. When the Rct values of the modified electrodes were examined respectively, it was seen that the Rct values of PCR/GC electrode were 7.64 Ω and the Rct values decreased with increasing surface modification towards the optimum electrode. Thus, the Rct value for the ZnO/MWCNT/PCR/GC electrode showing the highest electroconductivity is 1.10 μΩ. These results introduced that the synergistic effect of CNTs with PCR and ZnO particles effectively increased the conductivity of the electrode and promoted the electron transfer rate.

3.5. Voltammetric Behaviour of Melatonin and Caffeine at Bare and Modified Electrodes

The electrochemical behaviour of melatonin and caffeine in pH 7.0 phosphate buffer solution were examined at different electrodes such as bare, PCR/GCE,

MWCNT/PCR/GCE, MWCNT/GCE, ZnO/MWCNT/GCE, Ni/MWCNT/PCR/GCE, Cu/MWCNT/PCR/GCE, Au/MWCNT/PCR/GCE and Co/MWCNT/PCR/GCE and the obtaining results from each electrode were compaired with the voltammograms obtained in the absence and presence of metatonin and caffein in pH 7.0 phosphate buffer solution (Figure 3.11 and 3.12). Only a reduction peak for gold ions which are formed during the anodic current-potential scan, was observed on the Au/MWCNT/PCR/GCE. In the case of other electrodes, there was no any electrochemical signal on voltammograms for the other electrodes in pH 7.0 phosphate buffer solution (Figure 3.11 inset). In the presence of melatonin and caffeine, there were poor irreversible oxidation peaks in the CV responses of Bare GCE, PCR/GCE and MWCNT/PCR/GCE. This indicates the slow electron transfer rates for the oxidation of these molecules. Conversely, remarkable current increase of irreversible three oxidation peaks at about 0.65 V, 1.05V and 1.15V for melatonin and a single oxidation peak at 1.42 for caffeine were observed at MWCNT/GCE, ZnO/MWCNT/GCE, Ni/MWCNT/PCR/GCE, Cu/MWCNT/PCR/GCE, Au/MWCNT/PCR/GCE and Co/MWCNT/PCR/GCE, indicating the catalytic activity of the metal/metal oxide particles modified electrodes.

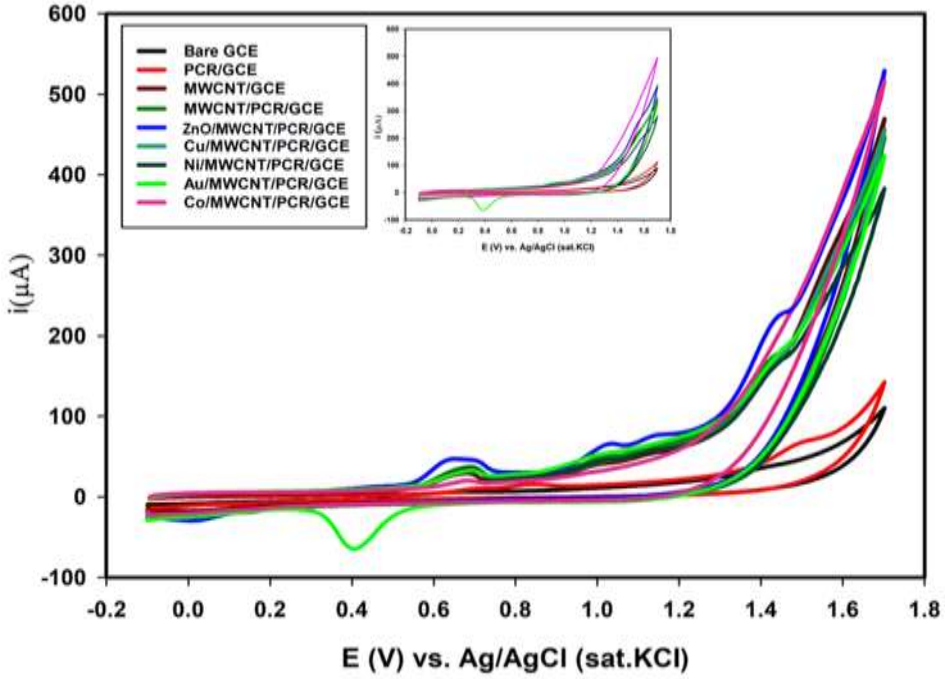

Figure 3.11 CV of bare GCE, PCR/GCE, MWCNT/PCR/GCE, MWCNT/GCE, ZnO/MWCNT/GCE, ZnO/MWCNT/PCR/GCE, Ni/MWCNT/PCR/GCE, Cu/MWCNT/PCR/GCE, Au/MWCNT/PCR/GCE and Co/MWCNT/PCR/GCE in the 0.1 M pH 7.0 phosphate buffer ($1.0x10^{-4}$ M melatonin and caffeine). Inset: CV's obtained at bare GCE, PCR/GCE, MWCNT/PCR/GCE, MWCNT/GCE, ZnO/MWCNT/GCE, ZnO/MWCNT/PCR/GCE, Ni/MWCNT/PCR/GCE, Cu/MWCNT/PCR/GCE, Au/MWCNT/PCR/GCE and Co/MWCNT/PCR/GCE in the absence

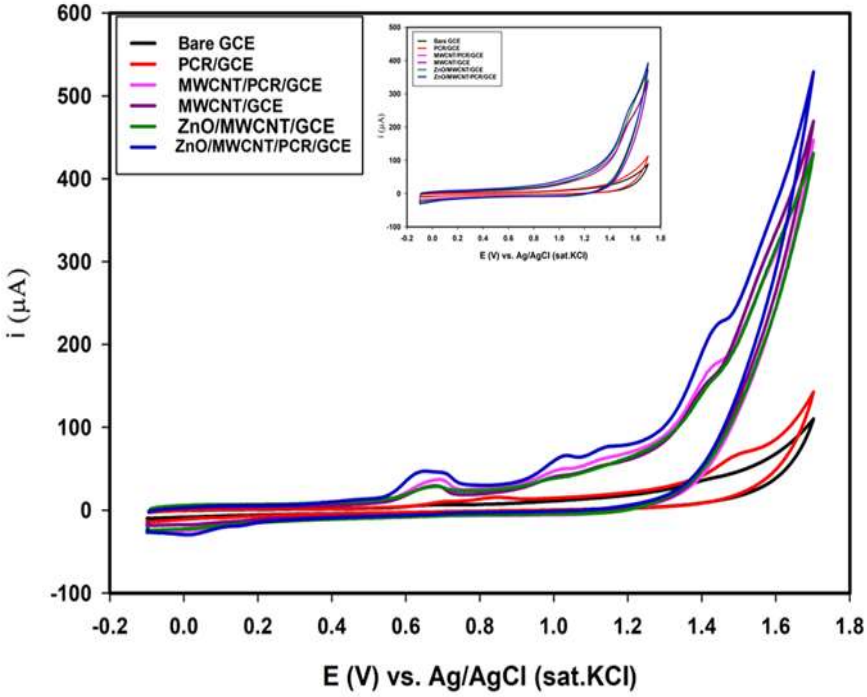

Figure 3.12 CV behaviors of bare GCE, PCR/GCE, MWCNT/PCR/GCE, MWCNT/GCE, ZnO/MWCNT/GCE and ZnO/MWCNT/PCR/GCE electrodes with $1.0x10^{-4}$ M melatonin and caffeine in pH 7.0 PBS. Inset: CV's obtained at bare GCE, PCR/GCE, MWCNT/PCR/GCE, MWCNT/GCE, ZnO/MWCNT/GCE and ZnO/MWCNT/PCR/GCE in the absence

The overall Table 3.2 demostrate ZnO particles modified MWCNT/PCR/GCE displayed best electrocatalytic activity for melatonin and caffein oxidation in terms of both peak current potentail values as compared to the almost all other electrodes. Therefore, the ZnO/ MWCNT/PCR/GCE will be used in detailed investigation of electrochemical behaviour melatonin and caffeine.

Table 3.2 Peak characteristics of melatonin and caffeine at all electrodes

Type of electrode	Melatonin		Caffeine	
	E(mV)	i (μA)	E(mV)	i (μA)
Bare GCE	666	1.43	1411	0.687
PCR/GCE	701/845	1.55/3.24	1489	5.19
MWCNT/PCR/GCE	676	14.07	1414	12.02
MWCNT/GCE	672	14.77	1404	5.91
ZnO/MWCNT/GCE	676	10.25	1408	4.24
ZnO/MWCNT/PCR/GCE	**645**	**25.16**	**1424**	**21.06**
Cu/MWCNT/PCR/GCE	686	14.68	1416	6.81
Ni/MWCNT/PCR/GCE	679	16.67	1416	7.53
Au/MWCNT/PCR/GCE	681	10.78	1424	4.89
Co/MWCNT/PCR/GCE	676	4.89	-	-

3.6. Optimization Studies for Melatonin and Caffeine Oxidation at bare and ZnO/MWCNT/PCR/GCE

3.6.1. Effect of supporting electrolyte pH on cyclic voltammetric behavior of melatonin and caffeine

The effect of pH on the electrochemical behaviour of melatonin and caffeine were studied by CV in the pH range of 3.76-8.00 (Figure 3.13, Figure 3.15) to elucidate the electrocatalytic oxidation of melatonin and caffein depending on pH at bare and ZnO/MWCNT/PCR/GCE. CV studies were performed in the presence

of $1.0x10^{-4}$ M melatonin and $1.0x10^{-4}$ M caffeine in different pH of supporting electrolytes. The peak currents increased in pH range between 3.76 to 7.00 and attained a highest value at pH 7.00, at high pH values (pH > 7.0) the currents value of both of melatonin and caffein were dropped (Figure 3.14 A and Figure 3.16A). Moreover, the oxidation peak potentials of melatonin and caffeine shifted to less positive potentails by increasing the supporting electrolyte solution of pH (Figure 3.14 B and Figure 16 B).

From the above results, pH 7.00 was chosen as optimum supporting electrolyte for the future studies.

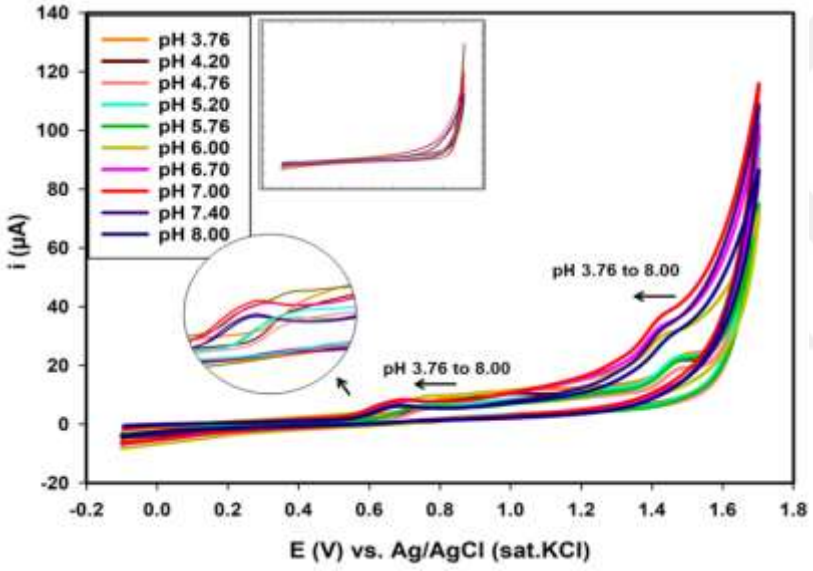

Figure 3.13 CV's of oxidation of melatonin and caffeine on bare GC electrode at different pH scale ranges in the presence of $1.0x10^{-4}$ M melatonin and caffeine at a scan rate of 50 mV/s and CV's obtained at bare GCE in the absence (inset)

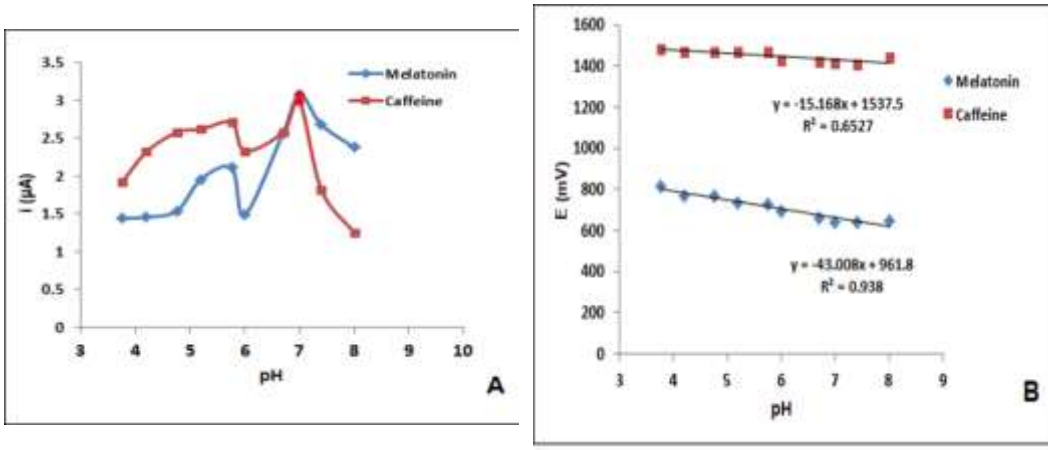

Figure 3.14 Effect of the pH on A) peak current B) peak potential of melatonin and caffeine on the bare GCE with cyclic voltammetry (pH: 3.76 to 8.00).

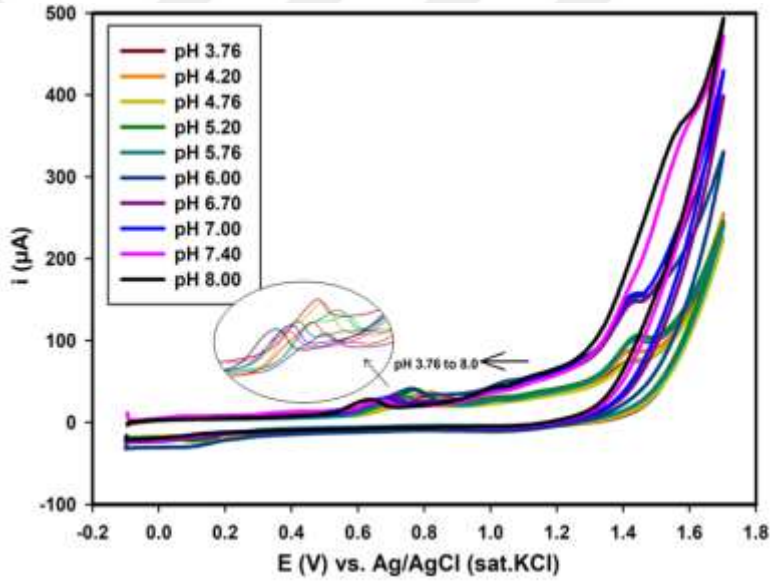

Figure 3.15 Cyclic voltammograms of oxidation of melatonin and caffeine on ZnO/MWCNT/PCR/GC electrode at different pH scale ranges in the presence of $1.0x10^{-4}$ M melatonin and caffeine at a scan rate of 50 mV/s.

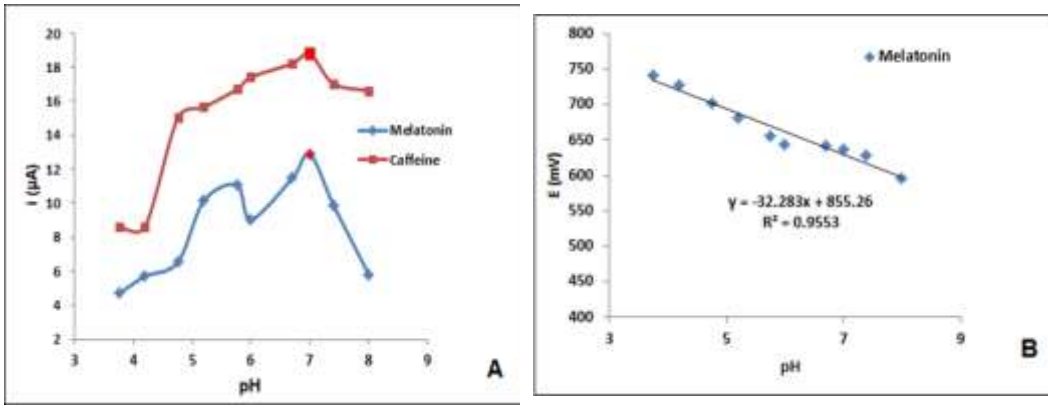

Figure 3.16 Effect of the pH on A) peak current B) peak potential of melatonin and caffeine on the ZnO/MWCNT/PCR/GCE with cyclic voltammetry (pH: 3.76 to 8).

Table 3.3 Cyclic Voltammograms of electrooxidation of melatonin and caffeine ($1.0x10^{-4}$ M), GC electrode in various pH (3.76 to 8.00) with 50 mV/s scan rate.

pH	Bare GCE			
	Melatonin		Caffeine	
	E(mV)	i (µA)	E(mV)	i (µA)
3,76	813	1.44	1482	1.92
4.20	766	1.46	1469	2.32
4.76	769	1.54	1469	2.58
5.20	737	1.96	1467	2.62
5.76	727	2.11	1472	2.71
6.00	693	1.49	1428	2.33
6.70	661	2.57	1425	2.58
7.00	**640**	**3.08**	**1418**	**2.98**
7.40	639	2.68	1410	1.82
8.00	645	2.38	1443	1.25

Table 3.4 Cyclic Voltammograms of electrooxidation of melatonin and caffeine ($1.0x10^{-4}$ M), ZnO/MWCNT/PCR/GC electrode in various pH (3.76 to 8.00) with 50 mV/s scan rate. (Ccresol red : 2 mM)

pH	ZnO/MWCNT/PCR/GCE			
	Melatonin		Caffeine	
	E(mV)	i (µA)	E(mV)	i (µA)
3,76	742	4.69	1469	8.60
4.20	728	5.69	1460	8.62
4.76	701	6.54	1453	15.04
5.20	681	10.14	1443	15.65
5.76	656	11.08	1436	16.71
6.00	644	9.06	1423	17.42
6.70	642	11.48	1421	18.23
7.00	**637**	**12.88**	**1418**	**18.80**
7.40	628	9.90	1517	17.04
8.00	596	5.80	1523	16.62

3.6.2. The effect of cresol red concentration on melatonin and caffeine oxidation

As shown in Figure 3.17, the PCR concentration stored by electrochemical polymerization on the GC electrode surface for the voltammetric behavior of melatonin and caffeine was examined. These concentrations range from $1.0x10^{-4}$ M

to 2.0x10^{-3} M. The highest peak current values among CR concentrations were read at 5.0x10^{-4} M concentration.

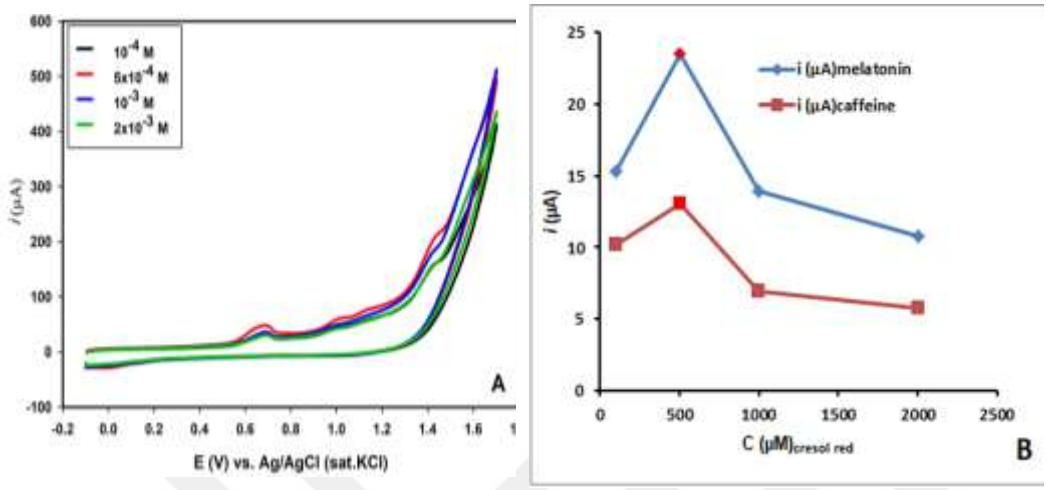

Figure 3.17 A) Cyclic voltammograms with different concentrations of PCR (10^{-4} M to 2x10^{-3} M) in the pH 7.00 (0.1 M) PBS on GC electrode **B)** The effect of PCR concentration on the peak current of 1.0x10^{-4} M melatonin and caffeine

Table 3.5 The effect of cresol red concentration on a melatonin and caffeine (1.0x10^{-4} M) oxidation.

Concentration of PCR (M)	Melatonin		Caffeine	
	E(mV)	i (µA)	E(mV)	i (µA)
1.0x10^{-4}	689	15.33	1419	10.15
5.0x10^{-4}	**681**	**23.53**	**1421**	**13.07**
1.0x10^{-3}	684	13.94	1414	6.97
2.0x10^{-3}	684	10.76	1414	5.72

3.6.3. Optimization study for the number of cycles of cresol red

In order to determine the optimum PCR cycle in the voltammetric determination of melatonin and caffeine ($1.0x10^{-4}$ M), different cycle numbers were studied at pH 7.00 PBS on the GC electrode surface with the optimum cresol concentration ($5.0x10^{-4}$ M) determined in the previous step Figure 3.17.

When the values of the polymerization cycle numbers in Figure 3.18A were examined, the highest peak current values were observed in 5th cycles in response to the electrochemical behavior of melatonin and caffeine Table 3.6.

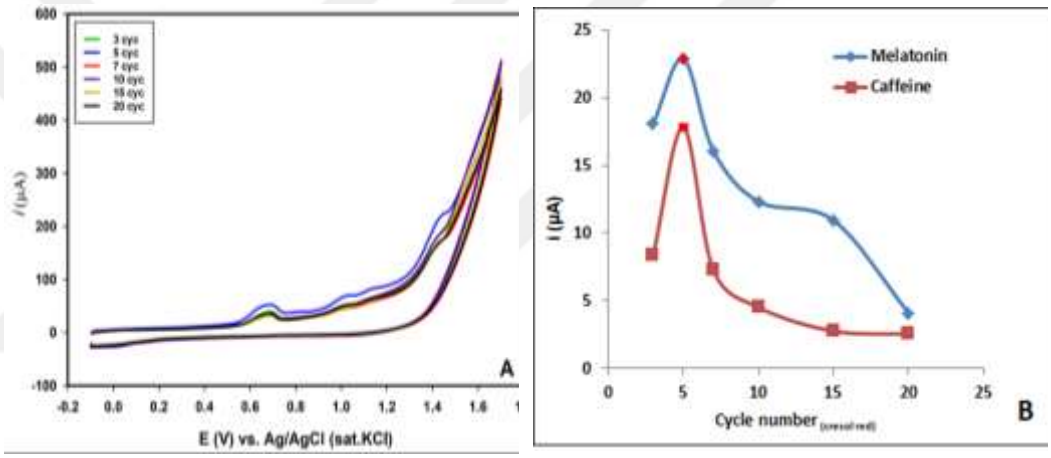

Figure 3.18 A) Cyclic voltammograms with different cycle numbers of PCR (3 to 20) in the pH 7.00 (0.1 M) PBS on GC electrode **B)** The effect of PCR cycle number on the peak current of $1.0x10^{-4}$ M melatonin and caffeine

Table 3.6 The effect of PCR on melatonin and caffeine ($1.0x10^{-4}$ M) oxidation in different cycle numbers

Cycle number of PCR	Melatonin		Caffeine	
	E(mV)	i (μA)	E(mV)	i (μA)
3	684	18.07	1419	8.39
5	**674**	**22.87**	**1426**	**17.79**
7	676	16.08	1426	7.28
10	679	12.33	1426	4.52
15	684	10.95	1436	2.76
20	689	4.11	1443	2.56

3.6.4. The effect of zinc sulfate concentration on melatonin and caffeine oxidation of ZnO nanoparticle formation

The effect of $ZnSO_4$ concentration during the ZnO particles deposition on MWCNT/ PCR/GCE on melatonin and caffeine oxidation was examined in the range of $1.0x10^{-4}$ M to $2.0x10^{-3}$ M and the results were displayed in Figure 3.19 and Table 3.7. The highest peak current value was determined at $1.0x10^{-3}$ M $ZnSO_4$ concentration and further studies will be performed under this condition.

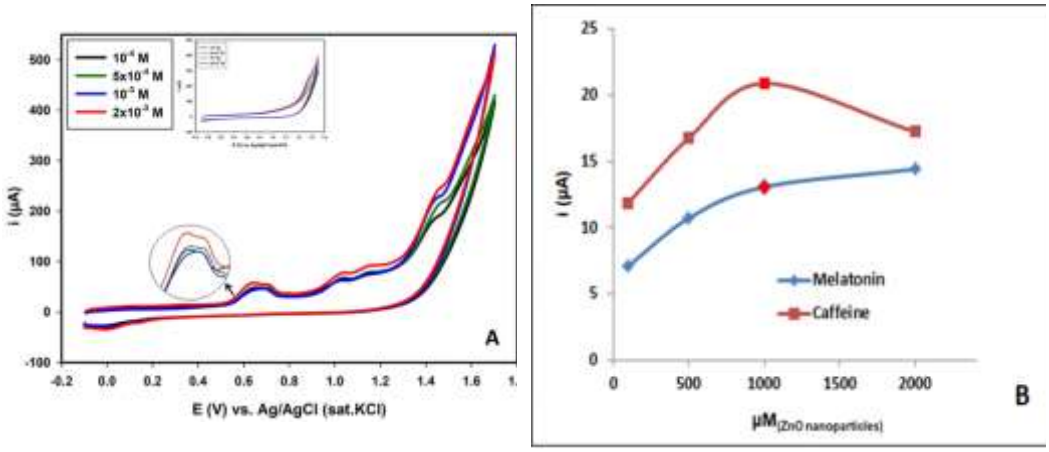

Figure 3.19 A) Cyclic voltammograms with different concentrations of $ZnSO_4$ (10^{-4} M to $2x10^{-3}$ M) in the pH 7.00 (0.1 M) PBS and **B)** The effect of $ZnSO_4$ concentration on the peak current of $1.0x10^{-4}$ M melatonin and caffeine. Inset: CV's obtained at MWCNT/PCR/GCE in the absence

Table 3.7 The effect of $ZnSO_4$ concentration during the $ZnSO_4$ deposition on MWCNT/ PCR/GCE for melatonin and caffeine($1.0x10^{-4}$ M) oxidation

The effect of $ZnSO_4$ concentration (M)	Melatonin		Caffeine	
	E(mV)	i (µA)	E(mV)	i (µA)
$1.0x10^{-4}$	632	7.13	1419	11.88
$5.0x10^{-4}$	630	10.74	1441	16.78
$1.0x10^{-3}$	**635**	**13.09**	**1424**	**20.9**
$2.0x10^{-3}$	625	14.43	1441	17.24

3.6.5. The effect of deposition potentials of ZnO particles on melatonin and caffeine oxidation

To obtained the best electrodeposition potentail of ZnO on MWCNT/ PCR/GCE for electrocatalytic oxidation of melatonin and caffeine, the deposition potentail was changed in the range between -1.40 V and -1.20 V (Figure 3.20 A and

B) The highest peak current value was achived at -1.3 V deposition potential and further studies will be carried out under this condition.

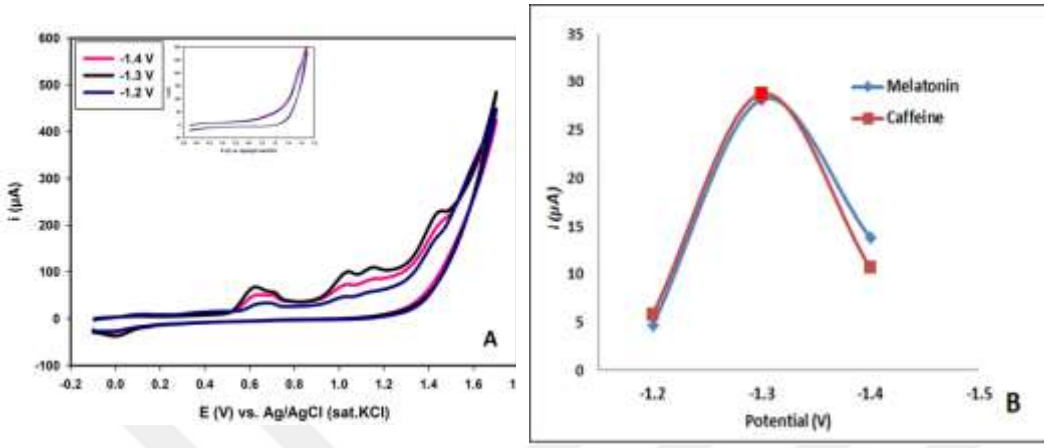

Figure 3.20 A) Cyclic voltammograms with different ZnO metal nanoparticles deposition potentials (-1.4 V to -1.2 V) in the pH 7.00 (0.1 M) PBS at MWCNT/PCR/GCE. **B)** The effect of ZnO metal nanoparticles deposition potentials on the peak current of $1.0x10^{-4}$ M melatonin and caffeine. Inset: CV's obtained at MWCNT/PCR/GCE in the absence

Table 3.8 The effect of ZnO metal nanoparticles deposition potentials on voltammetric behavior of a melatonin and caffeine ($1.0x10^{-4}$ M)

Potantials of ZnO (V)	Melatonin		Caffeine	
	E(mV)	i (µA)	E(mV)	i (µA)
-1.4	618	13.75	1438	10.60
-1.3	**613**	**28.15**	**1436**	**28.75**
-1.2	635	4.68	1421	5.77

3.6.6. Optimization study for the different deposition time of the ZnO nanoparticles on MWCNT/PCR/GC electrode surface

To obtained the best electrodeposition time of ZnO on MWCNT/ PCR/GCE for electrocatalytic oxidation of melatonin and caffeine, the deposition time was varied

from 30 s to 150 s (Figure 3.21A). The highest peak current was appeared at 60 s electrodeposition time of ZnO and further studies will be carried out under this condition.

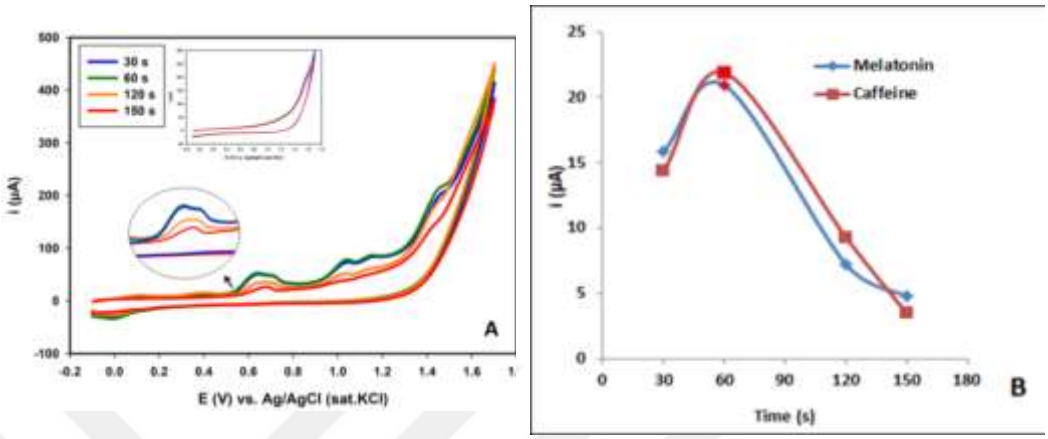

Figure 3.21 A) Cyclic voltammograms with different ZnO metal nanoparticles deposition times (30 s to 150 s) in the pH 7.00 (0.1 M) PBS at MWCNT/PCR/GCE. **B)** The effect of ZnO metal nanoparticles deposition times on the peak current of $1.0x10^{-4}$ M melatonin and caffeine. Inset: CV's obtained at MWCNT/PCR/GCE in the absence

Table 3.9 The effect of ZnO metal nanoparticles on melatonin and caffeine ($1.0x10^{-4}$ M) oxidation on various deposition times

Deposition times of ZnO (s)	Melatonin		Caffeine	
	E(mV)	i (µA)	E(mV)	i (µA)
30	625	15.85	1443	14.34
60	**623**	**20.93**	**1438**	**21.9**
120	634	7.23	1424	9.30
150	674	4.78	1416	3.5

In briefly, the optimum values and results of the experimental studies were given in Table 3.10.

Table 3.10 Optimum conditions for experimental studies

Experimental parameter	Optimum Conditions
pH of supporting electrolyte	pH 7.0 PBS
PCR concentration	5.0x10-4 M
Cycle number of PCR	5 cycles
ZnSO4 concentration	1.0x10-3 M
Deposition potential of ZnO nanoparticles	-1.3 V
Deposition time of ZnO nanoparticles	60 s
Volume of MWCNT	10 µL

3.7. Effect of potentail scan rate on electrochemical behavior of melatonin and caffeine at ZnO / MWCNT / PCR / GCE

The effect of different scan rate (5.0 – 150 $mV.s^{-1}$) on the electrochemical behaviour of $1.0x10^{-4}$ M melatonin and $1.0x10^{-4}$ M caffeine at ZnO / MWCNT / PCR / GCE was investigated in in pH 7.0 PBS using cyclic voltammetry. These cyclic voltammograms were showed in Figure 3.22.

The results indicated that the peak currents were linearly changed with the square root of scan rate over the range of 5.00–150.00 mVs^{-1} (Figure 3.23-A), indicating that the electrode process in the presence of melatonin and caffeine is controlled by diffussion at ZnO / MWCNT / PCR / GCE. On the other hand, the peak potential of both compounds shifted to more positive values with increasing the logaritmic scan rates. The linear relation between peak potential and logarithm of scan rate (Figure 3.23-B) indicated that an irreversible electrode process takes place on the electrode surface for both compounds.

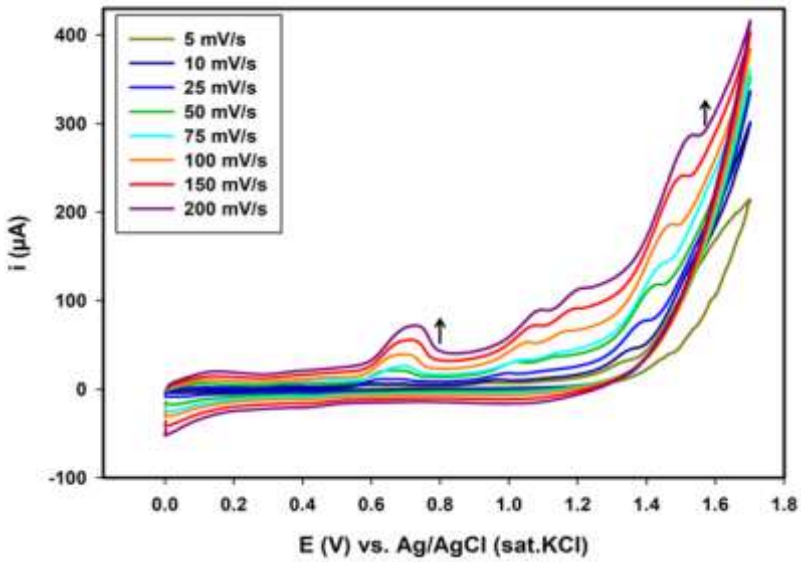

Figure 3.22 Cyclic voltammograms of melatonin and caffeine ($1.0x10^{-4}$ M) ZnO/MWCNT/PCR/GCE with different scan rates (5-200 mV/s).

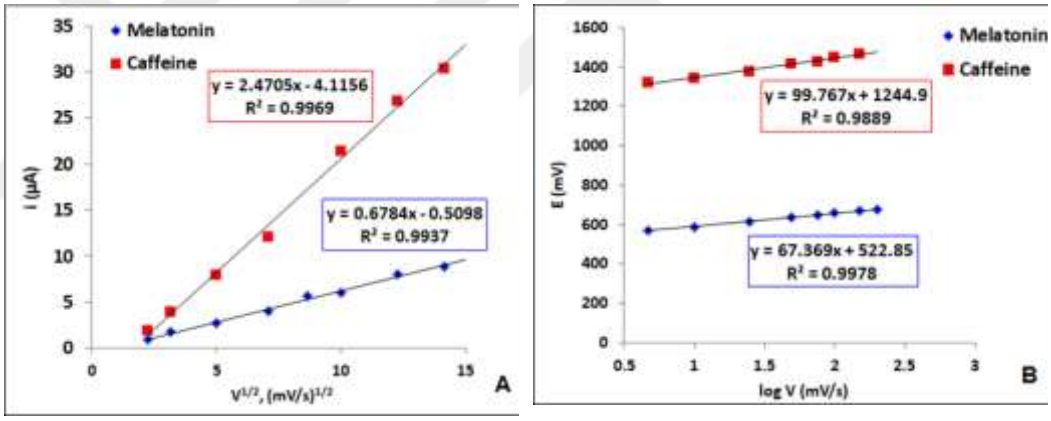

Figure 3.23 Square root of the scan rate vs. current and logoritm of scan rate vs. potential graphics from scan rate study at ZnO/MWCNT/PCR/GCE

3.8. Differential Pulse Voltammetric Determination of Melatonin and Caffeine

Determination of melatonin and caffeine under individual and simultaneous conditions is of great significance in the area of pharmacy and medicine as well as electrochemical analysis. Differential pulse voltammetry technique allows more sensitive analysis of melatonin and caffeine compared to cyclic voltammetry

technique. DPV has been used in experimental studies because the peak currents obtained were determined very well even at low concentrations. The optimization studies for melatonin and caffeine were firstly studied with DPV in the case of each species separately. The effect of different amplitute and different scan rate in DPV were performed for $1.0x10^{-5}$ M melatonin and $1.0x10^{-5}$ M caffeine (Figure 3.24 A and B, Figure 3.25 A and B) and the obtained results were given in Table 3.11 and Table 3.12 respectively. The parameters were also studied in the presence of both melatonin and caffeine (Figure 3.26 A and B) and the obtained results were recovered in Table 3.13. In the case of individual analyte, the optimum scan rate and amplitute were 5 mVs^{-1} and 100 mV for melatonin and 10 mV s^{-1} and 100 mV for caffeine respectively. Howver higher peak current were obtained with amplitudes upwards than 100 mV but the oxidation peak broaden at the high amplitude values. Therefore, the pulse amplitude of 100 mV was chosen to obtain a sharp and sufficiently high peak for further studies.

Table 3.11 Effect of amplitude (5-200 mV) (A) and effect of scan rate (3 mV-75mV) (B) on electrochemical behaviour of $1.0x10^{-5}$ M melatonin.

Melatonin	
Amplitude (mV)	**i (µA)**
5	0.069
10	0.117
25	0.565
50	2.11
75	4.41
100	**7.35**
150	7.98
200	6.5

Melatonin	
Scan Rate(mV/s)	**i (µA)**
3	2.16
5	**5.1**
10	4.51
20	3.47
50	3.24
75	2.24

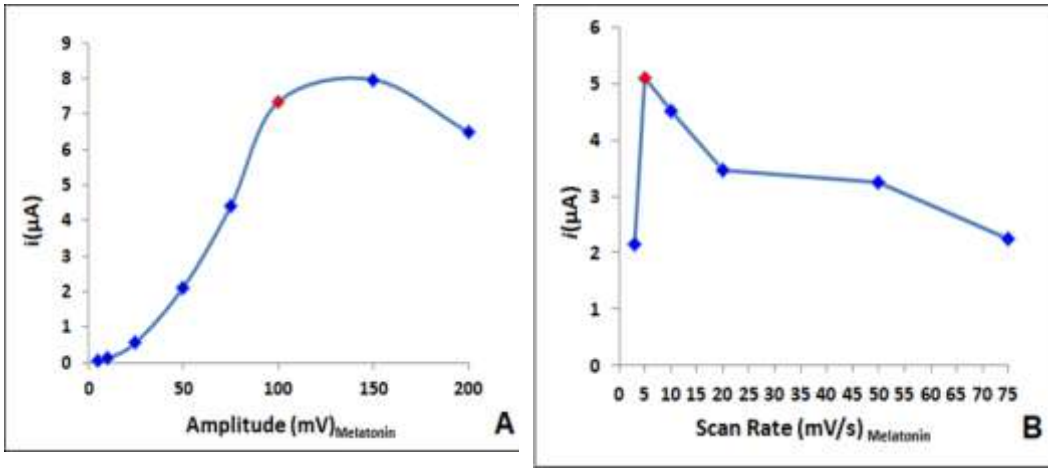

Figure 3.24 Effect of amplitude (5-200 mV) (A) and effect of scan rate (3 mV-75 mV) (B) on electrochemical behaviour of $1.0x10^{-5}$ M melatonin.

Table 3.12 Effect of amplitude (5-250 mV) (A) and effect of scan rate (3 mV-75mV) (B) on electrochemical behaviour of $1.0x10^{-5}$ M caffeine.

Caffeine	
Amplitude (mV)	**i (µA)**
5	0.367
10	0.483
25	1.32
50	5.32
75	9.98
100	11.22
150	15.74
200	16.66
250	13.82

Caffeine	
Scan Rate(mV/s)	**i (µA)**
3	5.91
5	7.6
10	8.88
20	12.48
50	7.67
75	4.88

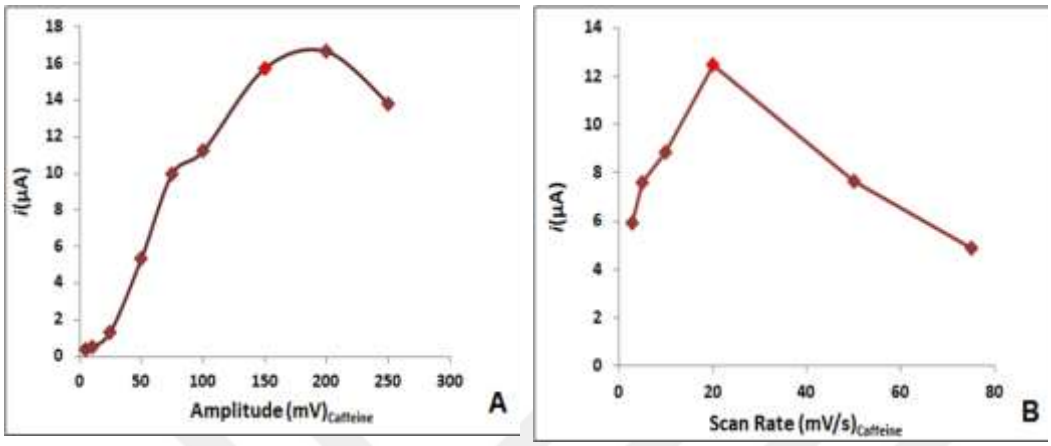

Figure 3.25 Effect of amplitude (5-200 mV) (A) and effect of scan rate (3 mV-75 mV) (B) on electrochemical behaviour of $1.0x10^{-5}$ M caffeine.

Table 3.13 Effect of amplitude (5-250 mV) (A) and effect of scan rate (3 mV-75mV) (B) on electrochemical behaviour of $5.0x10^{-5}$ M melatonin and caffeine.

(A) Melatonin+Caffeine		
Amplitude (mV)	**i (µA)$_{melatonin}$**	**i (µA)$_{caffeine}$**
5	0.0839	0.362
10	0.191	0.476
25	0.639	0.939
50	2.06	2.66
75	4.62	4.46
100	**9.08**	**9.12**
150	8.3	11.09

(B) Melatonin+Caffeine		
Scan Rate(mV/s)	**i (µA)$_{melatonin}$**	**i (µA)$_{caffeine}$**
3	3.57	2.99
5	6.54	5.32
10	7.28	6.40
20	**10.2**	**7.95**
50	5.89	6.08
75	4.99	3.05

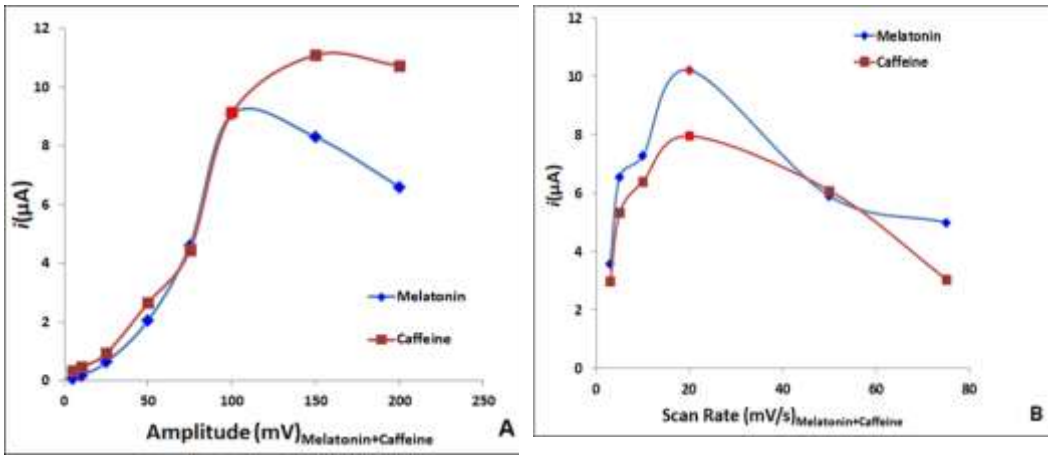

Figure 3.26 Effect of amplitude (5-200 mV) (A) and effect of scan rate (3 mV-75 mV) (B) on electrochemical behaviour of $5.0x10^{-5}$ M melatonin and caffeine.

After all DPV parameters were optimized, calibration curves were formed for each analyte in pH 7.00 PBS as individual and simultaneous conditions of melatonin and caffeine.

In the DPV studies of melatonin, two oxidation peaks were formed at 0.62 V and 0.85 V at bare GCE (Figure 3.27). Both peaks currents were increased by increasing of melatonin concentration (Figure 3.27). The first oxidation peak currents of melatonin were found to be proportional to its concentration over linear ranges $1.0x10^{-7}$ M to $8.0x10^{-7}$ M and the linear regression equations of ip_a=2.3372 C_M-0.1776 (R^2=0.9979) for $(A)_{Melatonin}$ and ip_a=0.1151 c_M-0.008 (R^2=0.9981) for $(B)_{Melatonin}$. The detection limit at bare GC electrode was calculated as $4.28x10^{-8}$ M and $3.33x10^{-8}$ M (S/N=3).

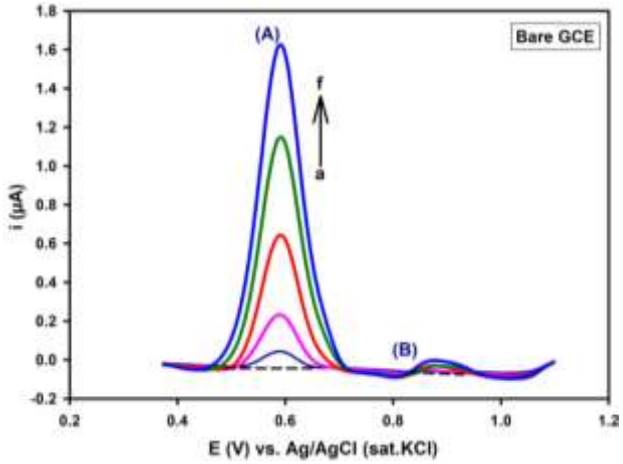

Figure 3.27 Differential pulse voltammograms of bare GCE for increasing concentrations of melatonin in pH 7.0 PBS (0.1 M). The scan rate was 5 mV/s and pulse amplitude 100 mV. Melatonin concentrations a) blank, b) $1.0x10^{-7}$ c) $2.0x10^{-7}$ d) $4.0x10^{-7}$ e) $6.0x10^{-7}$ f) $8.0x10^{-7}$ M

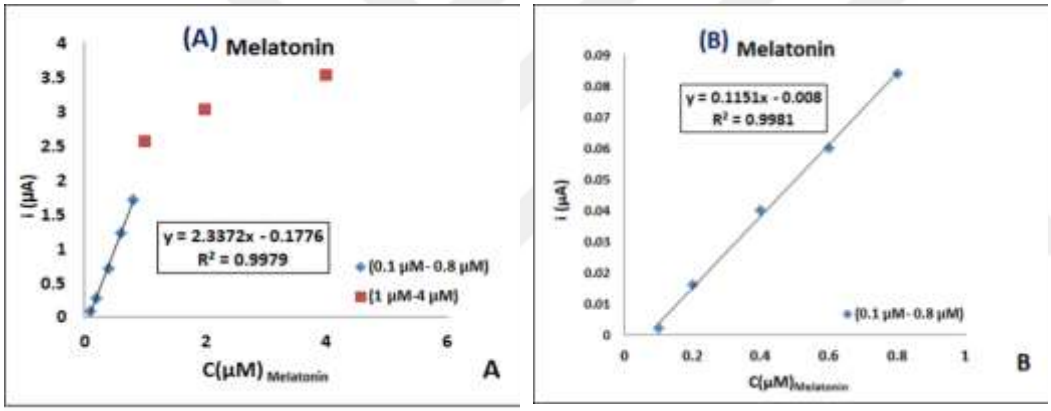

Figure 3.28 Calibration curves for a melatonin oxidation at bare GC electrode concentration ranges between $1.0x10^{-7}$ M– $8.0x10^{-7}$ M

For the PCR / GC electrode, the similar DPV behaviour was obtained for melatonin and the oxidation peaks were appeared at 0.60 V and 0.85 V (Figure 3.29). The both oxidation peaks current were linearly increased by increasing the melatonin concentration in the range $1.0x10^{-7}$-$1.0x10^{-6}$ M (Figure 3.29) and the linear regression equations of $ip_a=3.5116c_A+0.2671$ ($R^2=0.9943$) for $(A)_{Melatonin}$ first oxidation peak and linear regression equations of $ip_a=0.1852\ c_A+0.0424$ ($R^2=0.9958$) for $(B)_{Melatonin}$. The detection limit at PCR/GC electrode was calculated as $2.85x10^{-8}$ M and $5.28x10^{-8}$ M (S/N=3).

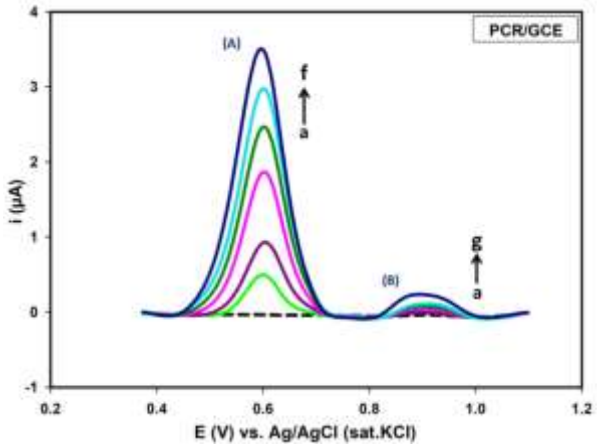

Figure 3.29 Differential pulse voltammograms of PCR/GCE for increasing concentration of melatonin in pH 7.0 PBS (0.1 M) with 5 mV/s scan rate and 100 mV pulse amplitude. Melatonin concentrations a) blank, b)$1.0x10^{-7}$ c) $2.0x10^{-7}$ d) $4.0x10^{-7}$ e) $6.0x10^{-7}$ f) $8.0x10^{-7}$ g) $1.0x10^{-6}$ M

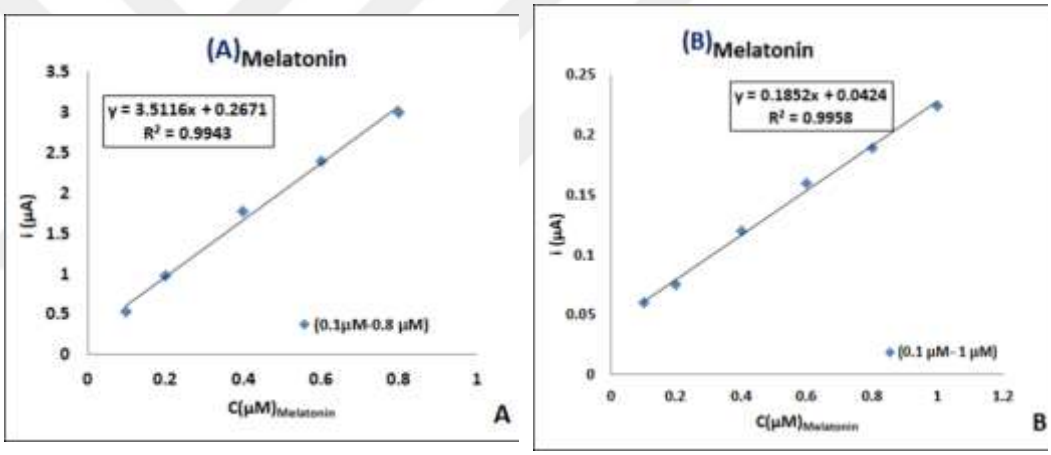

Figure 3.30 Calibration curves for a melatonin oxidation at PCR/GCE concentration ranges between $1.0x10^{-7}$ M – $1.0x10^{-6}$ M

In the case of MWCNT/GCE, two oxidation peaks were appeared at 0.3 V and 0.65 V for melatonin (Figure 3.31). The oxidation peak potentials of melatonin were shifted to low positive values on MWCNT/GCE compare to bare and PCR/GCE. These shifting could be explained by the catalytic acitvity of MWCNT on GCE. The current of both oxidation peaks of melatonin were increased linearly with the increase of melatonin concentration in the range of $8.0x10^{-8}$ M – $1.0x10^{-6}$ M at MWCNT/GCE (Figure3.31) and the linear regression equations of $ip_a=3.0019\ c_M+0.7606$ ($R^2=0.9971$) and $ip_a=1.4987\ c_M+0.1763$ ($R^2=0.9965$) (Figure3.32 A and

B) respectively. The detection limit at MWCNT/GC electrode was calculated as $2.66x10^{-8}$ M and $5.33x10^{-8}$ M (S/N=3).

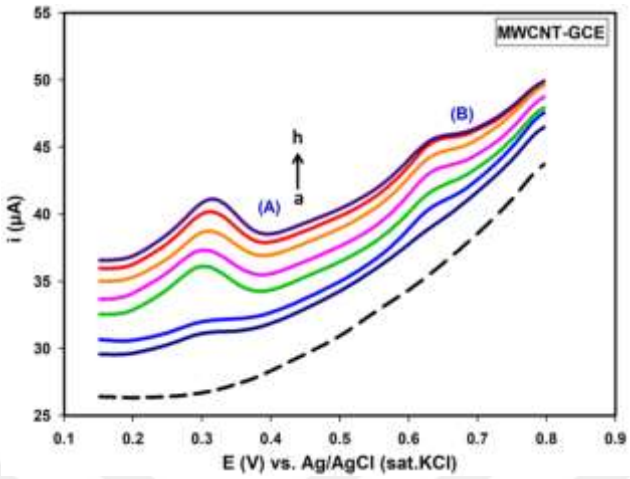

Figure 3.31 Differential pulse voltammograms of MWCNT/GCE for increasing concentration of melatonin in pH 7.0 PBS (0.1 M) with 5 mV/s scan rate and 100 mV pulse amplitude. Melatonin concentrations a) blank, b) $8.0x10^{-8}$ c) $1.0x10^{-7}$ d) $2.0x10^{-7}$ e) $4.0x10^{-7}$ f) $6.0x10^{-7}$ g) $8.0x10^{-7}$ h) $1.0x10^{-6}$ M

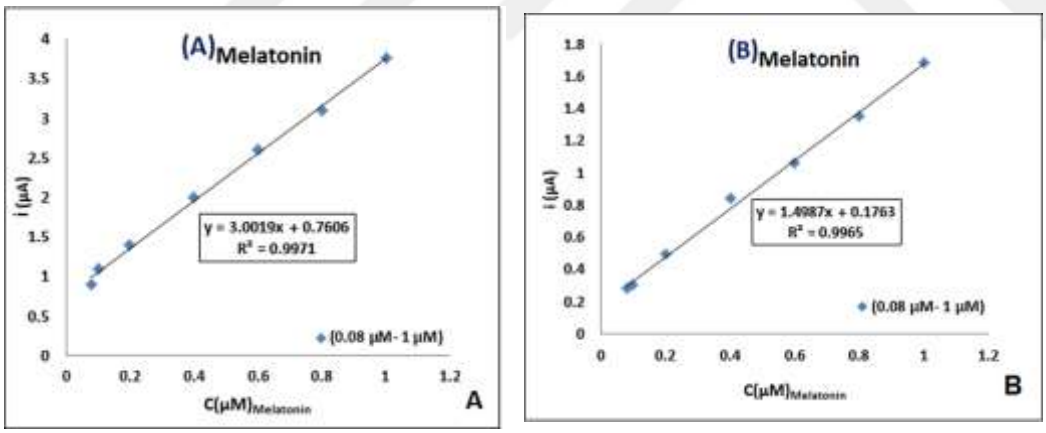

Figure 3.32 Calibration curves for a melatonin oxidation at MWCNT/GCE concentration ranges between $8.0x10^{-8}$ M– $1.0x10^{-6}$ M.

The DPV behaviour of melatonin was studied at MWCNT/PCR/GCE and two oxidation peaks were also observed at 0.3 V and 0.65 V on the MWCNT/PCR/GCE (Figure 3.33). The current values of both oxidation were linearly increased proportional to the concentration of melatonin. The linear range of melatonin on

MWCNT/PCR/GCE was varied from $1.0x10^{-7}$ M to $4x10^{-6}$ M with equation Ip=0.8201 C_A+0.2075 (R^2=0.9939) for first oxidation peak with equation Ip=0.5453 C_A+0.3697 (R^2=0.9905) for second oxidation peak (Figure 3.34A-B) . The detection limit at MWCNT/PCR/GCE was calculated as 9.32 $x10^{-8}$ M and $3.33x10^{-8}$ M (S/N=3).

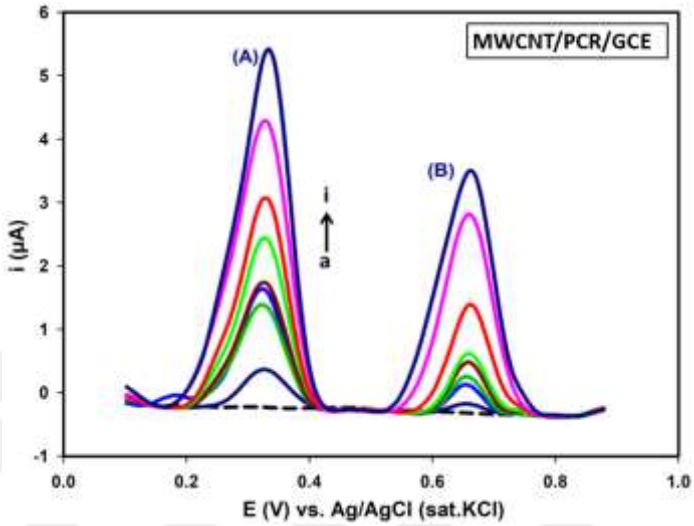

Figure 3.33 Differential pulse voltammograms of MWCNT/PCR/GCE for increasing concentration of melatonin in pH 7.0 PBS (0.1 M) with 5 mV/s scan rate and 100 mV pulse amplitude. Melatonin concentrations a) blank, b)$1.0x10^{-7}$ c) $2.0x10^{-7}$ d) $4.0x10^{-7}$ e)$6.0x10^{-7}$ f) $8.0x10^{-7}$ g)$1.0x10^{-6}$ h) $2.0x10^{-6}$ i) $6.0x10^{-6}$ M

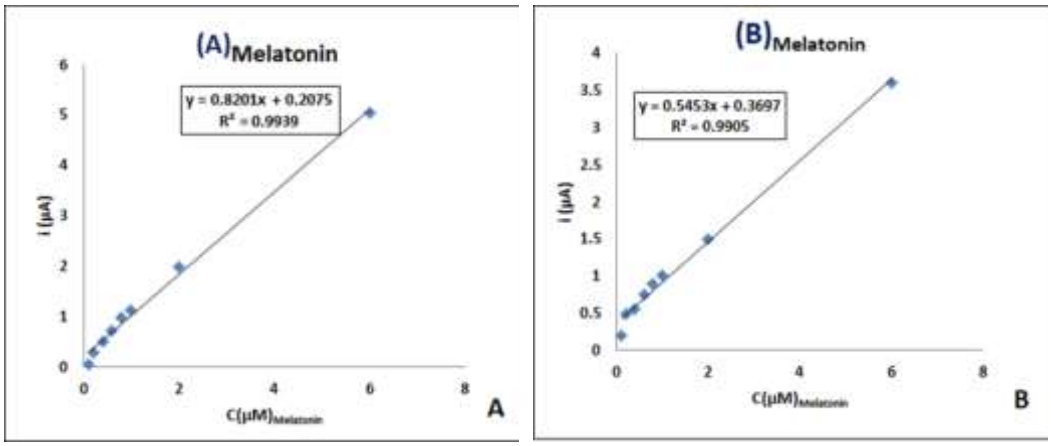

Figure 3.34 Calibration curves for melatonin at MWCNT/PCR/GCE in pH 7.00 PBS

The DPV behaviour of melatonin was investigated at ZnO/MWCNT/GCE and two oxidation peaks were observed at the ZnO/MWCNT/GCE (Figure 3.35). The current values of both oxidation were linearly increased proportional to the concentration of melatonin. The linear range of melatonin on ZnO/MWCNT/GCE was varied from $6.0x10^{-8}$ M to $8.0x10^{-7}$ M with equation $Ip_a=1.2183C_M+0.1581$ ($R^2=0.9967$) for first oxidation peak and $Ip_a=0.5147C_M+0.0981$ ($R^2=0.9917$) for second oxidation peak (Figure 3.36A-B) . The detection limits at MWCNT/GCE were calculated as $4.92x10^{-8}$ M and 1.17 $x10^{-8}$ M (S/N=3) respectivel for both oxidations.

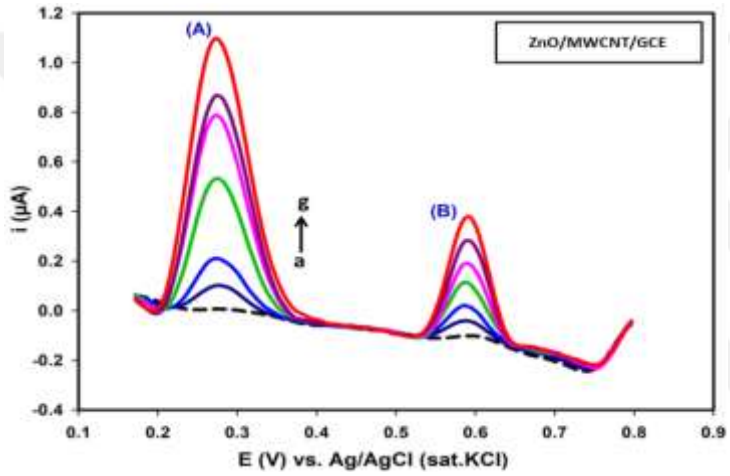

Figure 3.35 Differential pulse voltammograms of ZnO/MWCNT/GCE for increasing concentration of melatonin in pH 7.0 PBS (0.1 M) with 5 mV/s scan rate and 100 mV pulse amplitude. Melatonin concentrations a) blank, b) $6.0x10^{-8}$ c) $8.0x10^{-8}$ d) $2.0x10^{-7}$ e) $4.0x10^{-7}$ f) $6.0x10^{-7}$ g) $8.0x10^{-7}$ M

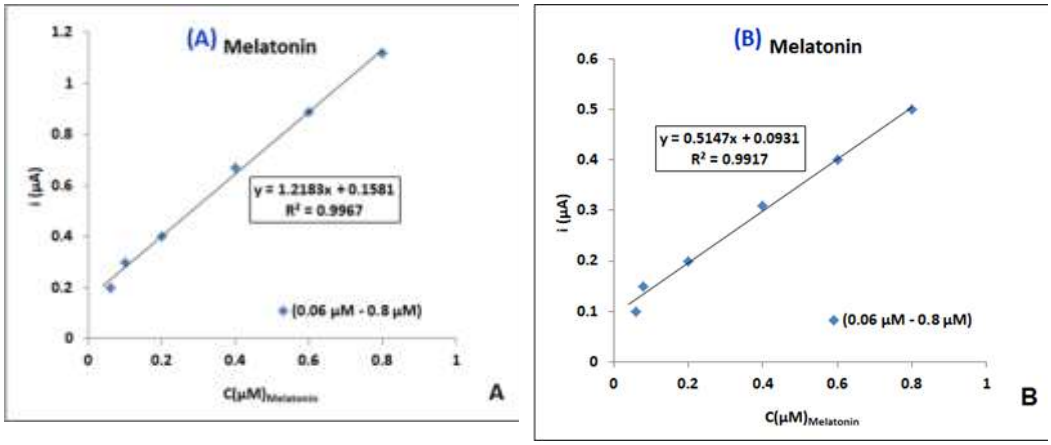

Figure 3.36 Calibration curves for a melatonin oxidation at ZnO/MWCNT/GCE concentration ranges between 6.0x10-8 M– 8.0x10-7 M.

Finally, the DPV behaviour of melatonin was investigated at ZnO/MWCNT/PCR/GCE and two oxidation peaks were observed at the ZnO/MWCNT/PCR/GCE (Figure 3.37). The current values of both oxidation were linearly increased proportional to the concentration of melatonin. The linear range of melatonin on ZnO/MWCNT/PCR/GCE was varied from $1.0x10^{-8}$ M to $6.0x10^{-5}$ M with equation $Ip_a=0.7262C_M+0.0433$ ($R^2=0.9892$) for first oxidation peak and $Ip_a=0.1319C_M+0.0972$ ($R^2=0.9915$) for second oxidation peak (Figure 3.38) . The detection limit at ZnO/MWCNT/PCR/GCE was calculated as $3.33x10^{-9}$ M and $6.67x10^{-7}$ M (S/N=3).

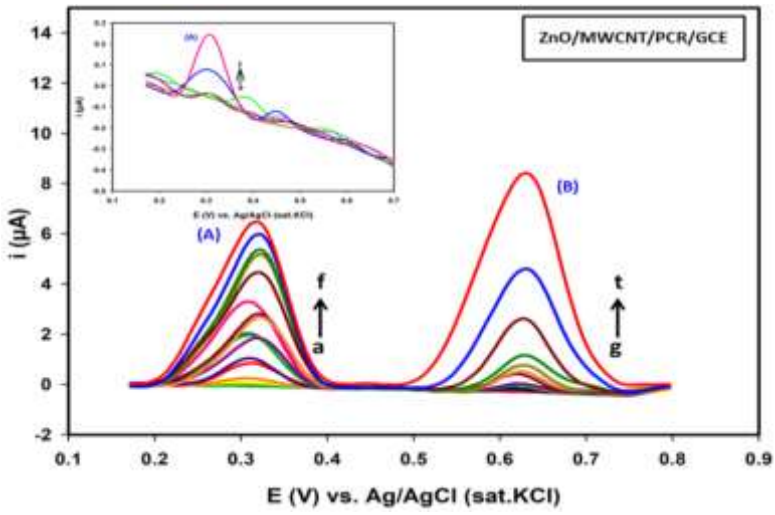

Figure 3.37 Differential pulse voltammograms of ZnO/MWCNT/PCR/GCE for increasing concentrations of melatonin in pH 7.0 PBS (0.1 M) with 5 mV/s scan rate and 100 mV pulse amplitude. Melatonin concentrations For (A) a) blank, b) $1.0x10^{-8}$ c) $2.0x10^{-8}$ d) $4.0x10^{-8}$ e) $6.0x10^{-8}$ f) $8.0x10^{-8}$ M. For (B) g) $2.0x10^{-7}$ h) $4.0x10^{-7}$ i) $6.0x10^{-7}$ j) $8.0x10^{-7}$ k) $1.0x10^{-6}$ l) $2.0x10^{-6}$, m) $4.0x10^{-6}$ n) $6.0x10^{-6}$ o) $8.0x10^{-6}$ p) $1.0x10^{-5}$ r) $2.0x10^{-5}$ s) $4.0x10^{-5}$ t) $6.0x10^{-5}$ M

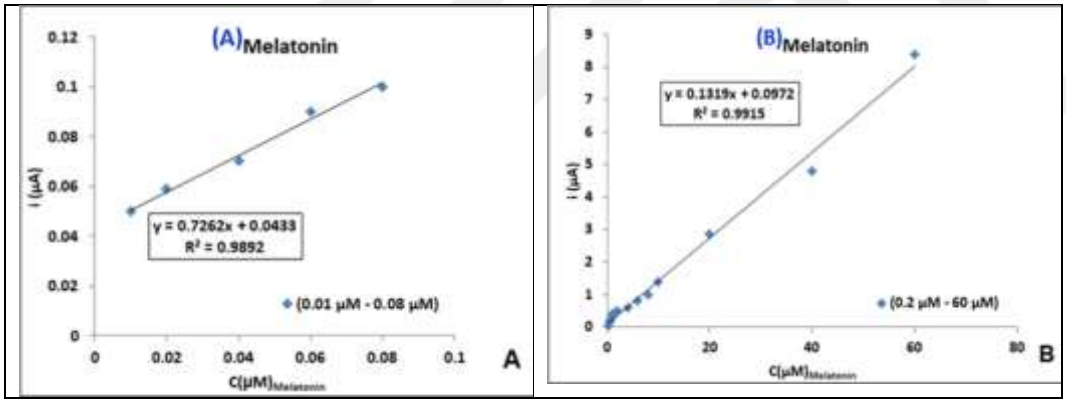

Figure 3.38 Calibration curves for a melatonin oxidation at ZnO/MWCNT/PCR/GCE concentration ranges between $1.0x10^{-8}$ – $6.0x10^{-5}$ M

Comparisons of the bare and modified electrodes in terms of sensitivity, detection limit (LOD) and linear concentration range of melatonin were given in Table 3.14. As seen in Table 3.14 data, **ZnO/MWCNT/PCR/GCE** shows higher activity towards melatonin oxidation and the higher sensitivity low detection limit compare with all electrodes.

Table 3.14 Analytical characteristics for determination of melatonin under optimum conditions.

ANALYTES	MELATONIN (A)	MELATONIN (B)
ELECTRODE	**BARE GCE**	
Calibration Equation	ip_a=2.3372 C_M-0.1776 (R^2=0.9979)	ip_a=0.1151 c_M-0.008 (R^2=0.9981)
Linear Range	$1.0x10^{-7}$ M-$8.0x10^{-7}$ M	$1.0x10^{-7}$ M-$8.0x10^{-7}$ M
LOD	$4.28x10^{-8}$ M	$3.33x10^{-8}$ M
ELECTRODE	**PCR/GCE**	
Calibration Equation	ip_a=3.5116c_A+0.2671 (R^2=0.9943)	ip_a=0.1852 c_A+0.0424 (R^2=0.9958)
Linear Range	$1.0x10^{-7}$ M– $8.0x10^{-7}$ M	$1.0x10^{-7}$ M– $8.0x10^{-7}$ M
LOD	$2.85x10^{-8}$ M	$5.28x10^{-8}$ M
ELECTRODE	**MWCNT/GCE**	
Calibration Equation	ip_a=3.0019 c_M+0.7606 (R^2=0.9971)	ip_a=1.4987 c_M+0.1763 (R^2=0.9965)
Linear Range	$8.0x10^{-8}$ M – $1.0x10^{-6}$ M	$8.0x10^{-8}$ M – $1.0x10^{-6}$ M
LOD	$2.66x10^{-8}$ M	$5.33x10^{-8}$ M
ELECTRODE	**MWCNT/PCR/GCE**	
Calibration Equation	Ip=0.8201 C_A+0.2075 (R^2=0.9939)	Ip=0.5453 C_A+0.3697 (R^2=0.9905)
Linear Range	$1.0x10^{-7}$ M - $4x10^{-6}$ M	$1.0x10^{-7}$ M - $4x10^{-6}$ M
LOD	9.32 $x10^{-8}$ M	$3.33x10^{-8}$ M
ELECTRODE	**ZnO/MWCNT/GCE**	
Calibration Equation	Ip_a=1.2183C_M+0.1581 (R^2=0.9967)	Ip_a=0.5147C_M+0.0981 (R^2=0.9917)
Linear Range	$6.0x10^{-8}$ M - $8.0x10^{-7}$ M	$6.0x10^{-8}$ M - $8.0x10^{-7}$ M
LOD	$4.92x10^{-8}$ M	1.17 $x10^{-8}$ M
ELECTRODE	**ZnO/MWCNT/PCR/GCE**	
Calibration Equation	Ip_a=0.7262C_M+0.0433 (R^2=0.9892)	Ip_a=0.1319C_M+0.0972 (R^2=0.9915)
Linear Range	$1.0x10^{-8}$ M - $8.0x10^{-8}$ M	$2.0x10^{-7}$ M - $6.0x10^{-5}$ M
LOD	$3.33x10^{-9}$ M	$6.67x10^{-7}$ M

Additionally, the obtained data with this study was also compared with the other related published paper on the determination of melatonin Table 3.15. , the developed ZnO/MWCNT/PCR/GCE demostrate high selectivity, LOD and a wide linear range.

Table 3.15 Comparison of some characteristics of the different modified electrodes for the determination of melatonin

Modified electrode	Linear range (M)	LOD (M)	Ref.
GPE Modified with ZnO nanorods and 3-(4-amino-3-hydroxy-biphenyl-4-yl)-acrylic acid (3,4 AAZCPE)	$3.0x10^{-7}$ - $1.0x10^{-4}$	5.6×10^{-8}	Molaakbari et al, 2015
graphene-based sensor screen-printed carbon electrode	$1.0x10^{-6}$ - $3.0x10^{-5}$	0.87×10^{-6}	Apetrei et al, 2016
CPE modified with Al_2O_3-supported palladium nanoparticles	$6.0x10^{-8}$ - $1.4x10^{-4}$	2.1×10^{-8}	Soltani et al, 2019
Carbon black as a GCE	$5.0x10^{-8}$ - $12.0x10^{-6}$	1.9×10^{-8}	Smajdor et al, 2017
AHNSA:PdNPs:ErGO/GCE	$5.0x10^{-6}$ - $1.0x10^{-4}$	$9.0x10^{-8}$	Kumar et al, 2016
ZnO/MWCNT/PCR/GCE	$1.0x10^{-8}$ - $6.0x10^{-5}$	$3.33x10^{-9}$ - $6.67x10^{-7}$	This study

A comparative DPV studies were performed for caffeine depending on its concentration increasing at bare GCE, PCR/GCE, MWCNT/GCE, MWCNT/PCR/GCE, ZnO/MWCT/GCE and ZnO/MWCNT/PCR/GCE. The dependence of peak current on caffeine concentration were shown for each electrode in Figure 3.39-44 respectively. The current respons by increasing concentration of caffeine was linear in the range of $2.0x10^{-5}$ M – $1.0x10^{-4}$ M at bare GCE, $6.0x10^{-7}$ M – $6.0x10^{-5}$ M at PCR/GCE, $1.0x10^{-7}$ M – $6.0x10^{-5}$ M at MWCNT/GCE, $4.0x10^{-7}$ M–$6.0x10^{-5}$M at MWCT/PCR/GCE and $1.0x10^{-7}$M–$2.0x10^{-6}$ M at ZnO/MWCNT/PCR/GCE. Lineer regression equations of i_{pa} $=0.1515c_c$ -2.454 (R^2=9942), i_{pa} $=0.213c_{c+}$ 0.4944 (R^2=99), i_{pa} $=0.1653c_c$ + 0.4332

(R^2=9946), i_{pa} =0.141c_c +0.1131 (R^2=9983), i_{pa} =0.1893c_c +0.5069 (R^2=997), i_{pa} =0.4787c_c +0.0512 (R^2=9971) were obtained, respectively. The detection limits were 6.67x10^{-6} M, 2.0x10^{-7} M, 3.3x10^{-8} M, 1.33x10^{-7} M, 2.67x10^{-8} M, 4.28x10^{-8} M, 3.0x10^{-8}M for caffeine, respectively. The best result was obtained with ZnO/MWCNT/PCR/GCE.

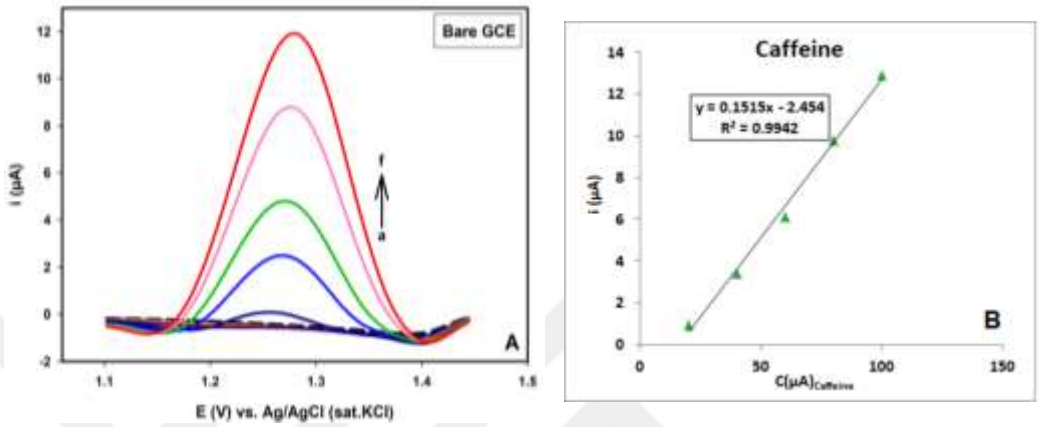

Figure 3.39 A) Differential pulse voltammograms of bare GCE for increasing concentrations of caffeine in pH 7.0 PBS (0.1 M) with 20 mV/s scan rate and 150 mV pulse amplitude. **B)** Calibration curves for caffeine oxidation at bare GCE. Caffeine concentrations: a) blank, b) 2.0x10^{-5} c) 4.0x10^{-5} d) 6.0x10^{-5} e) 8.0x10^{-5} f) 1.0x10^{-4} M

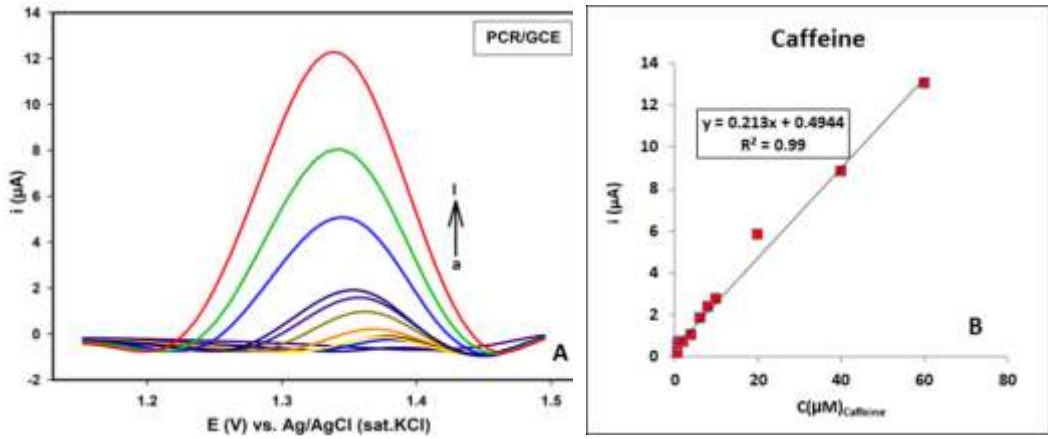

Figure 3.40 A) Differential pulse voltammograms of PCR/GCE for increasing concentrations of caffeine in pH 7.0 PBS (0.1 M) with 20 mV/s scan rate and 150 mV pulse amplitude. **B)** Calibration curves for caffeine oxidation at PCR/GCE. Caffeine concentrations: a) blank, b) 6.0x10^{-7} c) 8.0x10^{-7} d) 1.0x10^{-6} e) 2.0x10^{-6} f) 4.0x10^{-6} g) 6.0x10^{-6} h) 8.0x10^{-6} i) 1.0x10^{-5} j) 2.0x10^{-5} k) 4.0x10^{-5} l) 6.0x10^{-5} M

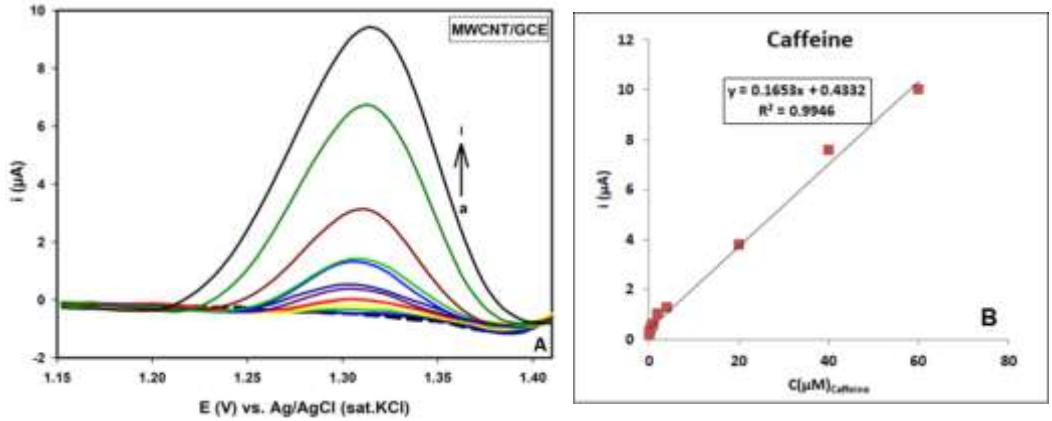

Figure 3.41 A) Differential pulse voltammograms of MWCNT/GCE for increasing concentrations of caffeine in pH 7.0 PBS (0.1 M) with 20 mV/s scan rate and 150 mV pulse amplitude. **B)** Calibration curves: Caffeine concentrations a) blank, b) $1.0x10^{-7}$ c) $2.0x10^{-7}$ d) $4.0x10^{-7}$ e) $6.0x10^{-7}$ f) $8.0x10^{-7}$ g) $1.0x10^{-6}$ h) $2.0x\ 10^{-6}$ i) $4.0x10^{-6}$ j) $2.0x\ 10^{-5}$ k) $4.0x\ 10^{-5}$ l) $6.0x\ 10^{-5}$ M

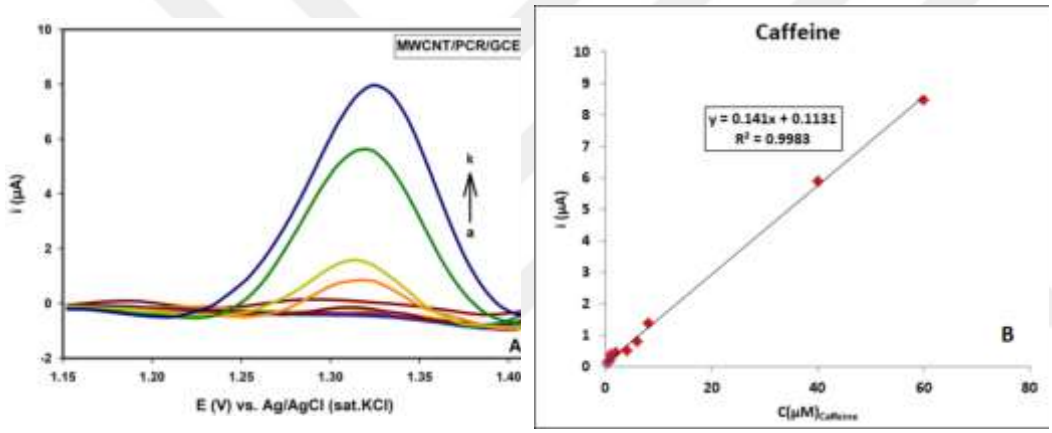

Figure 3.42 A) Differential pulse voltammograms of MWCNT/PCR/GCE for increasing concentrations of caffeine in pH 7.0 PBS (0.1 M) with 20 mV/s scan rate and 150 mV pulse amplitude. **B)** Calibration curves for caffeine oxidation at MWCNT/PCR/GCE. Caffeine concentrations: a) blank, b) $4.0x10^{-7}$ M, c) $6.0x10^{-7}$ M d) $8.0x10^{-7}$ e) $1.0x10^{-6}$ f) $2.0x10^{-6}$ g) $4.0x10^{-6}$ h) $6.0x\ 10^{-6}$ i) $8.0x10^{-6}$ j) $4.0x10^{-5}$ k) $6.0x10^{-5}$ M

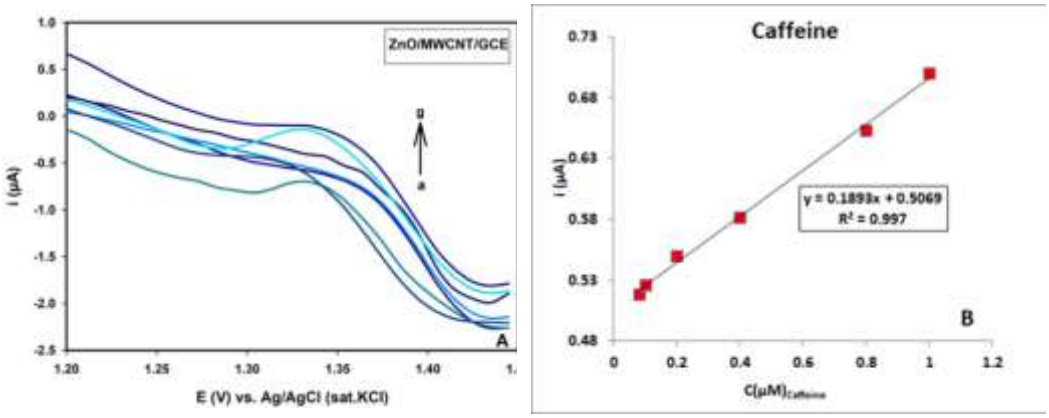

Figure 3.43 A) Differential pulse voltammograms of ZnO/MWCNT/GCE for increasing concentrations of caffeine in pH 7.0 PBS (0.1 M) with 20 mV/s scan rate and 150 mV pulse amplitude.**B)** Calibration curves for caffeine oxidation at ZnO/MWCNT/GCE. Caffeine concentrations: a) blank, b) $8.0x10^{-8}$ c) $1.0x10^{-7}$ d) $2.0x10^{-7}$ e) $4.0x10^{-7}$ f) $8.0x10^{-7}$ g) $1.0x10^{-7}$ M

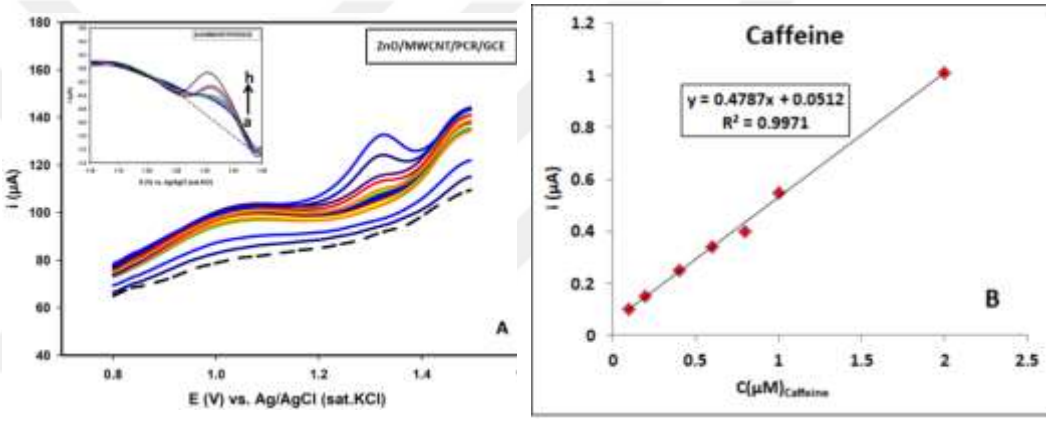

Figure 3.44 A) Differential pulse voltammograms of ZnO/MWCNT/PCR/GCE for increasing concentrations of caffeine in pH 7.0 PBS (0.1 M) with 20 mV/s scan rate and 150 mV pulse amplitude. Inset: DPV's obtained at ZnO/MWCNT/PCR/GCE in the absence. **B)** Calibration curves for caffeine oxidation at ZnO/MWCNT/PCR/GCE. Caffeine concentrations: a) blank, b) $1.0x10^{-7}$ c) $2.0x10^{-7}$ d) $4.0x10^{-7}$ e) $6.0x10^{-7}$ f) $8.0x10^{-7}$ g) $1.0x10^{-6}$ h) $2.0x10^{-6}$ M

Comparisons of the bare and modified electrodes in terms of sensitivity, detection limit (LOD) and linear concentration range of caffeine were given in Table 3.16. As seen in Table 3.16 data, **ZnO/MWCNT/PCR/GCE** shows higher activity towards melatonin oxidation and the higher sensitivity low detection limit compare with all electrodes.

Table 3.16 Analytical characteristics for determination of caffeine under optimum conditions.

ANALYTES	CAFFEINE
ELECTRODE	**BARE GCE**
Calibration Equation	ipa =0.1515cc -2.454 (R^2=9942)
Linear Range	$2.0x10^{-5}$ M – $1.0x10^{-4}$ M
LOD	$6.67x10^{-6}$ M
ELECTRODE	**PCR/GCE**
Calibration Equation	ipa =0.213cc+ 0.4944 (R^2=99)
Linear Range	$6.0x10^{-7}$ M – $6.0x10^{-5}$ M
LOD	$2.0x10^{-7}$ M
ELECTRODE	**MWCNT/GCE**
Calibration Equation	ipa =0.1653cc + 0.4332 (R^2=9946)
Linear Range	$1.0x10^{-7}$ M – $6.0x10^{-5}$ M
LOD	$3.3x10^{-8}$ M
ELECTRODE	**MWCNT/PCR/GCE**
Calibration Equation	ipa =0.141cc +0.1131 (R^2=9983)
Linear Range	$4.0x10^{-7}$ M–$6.0x10^{-5}$M
LOD	$1.33x10^{-7}$ M
ELECTRODE	**ZnO/MWCNT/GCE**
Calibration Equation	ipa =0.1893cc +0.5069(R^2=997)
Linear Range	$8.0x10^{-8}$ M- $1.0x10^{-7}$ M
LOD	$2.67x10^{-8}$ M
ELECTRODE	**ZnO/MWCNT/PCR/GCE**
Calibration Equation	ipa =0.4787cc +0.0512 (R^2=9971)
Linear Range	$1.0x10^{-7}$M – $2.0x10^{-6}$ M
LOD	$3.0x10^{-8}$M

Moreover, the obtained data with this study was also compared with the other related published paper on the determination of caffeine Table 3.17. , the developed ZnO/MWCNT/PCR/GCE demostrate high selectivity, LOD and a wide linear range.

Table 3.17 Comparison of some characteristics of the different modified electrodes for the determination of caffeine

Modified electrode	Linear range (M)	LOD (M)	Ref.
(Nafion–Gr/GCE)	$4.0x10^{-7}$-$4.0x10^{-5}$	$1.2x10^{-7}$	Yong-Sun et al, 2011
Bare/(EPPGE) edge plane pyrolytic graphite electrode	$2.0x10^{-8}$- $1.0x10^{-4}$	8.0×10^{-9}	Goyal et al, 2011
MWCNT/GCE	$1.0x10^{-5}$ - $5.0x10^{-4}$	3.52×10^{-9}	Gupta et al, 2013
Poly(AHNSA)/GCE	$6.0x10^{-8}$ – $4.0x10^{-5}$	6.7×10^{-8}	Amare et al, 2012
AHNSA:PdNPs:ErGO/GCE	$5.0x10^{-7}$ - $8.3x10^{-5}$	$3.5x10^{-8}$	Lourenção et al, 2016
ZnO/MWCNT/PCR/GCE	$1.0x10^{-7}$ - $2.0x10^{-6}$	$3.0x10^{-8}$	This study

3.9. Simultaneous Voltammetric Determination of Melatonin and Caffeine by Differential Pulse Voltammetry

DPV have higher current sensitivity towards the analytes than CV, especially for simultaneous determination Figure 3.45, Figure 3.46 and Figure 3.47 indicate DP voltammograms attained for only caffeine concentration varying, while the concentration of melatonin was kept constant as $5.0x10^{-6}$ M at MWCNT/GCE, MWCNT/PCR/GCE and ZnO/MWCNT/PCR/GCE in pH 7.00 PBS. As shown in Figures 3.45-46-47, the oxidation peak current of caffeine increased linearly with increasing of its concentration at all electrodes. The increasing of caffeine concentration did not cause a significant chance in both the peak potential and the peak current of melatonin. In this conditions, the peak current of caffeine was linear in the concentration range between $1.0x10^{-7}$ M– $6.0x10^{-6}$ M for MWCNT/GCE, $1.0x10^{-8}$ M to $1.0x10^{-6}$ M for MWCNT/PCR/GCE and

$6.0x10^{-8}$ M - $4.0x10^{-5}$ M for ZnO/MWCNT/PCR/GCE. For MWCNT/GCE, the linear regression equation of caffeine calibration curve was attined as $ip_a=0.2526c_C+0.2473$ ($R^2=0.9936$). For MWCNT/PCR/GCE, the linear regression equation of caffeine calibration curve was attined as $ip_a=6.0432c_C+0.0794$ ($R^2=0.9979$) and for ZnO/MWCNT/PCR/GCE, $ip_a=0.2341c_C+1.8085$ ($R^2=0.9992$) respectively. The detection limit was evaluated as $2.0x10^{-8}$ M for caffeine (S/N=3).

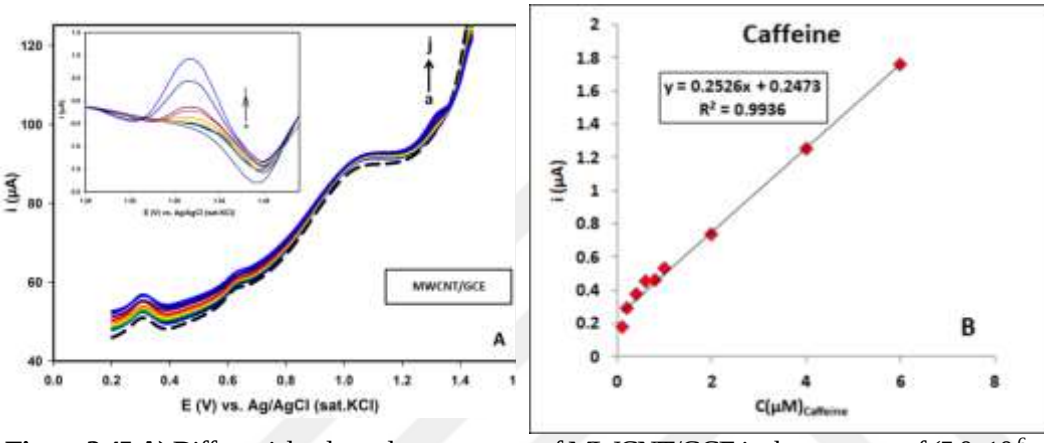

Figure 3.45 A) Differential pulse voltammograms of MWCNT/GCE in the presence of ($5.0x10^{-6}$ M) melatonin for increasing concentrations of caffeine in 0.1 M pH 7.0 posphate buffer solution (0.1 M) with 20 mV/s scan rate and 100 mV pulse amplitude. Inset: DPV's obtained at ZnO/MWCNT/PCR/GCE in the absence. **B)** Calibration curves for caffeine oxidation at MWCNT/GCE. Caffeine concentrations: a) blank, b) $1.0x10^{-7}$ c) $2.0x10^{-7}$ d) $4.0x10^{-7}$ e) $6.0x10^{-7}$ f) $8.0x10^{-7}$, g)$1.0x10^{-6}$ h) $2.0x10^{-6}$ i) $4.0x10^{-6}$ j) $6.0x10^{-6}$ M

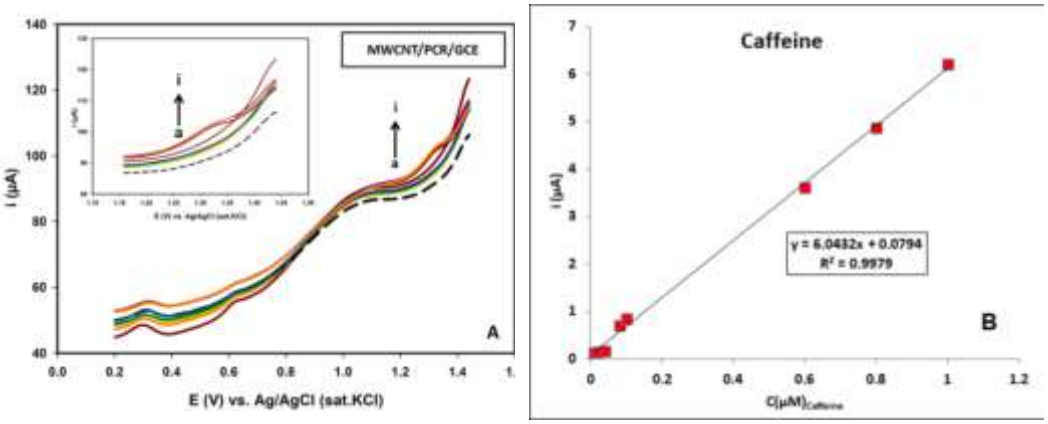

Figure 3.46 A) Differential pulse voltammograms of MWCNT/PCR/GCE in the presence of ($5.0x10^{-6}$ M) melatonin for increasing concentrations of caffeine in 0.1 M pH 7.0 posphate buffer solution (0.1 M) with 20 mV/s scan rate and 100 mV pulse amplitude. **B)** Calibration curves for caffeine oxidation at MWCNT/PCR/GCE. Caffeine concentrations: a) blank, b) $1.0x10^{-8}$ c) $2.0x10^{-8}$ d) $4.0x10^{-8}$ e) $8.0x10^{-8}$ f) $1.0x10^{-7}$, g) $6.0x10^{-7}$ h) $8.0x10^{-7}$ i) $1.0x10^{-6}$ M

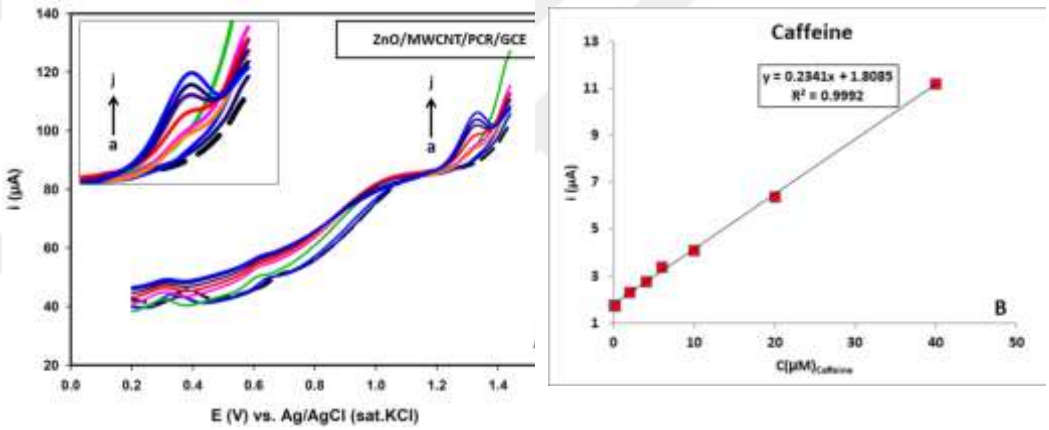

Figure 3.47 A) Differential pulse voltammograms of ZnO/MWCNT/PCR/GCE in the presence of ($5.0x10^{-6}$ M) melatonin for increasing concentrations of caffeine in 0.1 M pH 7.0 posphate buffer solution (0.1 M) with 20 mV/s scan rate and 100 mV pulse amplitude. **B)** Calibration curves for caffeine oxidation at ZnO/MWCNT/PCR/GCE. Caffeine concentrations: a) blank, b) $6.0x10^{-8}$ c) $8.0x10^{-8}$ d) $1.0x10^{-7}$ e) $2.0x10^{-6}$ f) $4.0x10^{-6}$, g) $6.0x10^{-6}$ h) $1.0x10^{-5}$ i) $2.0x10^{-5}$ j) $4.0x10^{-5}$ M

Comparisons of the bare and modified electrodes in terms of sensitivity, detection limit (LOD) and linear concentration range of caffeine in the presence of

($5.0x10^{-6}$ M) melatonin for increasing concentrations of caffeine in 0.1 M pH 7.0 posphate buffer solution (0.1 M) with 20 mV/s scan rate and 100 mV pulse amplitude.were given in Table 3.18.

Table 3.18 Analytical characteristics for determination of caffeine in the presence of ($5.0x10^{-6}$ M) melatonin for increasing concentrations of caffeine under optimum conditions

ANALYTES	**CAFFEINE**
ELECTRODE	**MWCNT/GCE**
Calibration Equation	$ip_a=0.2526c_C+0.2473$ ($R^2=0.9936$)
Linear Range	$1.0x10^{-7}$ M– $6.0x10^{-6}$ M
LOD	$3.33x10^{-8}$ M
ELECTRODE	**MWCNT/PCR/GCE**
Calibration Equation	$ip_a=6.0432c_C+0.0794$ ($R^2=0.9979$)
Linear Range	$1.0x10^{-8}$ M - $1.0x10^{-6}$ M
LOD	$3.32x10^{-9}$ M
ELECTRODE	**ZnO/MWCNT/PCR/GCE**
Calibration Equation	$ip_a=0.2341c_C+1.8085$ ($R^2=0.9992$)
Linear Range	$6.0x10^{-8}$ M - $4.0x10^{-5}$ M
LOD	$2.0x10^{-8}$ M

Figure 3.48, Figure 3.50, Figure 3.52 were demostrated DPV's achieved by increasing melatonin concentrations, meanwhile the concentration of caffeine was kept constant as $1.0x10^{-5}$ M in pH 7.00 PBS at MWCNT/GCE, MWCNT/PCR/GCE and ZnO/MWCNT/PCR/GCE.

The oxidation peaks current of melatonin linearly increased by depending on its concentration at three electrodes in the presence of $1.0x10^{-5}$ M in pH 7.00 PBS. The peak currents of caffeine were sligthly changed by increasing of melatonin concentration.

In the present conditions, the peaks current of melatonin were linear in the concentration range between $8.0x10^{-7}$ M- $1.0x10^{-5}$ M for MWCNT/GCE, $1.0x10^{-8}$ M- $1.0x10^{-6}$ M for MWCNT/PCR/GCE and $1.0x10^{-8}$ M - $1.0x10^{-6}$ M for ZnO/MWCNT/PCR/GCE. For MWCNT/GCE, the linear regression equations of two calibration curves for melatonin were obtained as $i_{pa}=0.5022c_M+1.0028$ ($R^2=0.9973$) for $(A)_{Melatonin}$ and $ip_a=0.1842c_M+0.4316$ ($R^2=0.9963$) for $(B)_{Melatonin}$. The detection limit was calculated as $2.67x10^{-7}$ M and $2.53x10^{-8}$ M (S/N=3). For MWCNT/PCR/GCE, the linear regression equations of two calibration curves for melatonin were obtained as $i_{pa}=1.9076c_M-0.0292$ ($R^2=0.9955$) for $(A)_{Melatonin}$ and $ip_a=1.5019c_M+0.0556$ ($R^2=0.9982$) for $(B)_{Melatonin}$. The detection limit was calculated as $3.3x10^{-9}$ M and $9.16x10^{-9}$ M (S/N=3). For ZnO/MWCNT/PCR/GCE, the linear regression equations of two calibration curves for melatonin were obtained as $i_{pa}=2.3204c_M-0.0403$ ($R^2=0.9986$) for $(A)_{Melatonin}$ and $ip_a=0.6305c_M-0.0137$ ($R^2=0.9968$) for $(B)_{Melatonin}$. The detection limit was calculated as $3.33x10^{-9}$ M and $2.0x10^{-8}$ M (S/N=3).

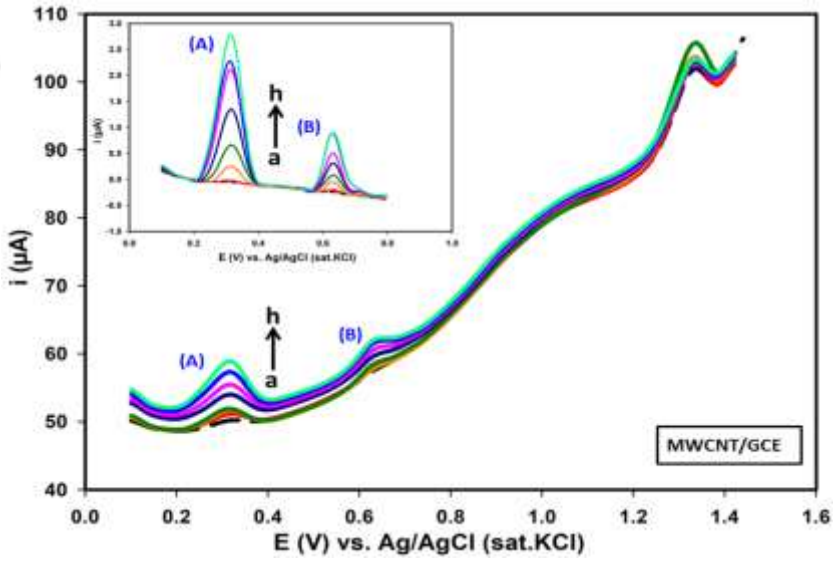

Figure 3.48 Differential pulse voltammograms of MWCNT/GCE in the presence of ($1.0x10^{-5}$ M) caffeine for increasing concentrations of melatonin in 0.1 M pH 7.0 PBS (0.1 M) with 20 mV/s scan rate and 100 mV pulse amplitude. Melatonin concentrations: a) $8.0x10^{-7}$ b) $1.0x10^{-6}$ d) $2.0x10^{-6}$ e) $4.0x10^{-6}$ f) $6.0x10^{-6}$ g) $8.0\ x10^{-6}$ h) $1.0x\ 10^{-5}$ M

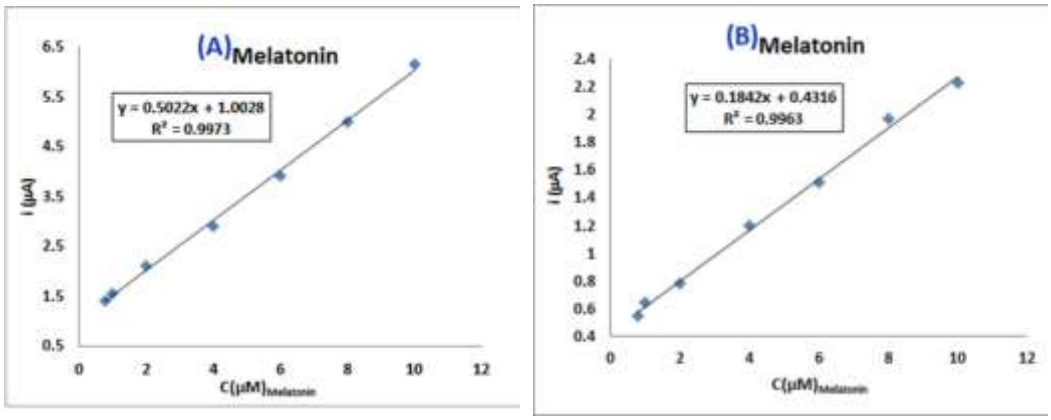

Figure 3.49 Calibration curves for a caffeine oxidation at MWCNT/GCE in the presence of ($1.0x10^{-5}$ M) caffeine for increasing of melatonin concentration ranges between $8.0x10^{-7}$ M-$1.0x10^{-5}$ M

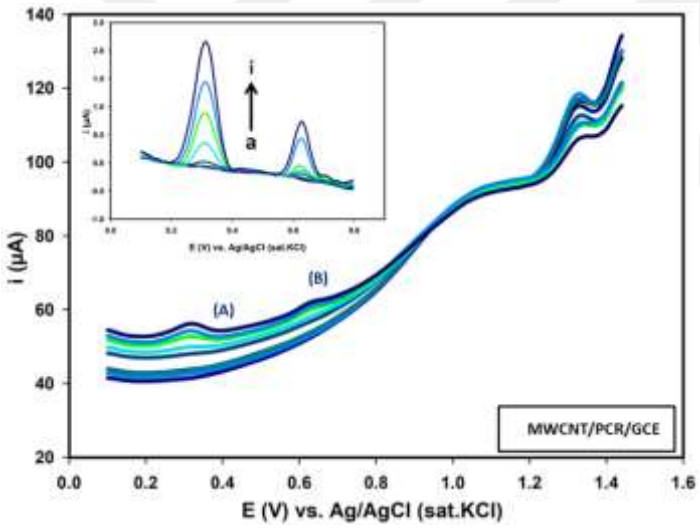

Figure 3.50 Differential pulse voltammograms of MWCNT/PCR/GCE in the presence of ($1.0x10^{-5}$ M) caffeine for increasing concentrations of melatonin in 0.1 M pH 7.0 PBS (0.1 M) with 20 mV/s scan rate and 100 mV pulse amplitude. For (A), a) blank, b) $1.0x10^{-8}$ c) $2.0x10^{-8}$ d) $4.0x10^{-8}$ e) $1.0x10^{-7}$ f) $2.0x10^{-7}$ g) $6.0x10^{-7}$ h) $8.0x10^{-7}$ i) $1.0x10^{-6}$ M. For (B) , b) $1.0x10^{-8}$ c) $2.0x10^{-8}$ d) $4.0x10^{-8}$ e) $1.0x10^{-7}$ f) $2.0x10^{-7}$, g) $6.0x10^{-7}$ M

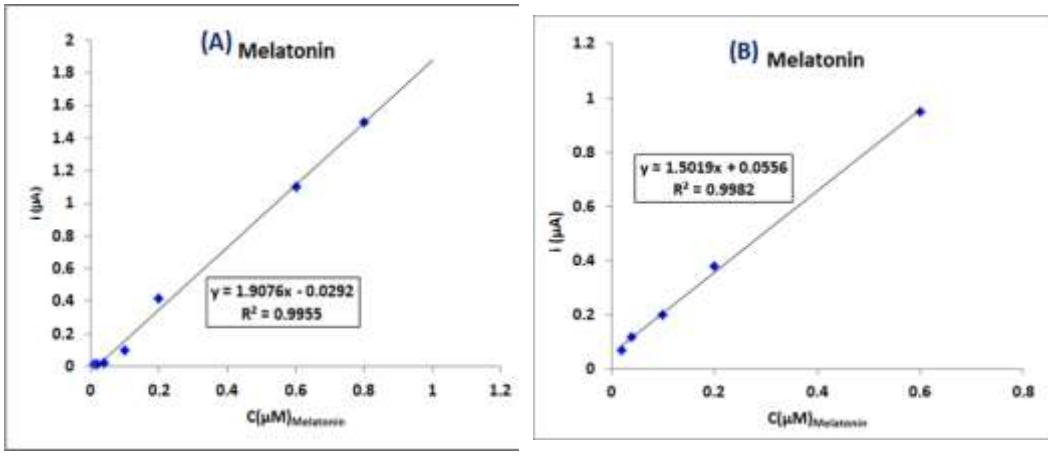

Figure 3.51 Calibration curves for a caffeine oxidation at MWCNT/GCE in the presence of ($1.0x10^{-5}$ M) caffeine for increasing of melatonin concentration ranges between $1.0x10^{-8}$- $1.0x10^{-6}$ M.

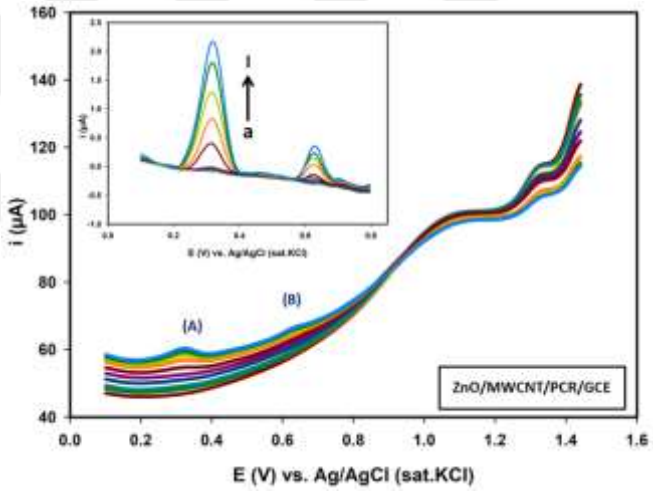

Figure 3.52 Differential pulse voltammograms of ZnO/MWCNT/PCR/GCE in the presence of ($1.0x10^{-5}$ M) caffeine for increasing concentrations of melatonin in 0.1 M pH 7.0 PBS (0.1 M) with 20 mV/s scan rate and 100 mV pulse amplitude.(Inset: Corresponding calibration curve of increasing melatonin concentrations). Melatonin concentrations For (A), a) blank, b) $1.0x10^{-8}$ c) $2.0x10^{-8}$ d) $4.0x10^{-8}$ e) $6.0x10^{-8}$ f) $8.0x10^{-8}$ g) $1.0x10^{-7}$ h) $2.0x10^{-7}$ i) $4.0x10^{-7}$ j) $6.0x10^{-7}$ k) $8.0x10^{-7}$ l) $1.0x10^{-6}$ M. For (B) e) $6.0x10^{-8}$ f) $8.0x10^{-8}$ g) $1.0x10^{-7}$ h) $2.0x10^{-7}$ i) $4.0x10^{-7}$ j) $6.0x10^{-7}$, k) $8.0x10^{-7}$ l) $1.0x10^{-6}$ M

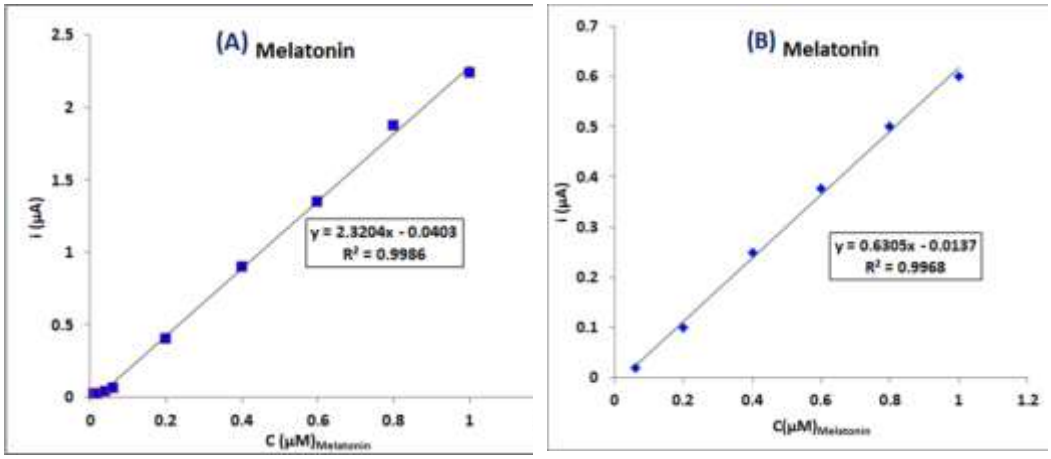

Figure 3.53 Calibration curves for a caffeine oxidation at ZnO/MWCNT/PCR/GCE in the presence of $(1.0x10^{-5}$ M) caffeine for increasing of melatonin concentration ranges between $1.0x10^{-8}$ M - 1.0x10-6 M

Comparisons of the bare and modified electrodes in terms of sensitivity, detection limit (LOD) and linear concentration range of melatonin in the presence of ($1.0x10^{-5}$ M) caffeine for increasing concentrations of melatonin in 0.1 M pH 7.0 posphate buffer solution (0.1 M) with 20 mV/s scan rate and 100 mV pulse amplitude.were given in Table 3.19.

Table 3.19 Analytical characteristics for determination of melatonin in the presence of ($1.0x10^{-5}$ M) caffeine for increasing concentrations of melatonin under optimum conditions

ANALYTES	**MELATONIN (A)**	**MELATONIN (B)**
ELECTRODE	**MWCNT/GCE**	
Calibration Equation	$i_{pa}=0.5022c_M+1.0028$ ($R^2=0.9973$)	$ip_a=0.1842c_M+0.4316$ ($R^2=0.9963$)
Linear Range	$8.0x10^{-7}$ M- $1.0x10^{-5}$ M	$8.0x10^{-7}$ M- $1.0x10^{-5}$ M
LOD	$2.67x10^{-7}$ M	$2.53x10^{-8}$ M
ELECTRODE	**MWCNT/PCR/GCE**	
Calibration Equation	$i_{pa}=1.9076c_M-0.0292$ ($R^2=0.9955$)	$ip_a=1.5019c_M+0.0556$ ($R^2=0.9982$)
Linear Range	$1.0x10^{-8}$ M- $1.0x10^{-6}$ M	$1.0x10^{-8}$ M- $6.0x10^{-7}$ M
LOD	$3.3x10^{-9}$ M	$9.16x10^{-9}$ M
ELECTRODE	**ZnO/MWCNT/PCR/GCE**	
Calibration Equation	$i_{pa}=2.3204c_M-0.0403$ ($R^2=0.9986$)	$ip_a=0.6305c_M-0.0137$ ($R^2=0.9968$)
Linear Range	$1.0x10^{-8}$ M- $1.0x10^{-6}$ M	$6.0x10^{-8}$ M- $1.0x10^{-6}$ M
LOD	$3.33x10^{-9}$ M	$2.0x10^{-8}$ M

As display in the Figure 3.54, Figure 3.56 and Figure 3.58, the oxidation peak currents were incraesed lienarly by simultaneously incraesing concentrations of melatonin and caffeine at the all electrodes. The linear variation of oxidation peaks current were obatained in the concentration for melatonin and caffeine in range between $8.0x10^{-7}$M- $8.0x10^{-5}$ M for MWCNT/GCE, 4.0 $x10^{-7}$ M- 2.0 $x10^{-5}$ M for MWCNT/PCR/GCE and $4.0x10^{-8}$ M-$4.0x10^{-7}$ M for ZnO/MWCNT/PCR/GCE. For MWCNT/GCE the linear regression equations of three calibration curves were obtained as $ip_a=0.1935c_M+4.727$ ($R^2=0.9972$) for $(A)_{Melatonin}$ and $ip_a=0.2226c_M+1.301$ ($R^2=0.9953$) for $(B)_{Melatonin}$ and $ip_a=0.1685c_C+0.7124$ ($R^2=0.9963$) for caffeine respectively. The detection limit was evaluated as $6.67x10^{-7}$ M, $2.67x10^{-7}$ M and 4.74 $x10^{-7}$ M (S/N=3) for MWCNT/GCE. For MWCNT/PCR/GCE the linear regression equations of three calibration curves were obtained as $ip_a=0.5026c_M+3.282$ ($R^2=0.9974$) for $(A)_{Melatonin}$ and $ip_a=0.1862c_M+0.5181$ ($R^2=0.9902$) for $(B)_{Melatonin}$ and $ip_a=0.1264c_C+0.5264$

(R^2=0.9918) for caffeine respectively. For MWCNT/PCR/GCE, the detection limit was evaluated as $2.0x10^{-7}$ M, $1.33x10^{-7}$ M and 1.33 $x10^{-7}$ M (S/N=3). For ZnO/MWCNT/PCR/GCE the linear regression equations of three calibration curves were obtained as $ip_a=2.881c_M-0.1624$ (R^2=0.9985) for $(A)_{Melatonin}$ and $ip_a=0.6308c_M+0.07$ (R^2=0.9959) for $(B)_{Melatonin}$ and $ip_a=0.8787c_C+0.1676$ (R^2=0.9994) for caffeine respectively. The detection limit was evaluated as $1.38x10^{-8}$ M for (A) and $(B)_{Melatonin}$ $1.33x10^{-8}$ M for caffeine (S/N=3).

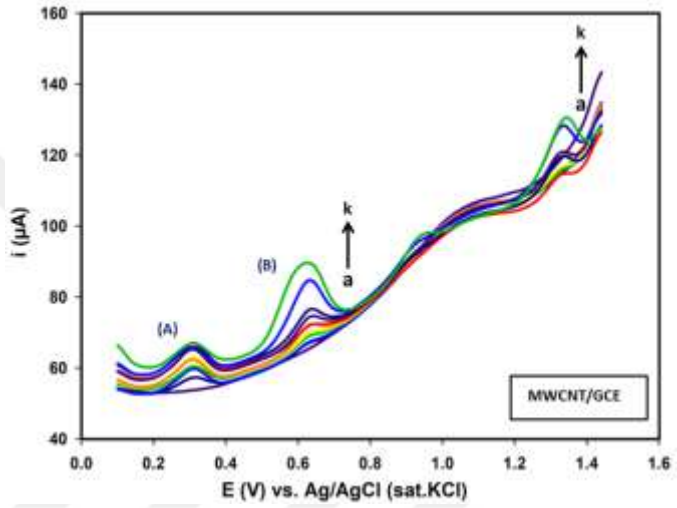

Figure 3.54 Differential pulse voltammograms of MWCNT/GCE in the presence of for increasing concentrations of melatonin and caffeine in 0.1 M pH 7.0 PBS (0.1 M) with 20 mV/s scan rate and 100 mV pulse amplitude. Melatonin and caffeine concentrations: For (B) and caffeine a) blank, b) $8.0x10^{-7}$ c) $1.0x10^{-6}$ d) $2.0x10^{-6}$ e) $4.0x10^{-6}$ f) $6.0x10^{-6}$ g) $8.0x10^{-6}$ h) $1.0x10^{-5}$ i) $2.0x10^{-5}$ j) $4.0x10^{-5}$ k) $8.0x10^{-5}$ M. For (A) d) $2.0x10^{-6}$ e) $4.0x10^{-6}$ f) $6.0x10^{-6}$ g) $8.0x10^{-6}$ h) $1.0x10^{-5}$ M

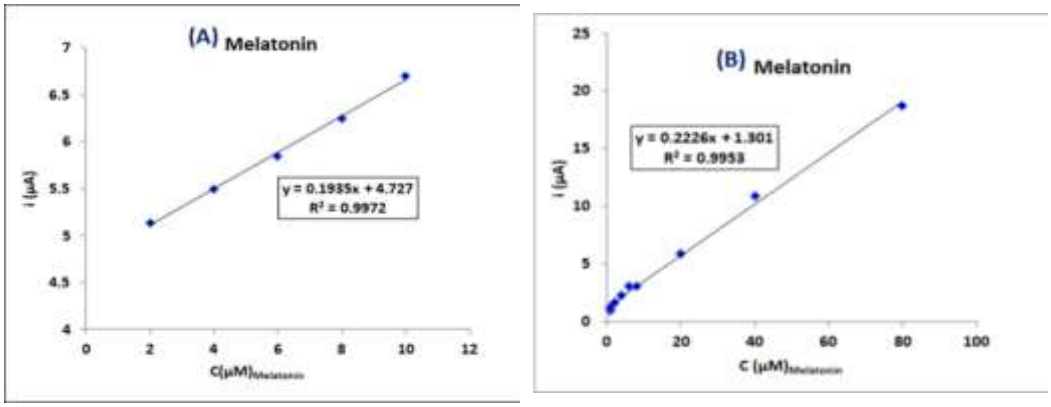

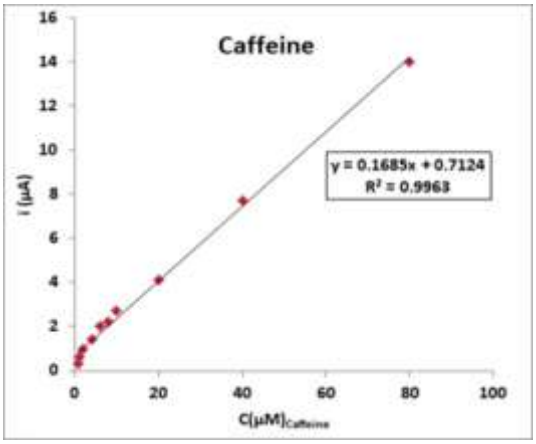

Figure 3.55 Calibration curves for a caffeine oxidation at MWCNT/GCE in the presence of for increasing of melatonin and caffeine concentration ranges between $8.0x10^{-7}$- $8.0x10^{-5}$ M

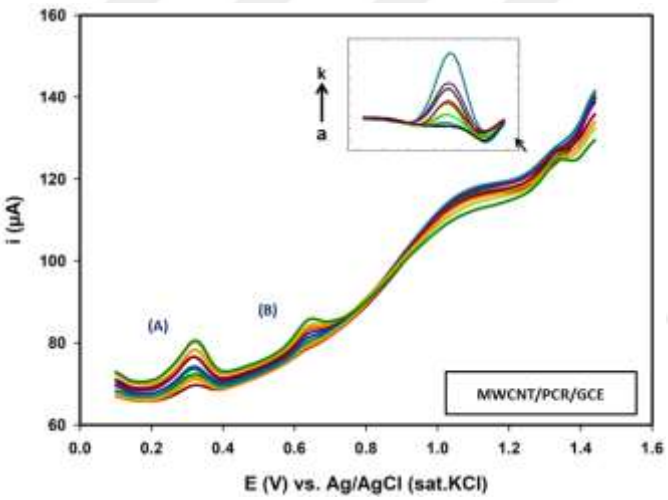

Figure 3.56 Differential pulse voltammograms of MWCNT/PCR/GCE in the presence of for increasing concentrations of melatonin and caffeine in 0.1 M pH 7.0 PBS (0.1 M) with 20 mV/s scan rate and 100 mV pulse amplitude. Melatonin and caffeine concentrations: For (B) and caffeine a) blank, b) $4.0x10^{-7}$ c) $6.0x10^{-7}$ d) $8.0x10^{-7}$ e) $1.0x10^{-6}$ f) $2.0x10^{-6}$ g) $4.0x10^{-6}$ h) $6.0x10^{-6}$ i) $8.0x10^{-6}$ j) $1.0x10^{-5}$ k) $2.0x10^{-5}$ M. For (A) c) $6.0x10^{-7}$ M, d) $8.0x10^{-7}$ M, e) $1.0x10^{-6}$M, f) $2.0x10^{-6}$ M, g) $4.0x10^{-6}$ M, h) $6.0x10^{-6}$ M, i) $8.0x10^{-6}$ M, j)$1.0x10^{-5}$ M

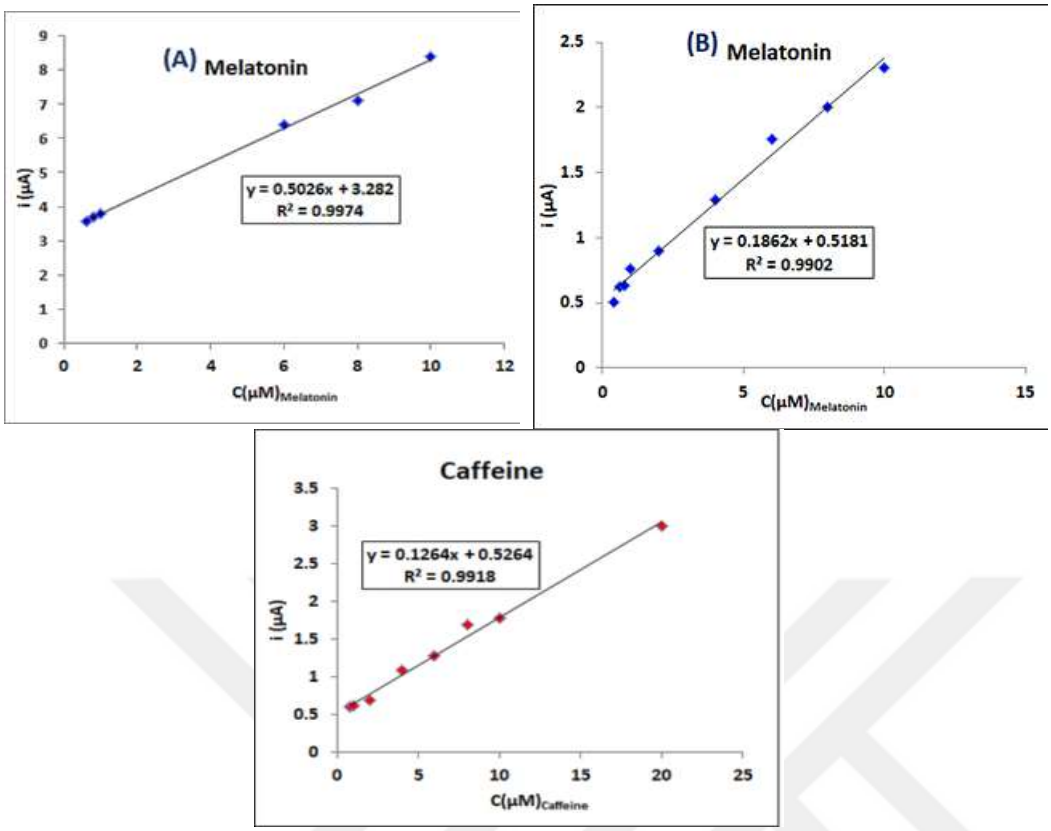

Figure 3.57 Calibration curves for a caffeine oxidation at MWCNT/PCR/GCE in the presence of for increasing of melatonin and caffeine concentration ranges between 4.0 x10^{-7}- 2.0 x10^{-5} M

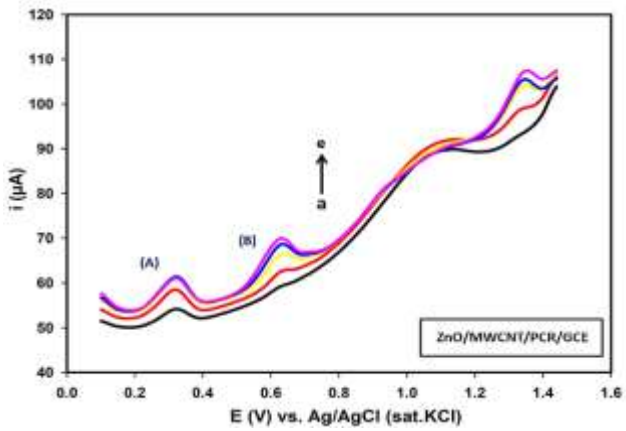

Figure 3.58 Differential pulse voltammograms of ZnO/MWCNT/PCR/GCE in the presence of for increasing concentrations of melatonin and caffeine in 0.1 M pH 7.0 PBS (0.1 M) with 20 mV/s scan rate and 100 mV pulse amplitude. Melatonin and caffeine concentrations: a) 4.0 x10^{-8} b) 6.0x10^{-8} c) 1.0x10^{-7} , d) 2.0 x10^{-7} , e) 4.0x10^{-7} M

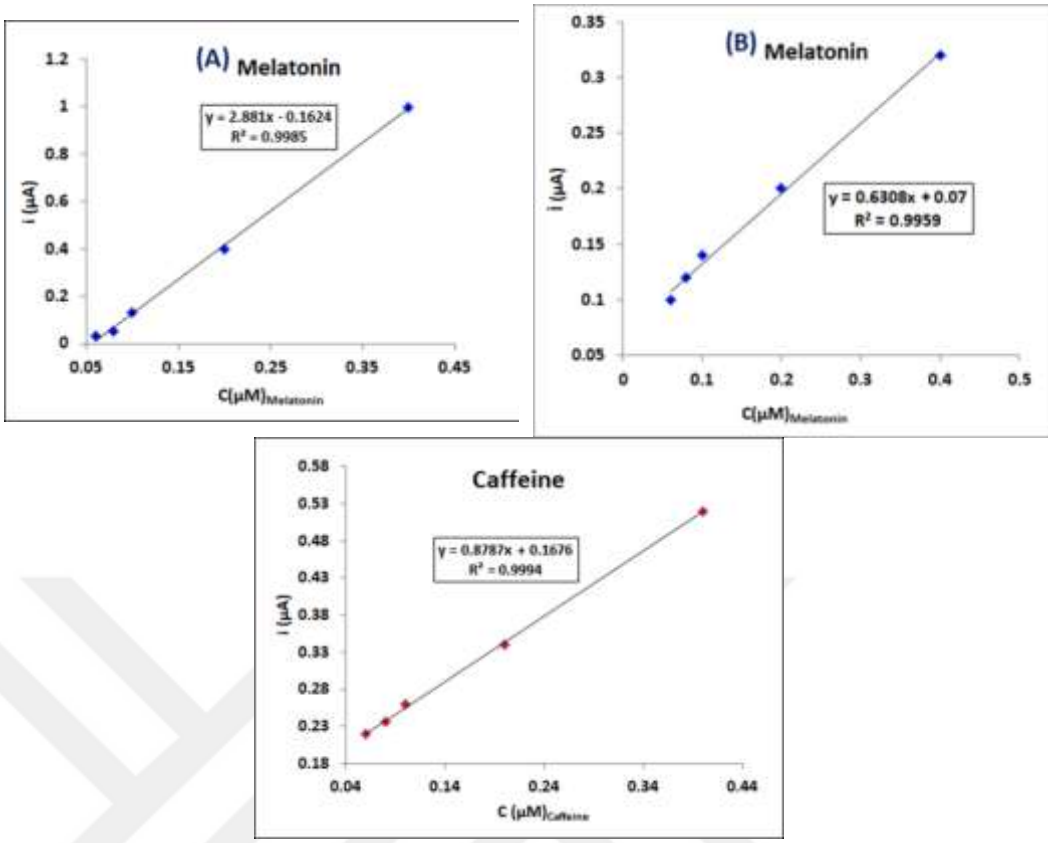

Figure 3.59 Calibration curves for a caffeine oxidation at ZnO/MWCNT/PCR/GCE in the presence of for increasing of melatonin and caffeine concentration ranges between $4.0x10^{-8}$-$4.0x10^{-7}$ M.

Comparisons of the bare and modified electrodes in terms of sensitivity, detection limit (LOD) and linear concentration range of melatonin and caffeine for all electrodes were given in Table 3.20. As seen in this comporison, **ZnO/MWCNT/PCR/GCE** shows higher activity towards melatonin and caffeine oxidation and the higher sensitivity low detection limit compare with all electrodes.

Table 3.20 Analytical characteristics for determination of melatonin and caffeine under optimum conditions

ANALYTES	MELATONIN (A)	MELATONIN (B)	CAFFEINE
ELECTRODE	**MWCNT/GCE**		
Calibration Equation	$ip_a=0.1935c_M+4.727$ ($R^2=0.9972$)	$ip_a=0.2226c_M+1.301$ ($R^2=0.9953$)	$ip_a=0.1685c_C+0.7124$ ($R^2=0.9963$)
Linear Range	$2.0x10^{-6}$ M- $1.0x10^{-5}$ M	$8.0x10^{-7}$ M- $8.0x10^{-5}$ M	$8.0x10^{-7}$ M- $8.0x10^{-5}$ M
LOD	$6.67x10^{-7}$ M	$2.67x10^{-7}$ M	$4.74\ x10^{-7}$ M
ELECTRODE	**MWCNT/PCR/GCE**		
Calibration Equation	$ip_a=0.5026c_M+3.282$ ($R^2=0.9974$)	$ip_a=0.1862c_M+0.5181$ ($R^2=0.9902$)	$ip_a=0.1264c_C+0.5264$ ($R^2=0.9918$)
Linear Range	$6.0x10^{-7}$ M - $1.0x10^{-5}$ M	$4.0x10^{-7}$ M- $2.0x10^{-5}$ M	$4.0x10^{-7}$ M- $2.0x10^{-5}$ M
LOD	$2.0x10^{-7}$ M	$1.33x10^{-7}$ M	$1.33\ x10^{-7}$ M
ELECTRODE	**ZnO/MWCNT/PCR/GCE**		
Calibration Equation	$ip_a=2.881c_M-0.1624$ ($R^2=0.9985$)	$ip_a=0.6308c_M+0.07$ ($R^2=0.9959$)	$ip_a=0.8787c_C+0.1676$ ($R^2=0.9994$)
Linear Range	$4.0\ x10^{-8}$ M - $4.0\ x10^{-7}$ M	$4.0\ x10^{-8}$ M - $4.0\ x10^{-7}$ M	$4.0\ x10^{-8}$ M - $4.0\ x10^{-7}$ M
LOD	$1.38x10^{-8}$ M	$1.38x10^{-8}$ M	$1.33x10^{-8}$ M

3.10. Interference Studies

The possible interfering compounds effect on melatonin and caffeine determination were investigated. For this studies, the potential interferences were added to fixed concentration of melatonin and caffeine containing pH.7.00 PB solution. Several organic molecules such as ascorbic acid, dopamine, uric acid and seratonin and different anionic and cationic species can be present in beverage samples and pharmaceuticals, thus their interference effect were examined at ZnO/MWCNT/PCR/GCE.

In this study, the effects of interference in the presence of melatonin and caffein were added to the solutions containing different organic and inorganic molecules. The anions and cations that can affect the interference positively or

negatively interact with the atoms in the molecular structure of melatonin and caffeine. For example the different types of organic molecules for example ascorbic acid, seratonin, uric acid, dopamine and different anions and cations can be studied in medicinal drugs and within biologic fluid samples in order to presented on ZnO/MWCNT/PCR/GCE under optimized conditions. Table 3.14 into 0.10 M PBS containing $5.0x10^{-5}$ M melatonin and caffeine. After adding the organic molecules like as sorted seratonin, uric acid, ascorbic acid and reduction signal was observed positive effect for interference. Inorganic compounds such as Na^{+}, K^{+}, NO_3^{-}, Mg^{2+} the reduction signals were influenced effect of interference for negatively.

Table 3.21 Relative (%) change of the analytical signal of melatonin and caffeine ($5.0x10^{-5}$ M) at ZnO/MWCNT/PCR/GCE in the (0.1 M) pH 7.00 PB solution.

Interfering species	Molar ratio ([Interfering species]/[M+C]	Change on the analytical signal of Melatonin (%)		Change on the analytical signal of Caffeine (%)
Ascorbic acid	1/10	33.55	58.41	86.51
	1	71.88	72.27	84.54
	10	-	78.50	59.54
Uric acid	1/10	55.33	-7.21	7.82
	1	523.36	-16.7	1.54
	10	-	-9.66	65.08
Dopamine	1/10	-43.96	30.02	-5.47
	10	-	0.995	-34.32
Seratonin	1/10	97.86	0.42	29.48
	1	341.99	-54.12	-14.23
Na^+	1/10	83.22	154.8	-34.02
	1	71.74	182.3	3.47
	10	105.55	143.3	-25.21
K^+	1/10	-22.77	+20.53	17.63
	100	-33.54	10.15	1.45
	1000	-9.67	-17.76	-18.63
NO_3^-	10	-41.47	5.45	27.75
	100	-49.61	10.02	34.69
	1000	-9.55	-32.67	23.37
Mg^{+2}	10	-41.47	5.45	27.75
	100	-49.61	10.02	34.69
	1000	-9.55	-32.67	23.37
Cl^-	10	-22.77	+20.53	17.63
	100	-33.54	10.15	1.45
	1000	-9.67	-17.76	-18.63
CO_3^{2-}	10	83.22	154.8	-34.02
	100	71.74	182.3	3.47
	1000	105.55	143.3	-25.21
SO_4^{2-}	1/10	-76.59	55.61	90.94
Al^{3+}	1/10	-76.59	55.61	90.94

3.11. Reproducibility, Repeatability and Stability of ZnO/MWCNT/PCR/GCE

Reproducibility, repeatability, and stability studies of ZnO/MWCNT/PCR/GCE were interpreted for electrochemical behaviour of both melatonin and caffeine. For these studies, five different ZnO/MWCNT/PCR/GCEs were prepared for investigation of melatonin and caffeine DPV behaviour to test the reproducibility of the modified electrode. As a result, the relative standart deviation (RSD) of the peak currents were 1.37% to 3.08% for melatonin and 2.24% for caffeine respectively.

The repeatability of ZnO/MWCNT/PCR/GCE was examined by monitoring the peaks current of the melatonin and caffeine at optimum experimental conditions for five successive measurements. The RSD were 1.709% and 2.32% for melatonin and for 1.730% caffeine.

In addition, a long-term stability of the ZnO/MWCNT/PCR/GCE was performed by keeping the electrode in pH 7.00 PB solution at laboratory conditions. The oxidation signals of $5x10^{-5}$ M melatonin and $5x10^{-5}$ M caffeine on ZnO/MWCNT/PCR/GCE were tested for six days.

The current siganls of ZnO/MWCNT/PCR/GCE remained about 98.2% and 97.5% for melatoinin and 97.3 % for caffeine, their initial current after 6 days respectively. The results of the ZnO/MWCNT/PCR/GCE represent the electrode possess great reproducibility, repeatability and stability.

3.12. Sample Analysis for Melatonin and Caffeine

The fabricated electrode and developed method were applied to pharmaceutical preparate and commercial coffee to determine the content of melatonin and caffeine respectively.

In the analysis of melatonin, five pharmaceutical preparate tablets were powdered separately and then each tablet was weighed and dissolved in ethanol, finally the total volume of sample solution was completed to 25 mL in the flask. The ZnO/MWCNT/PCR/GCE was immersed in directly the melatonin containing sample solution in 0.1 M PB solutions. The voltammograms were reported under optimum conditions in pH 7.00 PB solution by performing standard addition methods. The obtained voltammograms and standard addition plot were given in Figure 3.60. The oxidation currents increased with addition of melatonin standard solutions into sample and obeyed the equation: $ip_a = 0.1389C_M + 3.3622$, $R^2 = 0.9947$, n=5, which by extrapolation indicated that the concentration of melatonin in pharmacetic preparate was 2.43×10^{-4} M ±0.54. The result found using the proposed method was too close with expected value as 2.58×10^{-4} M in pharmacetic melatonin containing preparate.

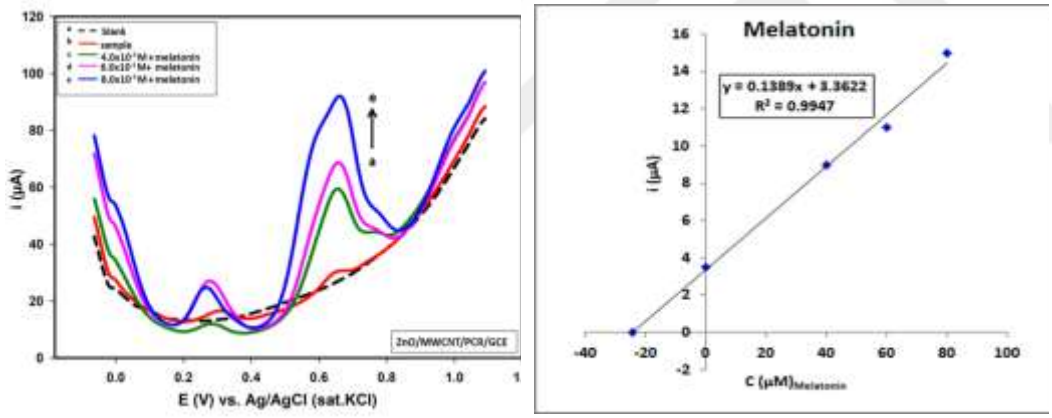

Figure 3.60 Application of the standard addition method for melatonin determination in melatonin containing sample DPV at ZnO/MWCNT/PCR/GCE

In the case of caffeine analysis in commercial coffee, granulated coffee was weighed approximately as 1.3407 g, and then it was dissolved in ultrapure water in 25 mL of flask. A portion of 1 mL was added into 9 mL pH 7.00 solution. The ZnO/MWCNT/PCR/GCE was immersed in directly the caffeine containing coffee sample solution in 0.10 M PB solutions. The voltammograms were reported under

optimum conditions in pH 7.00 PB solution by performing standard addition methods. The obtained voltammograms and standard addition plot were given in Figure 3.61. The oxidation currents increased with addition of caffeine standard solutions into sample and obeyed the equation: $ip_a = 0.0075C_C + 6.3049$, $R^2 = 0.9990$, n=5, which by extrapolation indicated that the amount of caffeine in commercial coffee was calculated as 1.2176 g ± 0.54.

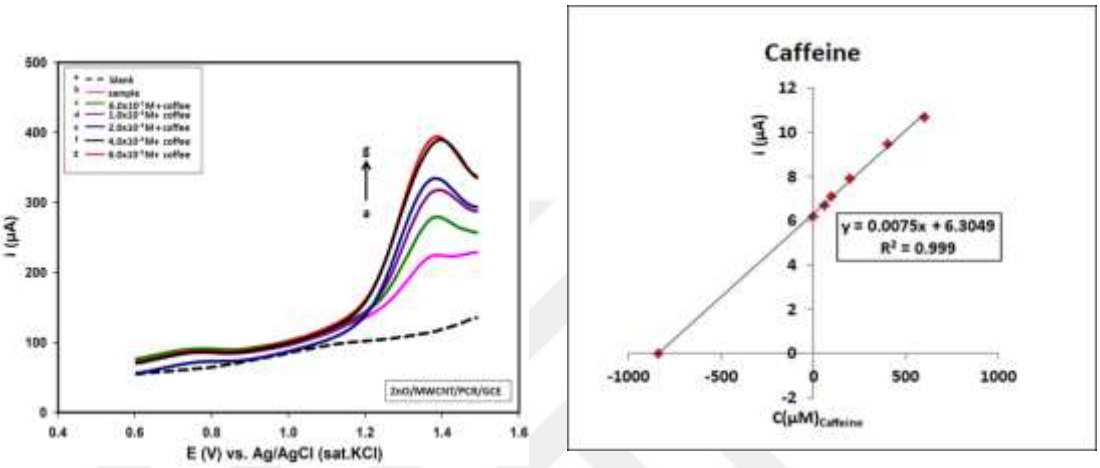

Figure 3.61 Application of the standard addition method for caffeine determination in coffee sample DPV at ZnO/MWCNT/PCR/GCE

4. CONCLUSIONS

In this thesis, the electrochemical behaviour of melatonin and caffeine were investigated in pH 7.00, (0.1 M) PBS by CV and DPV at different electrodes. The obtained results at ZnO/MWCNT/PCR/GC electrode were compared with GCE, PCR/GCE, MWCNT/GCE, MWCNT/PCR/GCE and ZnO/MWCNT/GCE. The best catalytic activity and selectivity for determination of melatonin and caffeine was obtained at ZnO/MWCNT/PCR/GC electrode.

Acetate buffer and different acidic solutions studied for selective determination of melatonin and caffeine that best peak separation and high peak currents were obtained at 0.1 M pH 7.00, PB solution.

In addition, DPV works were applied for the purpose of individual and simultaneous determination for both melatonin as well caffeine on GCE, PCR/GCE, MWCNT/GCE, ZnO/MWCNT/GCE, MWCNT/PCR/GCE, ZnO/MWCNT/PCR/GCE. The linear calibration ranges and dynamic range were plotted for all electrodes. The lowest detection limit and wider calibration range for melatonin and caffeine were obtained at ZnO/MWCNT/PCR/GCE in comparison to bare GCE, an another composite modified electrodes. As the results of studies, detection limits for individual determination of melatonin and caffeine were founded as $3.3x10^{-9}$ M ve $2.0x10^{-8}$ M, separately. The limit of detection values for simultanious determination of melatonin and caffeine were calculated as $1.38x10^{-8}$ M and $1.33x10^{-8}$ M, respectively.

Moreover, DPV technique was used to explain the stability, reproducibility, repeatability and studies due to the composite modified electrodes prepared in order to determination of melatonin and caffeine. During the studies, melatonin has two oxidation steps. Therefore, % relative standard deviation values of each melatonin peak were calculated separately. According to this result, The RSD% of the peak currents that obtained from reproducibility studies were found as 1.37% and 3.08% for melatonin and 2.24% for caffeine respectively (n=5). The measurements with

the same electrode for every hour during the day, represents the high repeatibility of the electrode with 1.709% and 2.32% RSD values for melatonin and 1.730% values for caffeine, respectively (n=5). Conversely, the long term stabilization studies of in this period of two weeks exhibits that this modified ZnO/MWCNT/PCR/GCE might be utilized as durable voltammetric sensor with only current decrease of 10.95% and 12.09% for melatonin and caffeine respectively.

In this study, the effects of interference in the presence of melatonin and caffein were added to the solutions containing different organic and inorganic molecules. The anions and cations that can affect the interference positively or negatively interact with the atoms in the molecular structure of melatonin and caffeine. For example the different types of organic molecules for example ascorbic acid, seratonin, uric acid, dopamine and different anions and cations can be studied in medicinal drugs and within biologic fluid samples in order to presented on ZnO/MWCNT/PCR/GCE under optimized conditions. Table 3.14 into 0.1 M PBS containing $5.0x10^{-5}$ M melatonin and caffeine. After adding the organic molecules like as sorted seratonin, uric acid, ascorbic acid and reduction signal was observed positive effect for interference. Inorganic compounds such as Na^{+}, K^{+}, NO_3^{-}, Mg^{2+} the reduction signals were influenced effect of interference for negatively.

Melatonin and caffeine determination and electrochemical behavior were also observed on ZnO/MWCNT/PCR/GCE modified electrode under conditions where the supporting electrolyte was pH 7.00 (0.1M) PBS. Remarkably of enhanced voltammetric signal of melatonin and caffeine oxidation the modified electrode can be attributed increasing conductivity and effective surface area electrode which can be played important role to accelerate the electron transfer. The presence of PCR films and effects of ZnO metal nano particles was also revealed by SEM, EDX and EIS.

The sample analysis of melatonin was based on these commonly used tablets as a daily food supplement and the sample analysis for caffeine was used granulated

coffee in real samples. The modified ZnO/MWCNT/PCR/GCE can be used for the fast, cheap and selective determination of melatonin and caffeine.

The general results show that ZnO/MWCNT composition with electropolimerization of PCR on GCE generate the catalytically active surface towards individual and simultaneous determination of melatonin and caffeine with high selectivity and sensitivity in real samples.

REFERENCES

Abid, A.D., Anderson, D.S., Das, G.K., Winkle, L.S.V. and Kennedy, I.M., 2013, Novel lanthanide-labeled metal oxide nanoparticles improve the measurement of in vivo clearance and translocation, Particle and Fibre Toxicology, 10(1):10 p.

Ando, Y., Zhao, X., Sugai, T., Kumar, M., 2004, Growing carbon nanotubes, Materials Today, 22-29 pp.

Ago, H., Komatsu, T., Ohshima, S., Kuriki, Y., Yumura, M., 2000, Dispersion of metal nanoparticles for aligned carbon nanotube arrays, Appl. Phys. Lett. 77-79 pp.

Aoiki, K., Osteryoung, J., Osteryoung, R. A., 1980, Differential normal pulse voltammetry-theory, J. Electroanal. Chem. Interfacial Electrochem. 110, 1-18 pp.

Agrawal, B., Chandra, P., Goyal, R. N., Shim, Y. B., 2013, Detection of norfloxacin and monitoring its effect on caffeine catabolism in urine samples, Biosens. Bioelectron. 47, 307–312 pp.

Ajayan, P. M., Charlier, J. -C., Rinzler, A. G., 1999, Carbon nanotubes: From macromolecules to nanotechnology, PNAS, 25(96), 14199-14200 pp.

Alyamani, A., Lemine, O. M., 2012, FE-SEM characterization of some nanomaterial, Scanning electron microscopy, In V. Kazmiruk (Ed.).

Apetrei, M. I., Apetrei C., 2016, Voltammetric determination of melatonin using a graphene-based sensor in pharmaceutical products, International Journal of Nanomedicine 11, 1859-1866 pp.

REFERENCES (continued)

Amare, M., Admassie, S., 2012, Polymer modified glassy carbon electrode for the electrochemical determination of caffeine in coffee, Talanta 93, 122– 128 pp.

Bakır, Ç. C., Şahin, N., Polat, R., Dursun, Z., 2011, Electrocatalytic reduction of oxygen on bimetallic copper-gold nanoparticles multiwalled carbon nanotube modified glassy carbon electrode in alkaline solution, Journal of Electroanalytical Chemistry, 662:275-280 pp.

Bandow, S., Rao, A. M., Williams, K. A., Thess, A., Smalley R. E., Eklund, P. C., 1997, Purification of Single-Wall Carbon Nanotubes by Microfiltration, *J. Phys. Chem. B*, 101, 44, 8839-8842 pp.

Brett, C. M. A., Brett, A. M. O., 1993, Electrochemistry Principles, Methods and Applications, Oxford University Pres Inc., Newyork.

Brabazon, D., Raffer, A., 2010, Advanced characterization techniques for nanostructures, Emerging nanotechnologies for manufacturing, 59–91pp., (William Andrew Publishing)

Bagheri, H., Afkhami, Hashemib, A., Ghaneia, P. M., 2015, Simultaneous and sensitive determination of melatonin and dopamine with Fe_3O_4 nanoparticledecorated reduced graphene oxide modified electrode, RSC Adv. 5, 21659 p.

Blecher, R., Lingens, F., Hoppe-Seyler's, Z., 1997, The Metabolism of Caffeine by a Pseudomonas putida Strain, Physiol. Chem., 358, 807 p.

Bubenik, G. A., 1999, in: R. Watson (Ed.), Melatonin in Health Promotion, CRC Press, Boca Raton, 21 p.

REFERENCES (continued)

Back, K., Tan, D. X., Reiter, R. J., 2016, Melatonin biosynthesis in plants: multiple pathways catalyze tryptophan to melatonin in the cytoplasm or chloroplasts. J Pineal Res. 61:426–37 pp.

Baker, R.T.K., Chludzinski, Jr. J. J., Dudash, N.S., Simoens, A.J., 1983, The formation of filamentous carbon from decomposition of acetylene over vanadium and molybdenum, 21(5), 463-468 pp.

Cardinali, D.P., 1981, Melatonin: A mammalian pineal hormon, Endocrinol. Rev. 2, 327–346 pp.

Corujo-Antuna, J. L., Abad-Villar, E. M., Fernandez-Abedul, M. T., 2003, Detecting and monitoring the production of melatonin and other related indole compounds in different Saccharomyces strains by solid-state electrochemical techniques, J. Pharm. Biomed Anal., 31, 421 p.

Charlier, J.-C., Blase, X., Roche, S., 2007, Electronic and transport properties of nanotubes, Reviews Of Modern Physics, 79, 677 p.

Chen, P., Lin, J., Tan, K. L., 2000, Carbon Nanotubes: A Future Material of Life, Life, 49,105-108 pp.

Colomer, J.-F., Henrard, L., Lambin, Ph., Van Tendeloo, G., 2002, Electron diffraction and microscopy of single-wall carbon nanotube bundles produced by different methods, Eur. Phys. J. B 27, 111-118 pp.

Chiang, C. K., Fincher Jr., C. R., Park, Y. W., Heeger, A. J., Shirakawa, H., Louis, E. J. Gau S. C., Alan, MacDiarmid, G., 1978, Electrical Conductivity in Doped Polyacetylene, Phys. Rev. Lett. 40, 1472 p.

REFERENCES (continued)

De Volder, M. F. L., Tawfick, S., Baughman, R. H., Hart J. A., 2013, Carbon nanotubes: present and future commercial applications, Science, 9, 339-535 pp.

Dai, H., 2002, Carbon nanotubes: opportunities and challenges, Surface Science, 500, 218-241 pp.

Dresselhaus, M. S., Dresselhaus, G., Jorio, A., 2004, Unusual Properties And Structure Of Carbon Nanotubes, Annu. Rev. Mater. Res. 34, 247-78 pp.

Dursun, Z., Karabiberoğlu, U. Ş., Koluaçık, E., 2018, Electrochemical Determination of Serotonin Using Pre-treated Multi-walled Carbon Nanotube-polyaniline Composite Electrode, Electroanalysis, 30, 2977 – 2987 pp.

Dursun, Z., Karabiberoğlu, U. Ş., 2010, Cu nanoparticles incorporated polypyrrole modified GCE for sensitive simultaneous determination of dopamine and uric acid, Talanta, 80(3): 1461-1466 pp.

Dursun, Z., Ceylan, K. Ç., 2018, Enhanced electrocatalytic activity of copper phthalocyanine/multiwalled carbon nanotube composite electrode via Pt nanoparticle modification for oxygen reduction, Turkish Journal of Chemistry, 42, 623 – 638 pp.

Eklund, P.C., Pradhan, B.K., Kim, U.J., Xiong, Q., Fischer, J.E., Friedman, A.D., Holloway, B.C. Jordan K., Smith, M.W., 2002, LargeScale Production of Single Walled Carbon Nanotubes Using Ultrafast Pulses from a Free Electron Laser, Nano Lett., Vol. 2, No.6.

REFERENCES (continued)

Fernandez, P. L., Martin, M. J., Gonzalez, A. G., Pablos, F., 2000, HPLC determination of catechins and caffeine in tea. Differentiation of green, black and instant teas, Analyst, 125, 421−425 pp.

Gupta, S., Price, C., Heintzman, E., 2016, Conducting polymer nanostructures and nanocomposites with carbon nanotubes: Hierarchical assembly by molecular electrochemistry, growth aspects and property characterization. J. Nanosci. Nanotechnol. 16, 374–391 pp.

Gupta, K. V., Jain, K. A., Shoora, K. S., 2013, Multiwall carbon nanotube modified glassy carbon electrode as voltammetric sensor for the simultaneous determination of ascorbic acid and caffeine, Electrochimica Acta 93, 248–253 pp.

Guo T., Nikolaev, P., Thess, A., Colbert, D., Smalley R., 1995, "Catalytic growth of single walled nanotubes by laser vaporization", Chemical Physics Letters, 243, 49 pp.

Guo, T., Diener, M. D., Chai, Y., Alford, M. J., Haufler, R. E., McClure, S. M., Ohno T., Weaver J. H., Scuseria, G. E., Smalley R. E., 1992, Uranium Stabilization of C_{28}: A Tetravalent Fullerene, 257, 1661-1664 pp.

Goldstein, J. I., Newbury, D. E., Echlin, P., Joy, D. C., 1992, Scanning electron microscopy and x-ray microanalysis, (2^{nd} ed.).

Goyal, N., R., Bishnoi, S., Agrawal, B., 2011, Electrochemical sensor for the simultaneous determination of caffeine and aspirin in human urine samples, Journal of Electroanalytical Chemistry 655, 97–102 pp.

REFERENCES (continued)

Hulla, J.E., Sahu, S.C., Hayes, A.W., 2015, Nanotechnology: History and future, Human and Experimental Toxicology, 34(12): 1318–1321 pp.

Huang, W. S., Humphrey, B. D., MacDiarmid, A. G., 1986, Polyaniline, a novel conducting polymer, Morphology and chemistry of its oxidation and reduction in aqueous electrolytes. Journal of the Chemical Society, Faraday Transactions 1: Physical Chemistry in Condensed Phases 82, 2385–2400 pp.

Horiuchi, S., Fujita, T., 2003, Three-Dimensional Nanoscale Alignment of Metal Nanoparticles Using Block Copolymer Films as Nanoreactors, Langmuir, 19, 2963–2973 pp.

Hilding, J., Grulke, E.A., Zhang, Z.G., Lockwood, F., 2003, Dispersion of Carbon Nanotubes in Liquids, Journal od Dispersion Science and Technology, 24(1): 1-41 pp.

Hamada, N., Sawada, S.-i., Oshiyama, A., 1992, New One-Dimensional Conductors: Graphitic Microtubules, Physical Review Letters, 10(68): 1579 p.

Iijima, S., 1991, Helical microtubules of graphitic carbon, Nature, 354, 56-58 pp.

Iijima, S., Ichihashi, T., 1993, Single-shell carbon nanotubes of 1-nm diameter, Nature 363, 603-605 pp.

Jayakumar, C., Magdalane, M. C., Kanimozhi, K., Kaviyarasu, K., Jeyaraj, B., 2017, Fabrication of Nano Poly Cresol Red over Glassy Carbon Electrode and its Application in Selective Determination of Uric acid in the Presence of Ascorbic Acid, Journal of Nanostructures, 7(2), 155-164 pp.

REFERENCES (continued)

Jones, J., Magri, R., Rios, R., Jones, M., Platea, C., Lewisa, D., 2011, The detection of caffeine and cotinine in umbilical cord tissue using liquid chromatography–tandem mass spectrometry, Anal. Methods, 3,1310−1315 pp.

Kam, N. W. S., Liu, Z., Dai, H., 2005, "Functionalization of carbon nanotubes via cleavable disulfide bonds for efficient intracellular delivery of siRNA and potent gene silencing," Journal of the American Chemical Society, vol. 127, 36, 12492–12493 pp.

Kaempgen, M., Ma, J., Gruner, G., Wee, G., Mhaisalkar, S. G., 2007, Bifunctional carbon nanotube networks for supercapacitors, Applıed Physıcs Letters, 90, 264104 p.

Kalmar, J. M., Cafarelli, E., 1999, Effects of caffeine on neuromuscular function, J. Appl. Physiol. 87, 801 p.

Kissinger, P. T., Heineman, R. W., 1983, Cyclic voltammetry, J. Chem. Educ., 60, 9, 702 p.

Kroto, H. W., Heath, J. R., O'Brien, S. C., Curl, R. F., Smalley, R. E., 1985, C_{60}: Buckminsterfullerene, Nature 318, 162-136 pp.

Kumar, H. K., Venkatesh, N., Bhowmik, H., Kuila, A., 2018, Metallic Nanoparticle: A Review, Biomedical Journal of Scientific and Technical Research 4(2)- 1318–1321 pp.

REFERENCES (continued)

Kumar, N., Sharma, R., Goyal, R. N., 2016, Nanopalladium grained polymer nanocomposite based sensor for the sensitive determination of Melatonin Electrochimica Acta, 211, 18–26 pp.

Kiselev, N.A. Zakharov, D.N., 2001, Electron Microscopy of Carbon Nanotubes, Crystallography Reports, Vol. 46, No. 4, pp. 577-585 pp.

Khan, I., Saeed, K., Khan, I., 2019, Nanoparticles: Properties, applications and Toxicities, Arabian Journal of Chemistry, 12: 908–931 pp.

Kuchibhatla, S. V. N. T., Karakoti, A. S., Bera, D., Seal, S., 2007, One dimensional nanostructured materials, Progress in Materials Science, 52, 699-913 pp.

Li, J., Jia, G., Zhang, Y., 2007, Chemical Anisotropies of Carbon Nanotubes and Fullerenes Caused by the Curvature Directivity, Chem. Eur. J., 13, 6430-6436 pp.

Lopez-Martinez, L., Lopez-de-Alba, P. L., Garcia-Campos, R., De Leon-Rodriguez, L.M., 2003, Simultaneous determination of methylxanthines in coffees and teas by UV-Vis spectrophotometry and partial least squares, Anal. Chim. Acta, 493, 83–94 pp.

Lourenção, C. B., Medeiros, A. R., Rocha-Filho, C. R., Mazo, H. L., Fatibello-Filho, O., 2009, Simultaneous voltammetric determination of paracetamol and caffeine in pharmaceutical formulations using a boron-doped diamond electrode, Talanta 78, 748–752 pp.

REFERENCES (continued)

Mayo, J.C., Sainz, R.M., Tan, D.X., Antolin, I., Rodriguez, C., Reiter, R.J., 2005, Melatonin and Parkinson's disease, Endocrine 27, 69–178 pp.

MacDonald, J. R., 1987, Impedance spectroscopy and its use in analyzing the steady-state AC response of solid and liquid electrolytes, J. Electroanal. Chem., 223, 25-50 pp.

Miyoshi, K., Surface Characterization Techniques, Mechanical Tribology, 2, 24 pp.

Mortier, J., Engelhardt, M., 2000, "Foreign body reaction to a carbon fiber implant in the knee: case report and literatüre survey," Zeitschrift f¨ur Orthop¨adie und ihre Grenzgebiete, vol. 138, no. 5, pp. 390–394 pp.

Maultzsch, J., 2004, Vibrational properties of carbon nanotubes and graphite, Fakultät II Mathematik und Naturwissenschaften, Technischen Universität Berlin, Germany, Doctor of Philosophy Thesis.

Mills, M. H., King, M. G., Keats, N. G., McDonald, R. A., 1986, Melatonin determination in human urine by high-performance liquid chromatography with fluorescence detection, J Chromatogr 377: 350 pp.

Miles, A., Philbrick, D., Tidmarsh, S. F., Shaw, D. M., 1985, Direct radioimmunoassay of melatonin in saliva, Clin. Chem., 31, 1412 p.

Molaakbari, E., Mostafavi, A., Beitollahi, H., 2015, Simultaneous electrochemical determination of dopamine, melatonin,methionine and caffeine, Sensors and Actuators B, 195–203 pp.

REFERENCES (continued)

Pizzariello, A., Svorc, J., Stred'ansky, M., Miertus, S., 1999, A biosensing method for detection of caffeine in coffee, J. Sci. Food Agric., 79, 1136 p.

Pons, F.W., Muller, P., 1990, Induction of frameshift mutations by caffeine in Escherichia coli K_{12}, Mutagen, 5, 173 p.

Qu, W., Wang, F., Hu, S., Cui, D., 2005, Electrocatalytic Properties and Voltammetric Determination of Melatonin at a Nanostructured Film Electrode, Microchim. Acta 150, 109–114 pp.

Radi, A., Bekhiet, G. E., 1998, Voltammetry of melatonin at carbon electrodes and determination in capsules, Bioelectrochem. Bioenerg. 45, 275–279 pp.

Rawat, A., Chandra, S., Sarkar, A., 2010, Easy Way of Sample Monitoring: Chemical Sensors and Biosensors, Anal. Bioanal. Electrochem. 2 , 212–216 pp.

Ramos, A., Hernández, Hernández, M. M., González, I., 2001, Influence of Chloride and Nitrate Anions on Copper Electrodeposition in Ammonia Media, Journal of The Electrochemical Society, 4(148).

Ratner, B. D., Hoffman, A. S., Schoen, F. J., Lemons, J. E., 1996, An Introduction to Materials in Medicine, Biomaterials Science, 447-449 pp.

Regan, F., Shakalisava, Y., 2005, Rapid simultaneous determination of alkylxanthines by CZE and its application in analysis of pharmaceuticals and food samples, Anal. Chim. Acta 540, 103–110 pp.

Reiter R. J., 1986, The pineal gland: An important link to the environment, News Physiol. Sci. 1, 202-205 pp.

REFERENCES (continued)

Reiter, R. J., 1991. Pineal Melatonin: Cell Biology of Its Synthesis and of Its Physiological Interactions, Endocrine Reviews, 2(12), 151–180 pp.

Robertson, J., 2004, Realistic applications of CNTs, Materials Today, 46-52 pp.

Rocheleau, M., Purdy, W. C., 1991. "Voltamınetric Studies with Quaternary An1monium Functionalized Polyn1er Film-coated Electrodes" Electroanalysis, 3, 935-939 pp.

Serp, P., Corrias, M., Kalck, P., 2003, Carbon nanotubes and nanofibers in catalysis, Applied Catalysis A: General 253 337-358 pp.

Sinnot, S. B. Andrews, R., 2001, Carbon Nanotubes: Synthesis, Properties, and Applications. Crit. Rev. Solid State Mater. Sci., 26(3), 145-249 pp.

Shirakawa, H., Louis, E. J., MacDiarmid, A. G., Chiang, C. K., Heeger, A. J., 1977, Synthesis of electrically conducting organic polymers: halogen derivatives of polyacetylene, $(CH)_x$, Journal of the Chemical Society,Chemical Communications, 578-580 pp.

Sun, X., Kiang, C. -H., Endo, M., Takeuchi, K., Furuta, T., Dresselhaus, M. S., 1996, Stacking characteristics of graphene shells in carbon nanotubes, 54(18): 12629-12632 pp.

Srisuphan, W., Bracken, M. B., 1986, Maternal Caffeine Intake and Intrauterine Growth Retardation, Am. J. Obstet. Gynecol., 155, 14 p.

Suni, I.I., 2008, Impedance methods for electrochemical sensors using nanomaterials, *Trends in Analytical Chemistry*, 27(7):604-611 pp.

REFERENCES (continued)

Sharma,V., Gulati, A., Ravindranath, S. D., Kumar, 2005, V., A simple and convenient method for analysis of tea biochemicals by reverse phase HPLC, J. Food Compos. Anal. 18, 583–594 pp.

Sun, W., Jiang, Q., Yang, M., Jiao, K., 2008, Electrochemical Behaviors of Hydroquinone on a Carbon Paste Electrode with Ionic Liquid as Binder, Bull. Korean Chem. Soc. 29, 915–920 pp.

Sun, J-Y., Huang, K-J., Wei, S-Y., Wu, Z-W., Ren, F-P., 2011, A graphene-based electrochemical sensor for sensitive determination of caffeine Colloids and Surfaces B: Biointerfaces, 84, 421–426 pp.

Soltani, N., Tavakkoli, N., Shahdost-fard, F., Salavati, H., Abdoli, F., 2019, A carbon paste electrode modified with Al_2O_3-supported palladium nanoparticles for simultaneous voltammetric determination of melatonin, dopamine, and acetaminophen, Microchimica Acta, 186:540, 7-13 pp.

Smajdor, J., Piech, R., Piech, M., Paczosa-Bator, B., 2017, Carbon black as a glassy carbon electrode modifier for high sensitive melatonin determination, Journal of Electroanalytical Chemistry 799, 278–284 pp.

Spataru, N., Sarada, B. V., Tryk, D.A., Fujishima, A., 2002, Anodic Voltammetry of Xanthine, Theophylline, Theobromine and Caffeine at Conductive Diamond Electrodes and Its Analytical Application, Electroanalysis, 14, 721 p.

Tan, D. X., Manchester, L. C., Esteban-Zubero, E., Zhou, Z., Reiter, R., 2015, Melatonin as a potent and inducible endogenous antioxidant: synthesis and metabolism. Molecules, 20:188-86 pp.

REFERENCES (continued)

Tsai, T.H., Huang, Y.C., Chen, S. M., 2011, Manganese hexacyanoferrate with poly(3, 4- ethylenedioxythiophene) hybrid film modified electrode for the determination of catechin and melatonin, Int. J. Electrochem. Sci. 6, 3238–3253 pp.

Thanh-Hai, L., Yukyung, K., Hyeonseok, Y., 2017, Electrical and Electrochemical Properties of Conducting Polymers, Polymers, 9, 150 p.

Terrones, M., 2003, Science and Technology of the Twenty-First Century: Synthesis, Properties, and Applications of Carbon Nanotubes, Annu. Rev. Mater.Res., 33, 419-501 pp.

Thess, A., Nikolaev, P., Dai, H., Xu, C., Rinzler, A. G., Colbert, D. T., Scuseria, G. E., Smalley, R. E., 1996, Crystalline Ropes of Metallic Carbon Nanotubes, 273, 483-487 pp.

Uslu, B., Demircigil, B.T., Ozkan, S.A., Sentürk, Z., Enein, H. Y. A., 2001, Simultaneous determination of melatonin and pyridoxine in tablet formulations by differential pulse voltammetry, Die Pharmazie 56, 938–942 pp.

Uygun, Z.O. and Uygun, H.D.E., 2014, A short footnote: Circuit design for faradaic impedimetric sensors and biosensors, *Sensors and Actuators, B*, 202:448–453 pp.

Vaisman, L., Wagner, H.D., Marom, G., 2006, The role of surfactants in dispersion of carbon nanotubes, Advances in Colloid and Interface Science, (128-130): 37-46 pp.

REFERENCES (continued)

Wang, J., 1991, "Modified Electrodes for Electrochemical Sensors", Electroanalysis, 4, 255-259 pp.

Wang, Y. R, Hu, P., Liang, Q. L., Luo, G. A., Wang, Y. M., 2008, Application of Carbon Nanotube Modified Electrode in Bioelectroanalysis, Chinese Journal of Analytic Chemistry, 8(36), 1011-1016 pp.

Wang, J., Dai, J., Yarlagadda, T., 2005, Carbon nanotube conducting polymer composite nanowires, Langmuir, 21, 9–12 pp.

Wang, A., Li, L., Zang, F., Fang, Y., 2000, Amperometric detection of three purine alkaloids following their separation by micellar electrokinetic capillary chromatography, Anal. Chim. Acta, 419, 235–242 pp.

Yang, S., Yang R., Li, G., Qua, L., Li, J., Yu, L., 2010, Nafion/multi-wall carbon nanotubes composite film coated glassy carbon electrode for sensitive determination of caffeine, Journal of Electroanalytical Chemistry, 639, 77-82 pp.

Zhou, W., Apkarian, R. P., Wang, Z. L., Joy, D., 2006, Fundamentals of scanning electron microscopy, In Scanning microscopy for nanotechnology, 1–40 pp.

Zheng, S., Huang, Y., Cai, J., Guo, Y., 2013, Nano-copper-mwcnt-modified glassy carbon electrode for selective detection of dopamine, International Journal of Electrochemical Science, 8:12296-12307 pp.

Zhu, W., Bartos, P. J. M., Porro, A., 2004, Application of nanotechnology in construction, Summary of a state-of-the-art report. Mater Struct, 37: 649–58 pp.

ACKNOWLEDGEMENT

I want to enounce my heartfelt much more thanks for study of my thesis dear supervisor, Prof. Dr. Zekerya DURSUN, for his leadership and mild understanding in cooperation academic and useful knowledges throughout the experimental studies. Further, thanks to Associate Prof. Dr. Şükriye KARABİBEROĞLU and Associate Prof. Dr. Aydan ELÇİ for them encouragement during the studies.

Special thanks to my friends in Electroanalitic Research Group, firstly PhD student Merve AKTÜRK, Berkay M. LEŞKERİ, PhD student Şebnem Gül İLARSLAN for their private attachments and helping in the course of my experimental works.

I am extending my thanks to Ege MATAL for XPS and SEM imaging studies. Also thanks to PhD Meral ESEN and PhD Ayşegül ERDOĞAN for their helping during my experimental studies.

Finally, I am extremely appreciatory to my grandmother for her love, prayers and endless supporting to finish for my experimental studies and I am also appreciative to my family for my educating and preparing me for my forward lives.

.... / .... / 20..

İmzası

Tansu DOĞAN

CURRICULUM VITAE

Name	: Tansu Doğan
Date of Birth	: June, 15, 1993
Place of Birth	: Marmaris, Turkey
Nationality	: Republic of Turkish
Marital Status	: Single
Adress	: Atatürk Mah. 8809/17 No :29 Çiğli/İzmir
Phone Number	: +90 5543774517
E-mail	: tansudgn@hotmail.com
Education	: 2012-2016, BSc Degree in Chemisty Department of Ege University, İzmir, Turkey
	: 2017-…., MSc Degree in Chemistry Department of Ege University, İzmir, Turkey.